THE ROLE OF SUPPORTED COBALT CATALYSTS IN THE METHANE PARTIAL OXIDATION REACTION

John Charl Jeannot

A dissertation submitted to the Faculty of Engineering, University of the Witwatersrand, Johannesburg, in fulfilment of the requirements for the degree of Masters of Science in Engineering.

Johannesburg, 1995

Abstract

The partial oxidation of methane by air to synthesis gas over supported cobalt catalysts was studied. The investigation included analysis of the products of this reaction at various temperatures, and of the structure of the catalysts using powder X-ray diffraction techniques. The most effective catalyst for this reaction was found to be metallic cobalt supported on rhombohedral alumina (prepared as 10%Co/C/γ-Al_2O_3). In the presence of this catalyst 96% of the feed was completely converted to synthesis gas (CO : $2H_2$) at 1000°C. This catalyst showed no evidence of coking or loss of activity at 1000°C over a period of 180 hours. The reaction mechanism is thought to occur in two stages over two distinct zones of the catalyst. Complete reaction of O_2 with CH_4 to form CO_2 and H_2O is followed, in the second stage, by reforming and the water gas shift reaction to produce synthesis gas.

Declaration

I declare that this is my own work, unaided except where acknowledged. It is being submitted to the University of the Witwatersrand for the degree of Masters of Science in Engineering. It has not been submitted for any other degree or examination in this or any other University.

J. C. Jeannot

John Charl Jeannot

This 24 day of July 1995.

Acknowledgements

I would like to express my gratitude to my project supervisor, Prof. V. D. Sokolovskii, for his unfailing support and encouragement, and always being ready to share his experience and expertise.

To Prof. N. J. Coville, Prof. D. Glasser and Dr D. Hildebrandt, my co-supervisors, I would like to express my appreciation for their time, advice and guidance.

To Brett and Clive for conducting the atomic absorption spectroscopy and temperature programmed reduction experiments, and Peter for conducting those rather tedious surface area experiments — my thanks. Keith, my gratitude for your patience in teaching me the finer points of powder X-ray diffraction.

My thanks too, to Basil, the glassblowers and workshop staff for their energetic technical support.

Paul Furber, Bunty and Joe Sutton, thank you for proofreading this.

And finally to those, who by their encouragement, love and prayers saw me through this project, my deepest gratitude.

Do you not know?
Have you not heard?
The LORD is the everlasting God,
the Creator of the ends of the earth.
He will not grow tired or weary,
and his understanding no one can fathom.
He gives strength to the weary
and increases the power of the weak.
Even youths grow tired and weary,
and young men stumble and fall;
but those who hope in the LORD
will renew their strength.
They will soar on wings like eagles;
they will run and not grow weary,
they will walk and not be faint.

ISAIAH 40^{28-31}

To my Lord and Saviour, Christ Jesus.

Do you not know?
Have you not heard?
The LORD is the everlasting God,
the Creator of the ends of the earth.
He will not grow tired or weary,
and his understanding no one can fathom.
He gives strength to the weary
and increases the power of the weak.
Even youths grow tired and weary,
and young men stumble and fall;
but those who hope in the LORD
will renew their strength.
They will soar on wings like eagles;
they will run and not grow weary,
they will walk and not be faint.

ISAIAH 40^{28-31}

To my Lord and Saviour, Christ Jesus.

Contents

List of Tables

List of Figures

List of abbreviations

A_B^R	:	Pseudonym for a catalyst awaiting patenting
BET	:	Brunauer, Emmett, Teller
F-T	:	Fischer-Tropsch
FID	:	Flame Ionisation Detector
TCD	:	Thermal Conductivity Detector
TPR	:	Temperature Programmed Reduction
XRD	:	X-Ray Diffraction

Chapter 1

Introduction

1.1 World energy resources

The global need and demand for energy is obvious. From making a cup of coffee to moving millions of people daily from home to work and back, modern society uses energy — and lots of it. This energy is provided in three ways: by large fixed installations (power stations) where coal and petroleum chemical energy, or nuclear energy from enriched uranium, is converted to electricity; by small fixed installations in the home or factory; and by small mobile engines which use natural gas and transport fuels. It is therefore obvious that, from power generation to transportation, man is almost completely dependent on the combustion of fossil fuels for his energy [1].

1.1.1 Fossil fuels

Coal is the most abundant fossil fuel making up 59,4% and 94% of fossil fuel reserves[1] and resources[2] respectively, table 1.1 [2]. Although coal is evenly distributed geographically, it is more costly to extract from the ground and transport than petroleum. It also has a lower calorific value than petroleum, is more hazardous, and importantly, more costly to process due to the often high levels of sulphur, nitrogen and minerals [1].

Table 1.1: World conventional fossil fuel reserves and resources

	Reserves		Resources	
	10^3 EJ	Percent of Total	10^3 EJ	Percent of Total
coal	19,7	59,4	314,0	94,0
peat	6,7	20,4		
oil	4,0	12,1	8,3-11,9	3,0
natural gas	2,7	8,1	10,0-10,3	3,0
Total	*33,1*	*100,0*	*332,0-336,2*	*100,0*

Reproduced from Kirk-Othmer Encyclopedia of Chemical Technology [2].

The world-wide reserves-to-production ratio of **petroleum oil** is the lowest of all the fossil fuels, 30, compared to 245 for coal, causing concern about future availability.

Although cheaper at source than petroleum, **Natural gas** is significantly more expensive to transport. Unless consumers are easily reached by pipeline the cost advantage is lost, making natural gas less accessible to world consumers.

Peat is largely under-utilized and consequently resources have not been thoroughly surveyed.

[1]Reserves consist only of those minerals which are economically extractable with current extraction technology.

[2]Resources are the total amounts of minerals, including reserves, that could possibly be exploited.

Resources of **heavy oil** have also not yet been estimated because they are unviable unless new recovery techniques are found or the price of other fuels increases.

Bituminous tar sands and oil shale are other unconventional fossil fuels that have not yet been exploited on a large scale. Oil shales have a widespread geographic distribution, and are estimated to be 500–2000 times the estimated total recoverable resources of petroleum. As well as being economically unviable to exploit, the potential environmental problems, especially the disposal of the solid wastes from the process, cannot be addressed with current technology.

Due to the massive amounts of fossil fuels that are produced, transported and consumed, difficult environmental problems have evolved. Emissions from the combustion of fossil fuels contain sulphur and nitrogen oxides, particulates, unburned hydrocarbons, trace metals and carbon monoxide. Some of these are believed to be related to long-term chronic health effects, and sulphur and nitrogen oxides are causes of acid rain. Coal is the most polluting of the fossil fuels, not only because of the emissions during combustion, but also because toxins can find their way into the water table after being leached from coal ash dumps. Natural gas is the most benign of the fossil fuels, creating a minimum of air pollutants.

Methods for reducing these emissions involve switching to higher-quality fuels, upgrading the fuels before use, finding better combustion technologies, and applying control technology to remove pollutants from the combustion products [2].

1.1.2 Alternate energy sources

Nuclear energy

Nuclear fission power plants create thermal, rather than air pollution as well as large volumes of hazardous radioactive waste. Accidents at nuclear power plants pose

a major threat to human health and the environment. However, using conventional reactor technology, western uranium reserves have approximately one half of the heat content of the world's coal reserves, and four times this using fast-breeder reactor technology [2].

Nuclear fusion is a potentially limitless fuel supply; the top 5 cm of Lake Erie has enough deuterium and tritium in it to produce energy equivalent to the world's petroleum reserves. However, while progress has been made, this technology appears to be decades away from commercial exploitation [3].

Renewable energy

Due to growing concern over the depletion of easily utilisable fossil fuels and the dangers associated with nuclear energy, interest in alternate sources of energy is growing. Wind, water, geothermal and solar energy are all commercially exploitable forms of energy. Although technology exists to harness the energy from the wind, falling water, tidal phenomena, hot-water springs, and the sun, the extent to which these technologies can be used is limited by geographical or climatological factors [2].

1.1.3 Into the future

Historically man has depended on carbonaceous fuels for his primary energy supplies. During the industrial revolution wood was replaced by coal and in the third quarter of the twentieth century, the consumption of oil superseded that of coal. Poirier, Sanger and Smith [4] reported that reserves of natural gas, representing some 4127 EJ would only last until 2029 (allowing for a 2% annual increase in consumption). Petroleum (4749 EJ) would last until 2008. These authors also expect discoverable reserves to play an important role in the future, even though these may be located in remote areas and are presently uneconomical to exploit. In spite of the possible discovery of

new reserves and the potential of improved technology[3] every non-renewable resource will eventually be depleted.

It appears as if man will again have to change his primary energy source. But to what? There is no new fuel or emerging technology which presents itself as able to solve the twin problems of being able to meet the increasing energy demands of a growing world population without large-scale environmental impact. This means that for the foreseeable future we remain dependent on fossil fuels. How efficiently we use them, and how effectively we control the impact of their consumption on our environment, will determine the quality of life in the next century.

1.1.4 The case for natural gas

Currently, only 7% of utilized natural gas is used in chemical industries. This is largely due to natural gas and petroleum occurring together. Natural gas, as a by-product of petroleum extraction, is burned as a fuel for heating and power generation [4]. Due to the high cost of transporting natural gas, if there is no population of significance located economically close to the oil field, the natural gas is often flared [5]. Recently pressure has been mounting against the flaring of natural gas. This practice is seen as a waste of an important natural resource and an unnecessary contribution of carbon dioxide to the atmosphere [6].

A large shift to the use of natural gas as a chemical feedstock has two advantages: since it would be replacing petroleum as a feedstock it would reduce the demand on petroleum reserves. Secondly, the impact on the environment would be reduced since less would be flared and it would replace less benign fossil fuels. The price advantage of natural gas, however, is diminished by the cost of transportation.

[3] If the amount of oil recovered from oil wells was to be increased from 25–30% to 45–50%, the estimate of recoverable oil reserves would increase dramatically.

Natural gas is located in most areas of the world, with the most important reserves located in the north and east of the former U.S.S.R. and in the Middle-East. Discoverable reserves will mainly be located in remote areas, where exploitation is presently uneconomic [4].

Natural gas can be transported as Liquid Natural Gas (LNG) after being cooled to -162^{o}C at 8 MPa. This is an expensive process and the cost is added onto the transport costs, which depend on the distance between the source and the consumer. In Europe the transportation costs contribute about 30% of the total consumer price.

The purification of natural gas to methane is relatively simple, making methane conversion technology more or less source independent and readily transferable. Natural gas is also often cheaper than alternative carbonaceous raw materials. Thus natural gas is an attractive raw material for producing synthetic petroleum products [7].

1.2 Natural gas — available technologies

Currently, methane is used in a number of industrial applications. It can be reacted with HCl and HF to produce halocarbons, with ammonia to produce hydrocyanic acid, and with sulphur to produce carbon disulphide. Using thermal electric arc technology acetylene can be produced, and carbon black can be made by pyrolysis. However, the most important direct methane conversion process is to synthesis gas [4].

1.2.1 The production of synthesis gas

Synthesis gas, or *syngas*, is the generic name for mixtures of hydrogen, carbon monoxide and carbon dioxide in various proportions. The industrial importance of syngas is twofold: it provides a cheap source of hydrogen for processes such as petroleum

reforming and ammonia synthesis; it can be used as a feedstock for the synthesis of many organic chemicals. [1]

Among the options for generating syngas from natural gas are partial oxidation, autothermal reforming, steam-reforming in tubular reactors, and a number of speciality processes [8]. In most cases the production of synthesis gas is achieved by steam-reforming methane, equation 1.1:

$$CH_4 + H_2O \rightleftharpoons CO + 3H_2 \qquad (\Delta H^{\circ}_{298} = 206\ \text{kJ/mol}) \tag{1.1}$$

Thermodynamically this reaction is only favoured at high temperatures (see table 1.3, section 1.3.1 for the thermodynamics of this reaction), where coking or sintering may occur. These problems can be overcome by careful catalyst selection. Nickel-based catalysts are used to control the balance between coke formation and removal. Careful control of the amount of nickel can result in a small loss of steam-reforming activity coupled with a marked decrease in coking [9].

This reaction is well established for the manufacture of syngas, but has the disadvantage of being highly endothermic. The supply of sufficient energy to sustain not only the high reactor temperatures, but also the reaction, results in high capital and operating costs[4] [11].

The result of these disadvantages is that up to 60% of the capital cost of a methane conversion plant involves gas cleaning and desulphurisation, and generation and compression of syngas [8].

The largest use of synthesis gas world-wide is in the manufacture of ammonia, where the hydrogen content is of most interest [12]. Production of synthesis gas via the

[4]A review of the processes and reactors used for methane conversion, and in particular steam-reforming, is presented in *Technology and Manufacture of Ammonia*, [10].

steam-reforming process (equation 1.1) produces a hydrogen to carbon monoxide ratio of three as opposed to two for the partial oxidation process, equation 1.2:

$$CH_4 + \frac{1}{2}O_2 \rightleftharpoons CO + 2H_2 \qquad (\Delta H^{\circ}_{298} = -36 \text{ kJ/mol}) \tag{1.2}$$

The higher hydrogen content of synthesis gas produced by steam-reforming may favour ammonia synthesis, but it is often too high for other downstream processes. The ratio of hydrogen to carbon monoxide produced by the partial oxidation may therefore be more suitable for certain chemical processes [13].

In this work the partial oxidation of methane is presented as a competitive process for the steam-reforming process, particularly for the production of hydrocarbons and other organic compounds. Thus in this section an overview of those technologies which would benefit from a cheaper source of synthesis gas consisting primarily of hydrogen and carbon monoxide in a 2 : 1 ratio, is presented. Bond [1] and Strelzhoff [10] have given detailed overviews of those technologies which are concerned with the hydrogen content of syngas.

1.2.2 Fischer-Tropsch synthesis

In 1923 Franz Fischer and Hans Tropsch discovered that in the presence of ferrous metals carbon monoxide and hydrogen react to form higher gaseous, liquid and solid aliphatic hydrocarbons. This reaction became known as the Fischer-Tropsch reaction (F-T) [14].

The SASOL process (South Africa) and the Shell Middle Distillate Synthesis process (Malaysia) are the only known operations at present using this technology on a large scale.

SASOL

Synthesis gas is produced from coal for the SASOL process. The coal is gasified and the gas purified before F-T reaction. A diverse range of products are recovered by processes which include cryogenic separation of the light ends and steam/oxygen reforming of methane back to syngas.

In 1980 and 1982, when the SASOL 2 and 3 plants came on line, the price of petroleum crude was around the US$ 30/bbl mark. Even if the coal price was only US$ 15/ton (ash free), at 1993 petroleum crude prices the construction of a new plant based on the SASOL process was not viable. However, for remote natural gas priced at US 50 cents per million BTU, a grassroots F-T syncrude plant would be viable at US$ 23/bbl (15% return on capital) [12].

SASOL manufactures straight-run F-T diesel which has lower sulphur, nitrogen and aromatics content and higher linear hydrocarbon levels compared to petroleum derived diesel. This makes it a high-quality product. However, for the same reason *i.e.* low aromatics and high linear hydrocarbon levels, F-T gasoline has a low octane number and requires upgrading.

The greatest advantage of the SASOL process is the diversity of the products which can be produced.

Other chemicals which can be recovered from the SASOL process include significant amounts of phenol and cresols, from the Lurgi gasifiers. Ethanol, n-propanol, acetone and methyl ethyl ketone can be recovered in high purity as byproducts if iron-based catalysts are used. In low temperature F-T processes over 50% of the hydrocarbon product consists of highly-linear paraffinic waxes, with molecular weights between 300 and about 1700. The fractionated and refined waxes can earn four times as much as diesel or gasoline fuels.

The largest potential for chemical production lies in the high content of linear alpha olefins produced in high temperature iron catalyst based F-T processes. C_2 to C_4 olefins are conventionally produced from ethane or petroleum naphtha cracking, which at low petroleum crude prices are more competitive than via F-T. Higher molecular mass olefins are conventionally produced by oligomerisation to a wide spectrum of olefins, and then only to even carbon-numbered products. The F-T route can produce olefins selectively with both odd and even carbon-numbered olefins. C_7 to C_9 olefins can be converted to the corresponding alcohols and used in the manufacture of plasticisers for PVC. They can also be converted, using metathesis processes, to more valuable higher-mass linear olefins. C_9 to C_{12} olefins are used in the manufacture of synthetic lubricating oils. These, as well as linear alcohols produced by hydroformylation of C_{12} to C_{15} olefins, fetch high prices [12].

Shell Middle Distillate Synthesis

The objective of this process is to make kerosine and gas oil from natural gas. The production of saturated hydrocarbons requires synthesis gas with a hydrogen/ carbon monoxide ratio of two, and is produced by non-catalytic, autothermal partial oxidation. The synthesis step is a highly modernised version of F-T chemistry, emphasising high yields and favourable catalyst performance. The waxy product from the synthesis step is hydroisomerised and hydrocracked to give the appropriate yields of distillate products. These products are free from sulphur and nitrogen and are easily blendable with conventional refinery streams [8].

1.2.3 Methanol synthesis

Apart from traditional markets, a significant demand for methanol in new markets, such as fuels, can be foreseen. In addition to this, a variety of chemicals which today are produced from petroleum or by other routes, can be based on methanol. Thus

the hydrogenation of carbon monoxide to methanol is of the greatest economical and technological importance [15].

The first industrial catalytic methanol synthesis process was introduced by BASF in 1923. The process was based on zinc chromite catalysts, which were used almost exclusively until 1966 when ICI introduced copper-based catalysts. With the new catalysts the operating temperature and pressure could be decreased from 350°C to around 250°C and from 20-30 MPa to 5-10 MPa respectively. Although a number of competitive catalysts have since been introduced, they are mostly variations of the co-precipitated Cu-ZnO catalysts. Research into these co-precipitated catalysts as well as Raney Cu-Zn catalysts, intermetallic catalysts, and noble-metal catalysts is ongoing and results in continual small improvements to the technology of this process. [16]

Since the direct oxidation of methane avoids the highly energy intensive steam-reforming reaction (equation 1.1), this reaction has long been conceived as the most desirable route for methanol production [16] and has become the subject of intensive research (section 1.3.1).

The conversion of synthesis gas to methanol remains a mature and highly optimised process, with 99% selectivity achievable. In table 1.2, the efficiency with which synthesis gas is converted to various organic products is shown. It is evident that the conversion of synthesis gas to low molecular mass oxygenated products such as methanol, is more efficient than the conversion of syngas to hydrocarbons.

Methanol is a very versatile chemical intermediate and has many outlets. The largest portion of methanol is currently used in formaldehyde manufacture. The best way of producing acetic acid is carbonylation of methanol. Methanol can be reacted with CO to produce methylformate and dimethyl formamide. Methanol is also used in the manufacture of the octane booster MTBE. The vinyl acetate monomer can be produced from methanol and syngas [12].

Table 1.2: The efficiency of producing various products from syngas[a].

Reaction	Syngas Efficiency[b]
$2H_2 + CO \rightleftharpoons CH_3OH$	100%
$2H_2 + 2CO \rightleftharpoons CH_3COOH$	100%
$3H_2 + 2CO \rightleftharpoons (CH_2OH)_2$	100%
$4H_2 + 2CO \rightleftharpoons C_2H_5OH + H_2O$	72%
$8H_2 + 4CO \rightleftharpoons C_4H_9OH + 2H_2O$	58%
$4H_2 + 2CO \rightleftharpoons C_2H_4 + 3H_2O$	43.8%
$17H_2 + 8CO \rightleftharpoons C_8H_{18} + 8H_2O$	44.2%

[a] mass percent of syngas converted to the desired product

[b] Reproduced from [12]

1.2.4 Methanol to gasoline

Methanol can be used as an automobile fuel, although this application has been limited to date [12]. However, it is possible to manufacture gasoline from methanol. This process is based on the catalytic conversion of methanol to hydrocarbons over zeolite catalysts. This process produces C_4 to C_{10}, and aromatic hydrocarbons, and very few of the light gas and higher molecular weight hydrocarbons produced by the Fischer-Tropsch process [14].

The energy crises of 1973 and 1979 severely weakened the economy of New Zealand as it saw the percentage of its export earnings spent on fuel rise from 5% to between 20 and 30%. As a result a project was implemented to achieve about 50% self-sufficiency in transport fuels.

The Synfuel gas-to-gasoline project at Motunui, New Zealand, was designed to produce 570 000 tonnes per annum of high-octane gasoline. The conversion takes place in two stages: first, from gas to methanol (GTM) and second, from methanol to gasoline (MTG). The GTM stage uses the ICI low-pressure methanol process, with synthesis gas as an intermediatory. The MTG stage uses a fixed-bed catalytic process with Mobil's proprietary ZSM-5 catalyst.

The plant is owned and operated by New Zealand Synthetic Fuels Corporation Limited, with 25% of the shares held by Mobil and the balance held by the government. In 1987 the cost of producing one barrel of gasoline by the Synfuel process was US$ 60[5,6] [17]. To be comparable to imports the cost of crude oil would have had to be US$ 55[7]. The cost to the government was US$ 45. By 1996 the loan capital will be repaid, reducing the cost per barrel of gasoline to US$ 27 and the government burden to US$ 18. However, in real terms the cost of gas would continue to decrease, further reducing the gasoline cost per barrel to US$ 21 and the cost to the state to US$ 14 by the year 2000.

In 1987 it was forecast that New Zealand would import 2,1 million tonnes of crude oil, less than half of that imported in 1973/74. The advantages of this increased self-sufficiency could be significant, especially in the medium to long term [17].

Mobil Olefin to Gasoline and Mobil Olefin to Gasoline Distillate

Mobil has developed an alternate process to that employed at Motunui, which also uses methanol as a feed and ZSM-5 catalysts. This process combines Mobil's methanol to olefin (MTO) and the Mobil olefin to gasoline and distillate (MOGD) processes. Product flexibility, which allows the plant to adapt to market demands, high yields and excellent product quality make this combined process an attractive alternative for producing a wide range of hydrocarbon products from natural gas or coal [18].

---

[5]The prices quoted are in 1987 US Dollars where US$ 1 = NZ$ 1,85.

[6]It is assumed that the plant operates at design efficiency and capacity.

[7]To calculate the equivalent crude oil cost price, subtract US$ 7 from the price per barrel of gasoline.

Topsøe Integrated Gasoline Synthesis

In the future synthetic fuel plants are most likely to be situated in areas where the cost of natural gas is very low. For plants of this kind a low investment is essential, since investment costs will constitute a high proportion of the production costs due to the low energy price. Consequently, further development of the New Zealand Synfuel process should aim at reducing the investment.

In contrast to the New Zealand Synfuel process, the Topsøe Integrated Gasoline Synthesis (TIGAS) process integrates the methanol synthesis and MTG process steps into a single synthesis loop. In the integrated loop the first step is a process developed by Haldor Topsøe A/S. It uses a multi-functional catalyst system to produce a mixture of oxygenates, not just methanol. The second step is similar to Mobil's MTG process. Using the integrated loop allows the process to operate at the same, relatively low pressure, keeping the process as simple and cost effective as possible [19].

1.3 Natural gas — future potential

From the discussion in the previous section, it is evident that for the production of organic compounds, processes using synthesis gas as a feedstock hold great potential. These well-established processes can flexibly produce a wide range of organic chemicals of a high quality and at high yields. Since synthesis gas manufacture represents the greatest capital and operational cost in such processes considerable effort has been dedicated to improving this process, and to processes that would eliminate the need for synthesis gas production.

The partial oxidation of methane to synthesis gas is concerned with the production of synthesis gas under thermodynamically favourable conditions. The oxidative coupling to ethene, partial oxidation of methane to oxygenates, and oxychloro routes would eliminate synthesis gas as an intermediate.

1.3.1 Oxidative coupling

In table 1.3 the free energies and enthalpies of formation are given for various methane conversion reactions at 25°C and 1000°C [8].

Table 1.3: Free energies and enthalpies of formation

Number	Reaction	$\Delta G_{25°C}$ [kJ/mol]	$\Delta G_{1000°C}$ [kJ/mol]	$\Delta H_{25°C}$ [kJ/mol]	$\Delta H_{1000°C}$ [kJ/mol]
Steam-reforming[a]:					
(i)	$CH_4 + H_2O \rightleftharpoons CO + 3H_2$	+142	-96	+206	+227
Partial Oxidation to Syngas:					
(ii)	$CH_4 + \frac{1}{2}O_2 \rightleftharpoons CO + 2H_2$	-86	-274	-36	-22
Coupling:					
(iii)	$2CH_4 \rightleftharpoons C_2H_6 + H_2$	+69	+70	+32	+38
(iv)	$2CH_4 \rightleftharpoons C_2H_4 + 2H_2$	+170	+42	+101	+110
(v)	$2CH_4 \rightleftharpoons C_2H_2 + 3H_2$	+311	+58	+375	+405
Oxidative Coupling:					
(vi)	$2CH_4 + \frac{1}{2}O_2 \rightleftharpoons C_2H_6 + H_2O$	-160	-107	-177	-174
(vii)	$2CH_4 + O_2 \rightleftharpoons C_2H_4 + 2H_2O$	-287	-313	-282	-278
(viii)	$2CH_4 + \frac{3}{2}O_2 \rightleftharpoons C_2H_2 + 3H_2O$	-375	-475	-349	-344
Partial Oxidation to Oxygenates:					
(ix)	$CH_4 + \frac{1}{2}O_2 \rightleftharpoons CH_4O$	-111	-58	-126	-127
(x)	$CH_4 + O_2 \rightleftharpoons CH_2O + H_2O$	-290	-307	-285	-287
Full Oxidation:					
(xi)	$CH_4 + \frac{3}{2}O_2 \rightleftharpoons CO + 2H_2O$	-546	-628	-519	-521
(xii)	$CH_4 + 2O_2 \rightleftharpoons CO_2 + 2H_2O$	-801	-910	-802	-803

[a] $\Delta G = 0$ at 620°C

[8] The values in table 1.3 were calculated using the software provided with *Chemical and Engineering Thermodynamics* [20].

The industrial importance of ethene as a feedstock is illustrated in figure 1.1 (reproduced from *Heterogeneous Catalysis: Principles and Applications* [1]).

Simple dehydrogenation to (predominantly) acetylene is possible by the electric arc process and by thermal-cracking. The fractional conversion of methane to C_2 hydrocarbons is relatively low, 10-20% by volume in the exit gas. Carbon and hydrogen are generated as byproducts. In the electric arc process hydrogen is a valuable byproduct, but in the thermal-cracking process the off gases are used for heat generation. The economic viability of both processes is dependent on good heat recovery, with the electric arc process strongly dependent on cheap electricity.

High-temperature gas-phase partial oxidation to acetylene is a flame process (1500-1550°C) achieving 95% methane conversion, but only about 30% acetylene selectivity. The remainder is converted to CO, CO_2 and H_2.

Due to the stability of the C-H bond (415,8 kJ/mol [21]) extremely high temperatures are needed to activate methane. The bond energy of an O-O bond is only 138 kJ/mol [21], and oxygen radicals are produced at lower temperatures than those needed for C-H bond breaking. The oxygen radicals remove hydrogen from the methane to produce water. The resulting radicals can then couple, or react to form CO and CO_2. The reaction is surface catalysed by O^- sites according to reaction 1.3:

$$2CH_4 + 4[O^-] \rightarrow 2[CH_3{-}O^-] + 2[H - O^-] \rightarrow C_2H_6 + H_2 + 4[O^-] \qquad (1.3)$$

The final step is not likely to be a surface reaction, but rather the result of gas-phase dimerisation of the two desorbed methyl radicals. Ethane may undergo dehydrogenation oxidatively on the surface via ethyl radicals. Non-selective oxidation is thought to occur via methyl peroxy radicals formed from methyl radicals reacting with O_2 or through the gas-phase combustion of the hydrocarbon products, especially ethylene [22]. In the presence of oxygen, gas-phase ethane is converted to ethene and water [23].

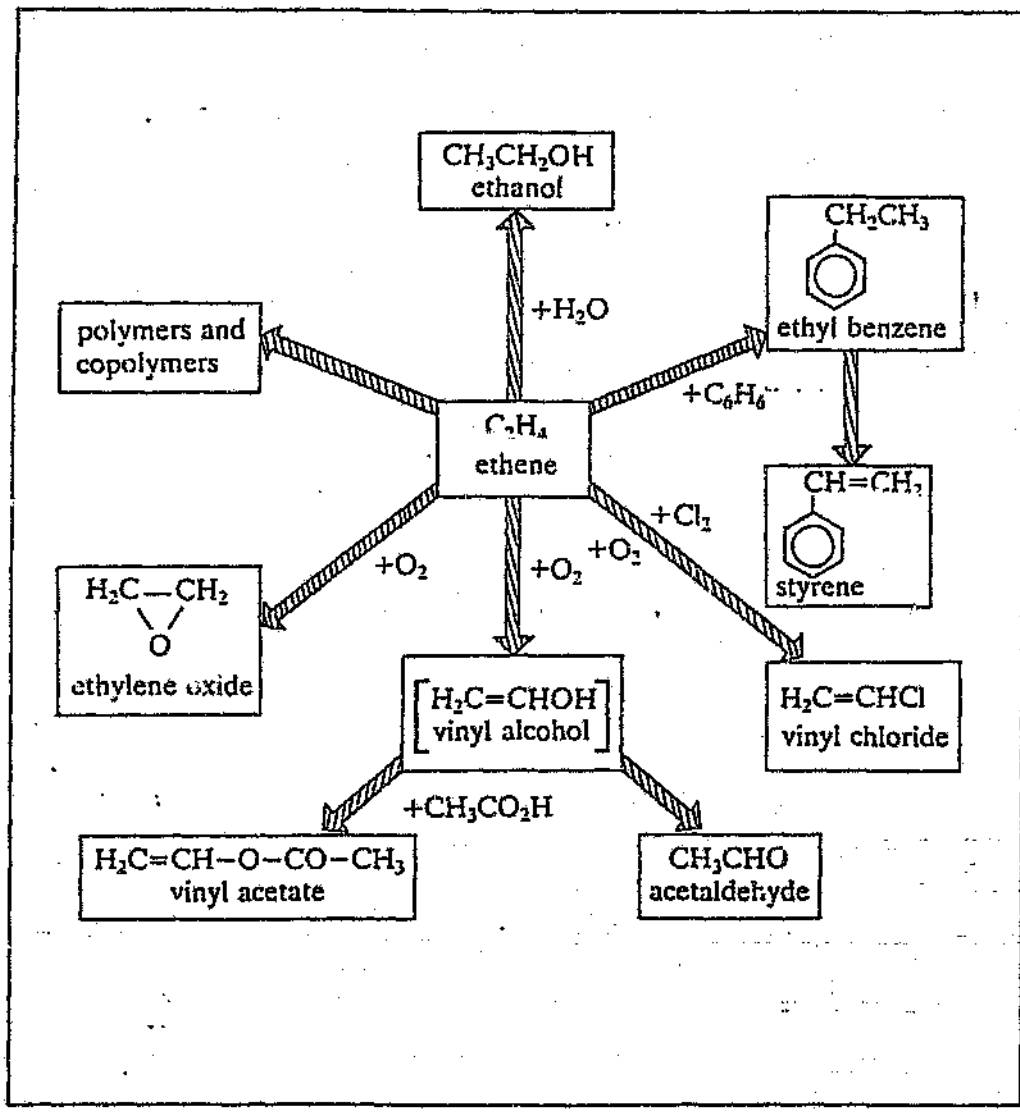

Figure 1.1: Some industrially important reactions of ethene

Using available technology, the cost of producing one gallon of gasoline at a 10600 bpd plant via an oxidative coupling route is US$ 2,09 compared to US$ 1,94 for a similar syngas-methanol process. The two routes are similar in that most fixed investment is in the methane conversion portion of the processes. The syngas-methanol route does have a cost advantage due to higher selectivity to final products (nearly 100% to methanol versus 77% to C_2's for methane coupling). The comparison, however, is encouraging since the oxidative coupling route is still in its early stages of development, while the syngas-methanol process has many years of development and commercial practice behind it [22].

1.3.2 Partial oxidation to oxygenates

The versatility of methanol and its industrial importance has already been discussed in section 1.2.3. The properties which make formaldehyde valuable are its chemical reactivity, its colourless nature, its stability and the purity of its commercial forms [24]. Formaldehyde is used as a basic chemical building unit in a large range of organic compounds, from amino and phenolic resins to slow-release fertilizers. It is also used in the synthesis of chelating agents, textile finishes and acetyl resins. Its significance is highlighted by the fact that, historically, almost half of all the methanol produced globally has been to produce formaldehyde [25]. Formaldehyde is easily reduced by hydrogen back to methanol over many metal and metal oxide catalysts [2].

Methanol is known to cause blindness if ingested, and 25-100 ml of methanol by mouth is reported to be fatal [25]. In spite of this methanol is dangerous to aquatic life only in high concentrations, while formaldehyde solutions are harmful to aquatic life in very low concentrations [26]. This makes methanol preferable for bulk transportation.

The direct partial oxidation of methane to formaldehyde or methanol would eliminate the need for synthesis gas as an intermediate for producing oxygenates. The partial oxidation of methane to formaldehyde and methanol occurs over the same acid based catalysts, but under different reaction conditions, with formaldehyde being the favoured product at higher temperatures and lower pressures.

Synthesis of methanol or formaldehyde implicitly requires the formation of a carbon-oxygen bond. As a result reactions *ix* to *xii* in table 1.3 form a sequence from the activation of methane via methanol and formaldehyde to full combustion products. The intermediate oxygenates are less stable and carbon oxide formation is favoured [4]. However, there is a redeeming advantage to these reactions, since good selectivities are achievable, albeit at low conversions, the liquid products are easily separated and the unreacted feed gases can be recycled [27].

Research by Foulds and Walker [28], suggests that the significance of gas-phase reactions has been largely underestimated. Results were obtained without a catalyst which were comparable to those obtained with catalysts present. This raises questions concerning the role of the catalyst. It has been suggested that future research be aimed at low-temperature catalytic radical initiation. A review of the mechanistic features of these reactions is presented Pitchai and Klier [29].

Using a novel process, workers at Catalytica [30] have claimed to achieve yields of 43% at the relatively low temperature of 180°C. The reaction takes place in two stages, the first a sulphuric acid bath in which the methane is converted to methyl bisulphate in the presence of a mercury catalyst. SO_2 is evolved from the second stage as the methyl bisulphate intermediate is dissolved in water. The SO_2 is recovered and used for sulphuric acid production.

1.3.3 Oxychloro routes

Methane can be selectively chlorinated by means of catalysts to methyl chloride (equation 1.4):

$$CH_4 + Cl_2 \rightarrow CH_3Cl + HCl \tag{1.4}$$

Methyl chloride in turn can be converted into higher hydrocarbons over ZSM-5, via reaction 1.5:

$$nCH_3Cl \rightarrow -(CH_2)_n- + nHCl \tag{1.5}$$

Where $-(CH_2)_n-$ represents aromatics, olefins and paraffins. The HCl could then be converted back to Cl_2 and recycled [7].

A process for the production of aromatic rich gasoline boiling range hydrocarbons from methane is therefore possible [31].

The oxidative coupling of methane to C_2 products using chlorine as an oxidant is also possible. In a flame reaction with $CH_4/Cl_2 \approx 1$ at 1700°C, the reaction produces mostly ethylene with chlorine emerging as HCl. Again this could be recycled as chlorine after conversion by the Deacon process [7].

These processes, however, suffer from the presence of high concentrations of corrosive HCl and the problem of converting HCl to Cl_2 for recycle [23].

1.4 Partial oxidation to synthesis gas

In general the oxidative conversion of methane to value-added products takes the form:

$$CH_4 \xrightarrow{k_1} \text{Product} \xrightarrow{k_2} CO_x + H_2O \quad (x = 1,2) \tag{1.6}$$

The desired intermediate products can only be obtained at high methane conversions if $k_2 < k_1$. Intermediate products are thermodynamically less stable than combustion products, and are also more easily activated than methane. Catalysts which activate methane usually activate the intermediate products, especially at high methane conversions. Thus as the methane conversion increases so the selectivity decreases, and thus there is an upper limit to the attainable yield of the desirable product.

This phenomena is evident in oxidative coupling (section 1.3.1) and the partial oxidation to oxygenates (section 1.3.2), but not in the partial oxidation of methane to synthesis gas [27].

For the production of synthesis gas the partial oxidation reaction is thermodynamically more favourable than the widely utilised steam-reforming route (table 1.3). The steam-reforming reaction is highly endothermic and is only favourable at high temperatures, which results in certain process disadvantages (section 1.2.1). The partial oxidation reaction is mildly exothermic and favourable even at low temperatures.

1.4.1 Reaction mechanism

Prettre, Eichner and Perrin [32] noted that the gas products from the partial oxidation of methane were not well represented by equation 1.7:

$$CH_4 + \frac{1}{2}O_2 \rightleftharpoons CO + 2H_2 \tag{1.7}$$

They also observed that the temperature at the front of their catalyst bed was very high and decreased rapidly before stabilising. Other workers have subsequently observed the same phenomena [33, 34]. This the authors proposed was consistent with an exothermic reaction followed by an endothermic one. The temperature observed at the front of the catalyst bed was too high to be caused by the partial oxidation reaction (equation 1.7). This prompted Prettre and his co-workers to propose a combustion and reforming mechanism.

It was reasoned that the high temperatures were caused by the combustion of methane in the relatively oxygen-rich feed as it first came into contact with the catalyst (equations 1.8 to 1.10).

$$CH_4 + 2O_2 \rightleftharpoons CO_2 + 2H_2O \tag{1.8}$$

$$CH_4 + \frac{3}{2}O_2 \rightleftharpoons CO + 2H_2O \tag{1.9}$$

$$CH_4 + O_2 \rightleftharpoons CO_2 + 2H_2 \tag{1.10}$$

This would result in the complete combustion of the oxygen, but not all the methane. The energy derived from these exothermic reactions would then drive the reforming reactions (equations 1.11 and 1.12) and the water gas shift reaction (equation 1.13):

$$CH_4 + H_2O \rightleftharpoons CO + 3H_2 \tag{1.11}$$

$$CH_4 + CO_2 \rightleftharpoons 2CO + 2H_2 \tag{1.12}$$

$$CO + H_2O \rightleftharpoons CO_2 + 2H_2 \tag{1.13}$$

A model was devised based on this mechanism, which predicted the gas product from the partial oxidation of methane, this time with greater accuracy.

Prettre *et al* [32] also observed that decreasing the length of the catalyst bed resulted in a greater yield of combustion products rather than reforming products. Further, uncombusted CH_4 was also more prevalent in the product stream. Similarly, other workers noted that at larger space velocities [35, 33] or higher oxygen/methane ratios [35, 36] that CO_2 and h_2O selectivities increased at the expense of CO and H_2.

Using this mechanism the conversion of methane is thermodynamically predicted to be 42%, with 21% selectivity to CO and a H_2/CO ratio of 4,7. This result is based on a methane to oxygen ratio of 2 : 1, at one atmosphere and 500°C. At 750°C these values change to 91% methane conversion, 96% selectivity to CO, and a H_2/CO ratio of 2,0.

Schmidt and his co-workers were unable to explain some of their results by means of the combustion and reforming mechanism, but found that their results were more consistent with a direct partial oxidation mechanism (equation 1.7) [37, 38]. These researchers developed a model using a 19-step surface mechanism, which allowed them to predict the behaviour of the partial oxidation reaction with reasonable accuracy under different conditions.

Schmidt's group studied pure metal surfaces, not supported metal catalysts. It is possible that the reaction mechanism in the presence of pure metals is different from that in the presence of supported metals.

Lapszewicz *et al* [13] carried out methane-deuterium exchange experiments over Rh, Ru, Pt and Pd supported on MgO. By passing a mixture of D_2 and CH_4 over these catalysts they found that the most active catalysts (Rh, Ru and Pt) favoured the formation of CD_4. The Rh catalyst showed very low conversions of methane and produced only CH_3D. This correlation between the most active catalysts and the complete dissociation of methane indicated that surface carbon is the precursor of CO_x products. They have also suggested that C-H bond scission is the rate limiting step.

1.4.2 Coke formation

Carbon deposition processes which are thermodynamically favourable below 1200°C are the Boudouard reaction, equation 1.14, and the catalytic decomposition of methane, equation 1.15.

$$2CO \rightleftharpoons C + CO_2 \tag{1.14}$$

$$CH_4 \rightleftharpoons C + 2H_2 \tag{1.15}$$

Claridge *et al* [39] passed pure CH_4 and pure CO over supported nickel catalysts at various temperatures and monitored the formation of amorphous surface carbon. They have shown that the Boudouard reaction dominates at lower temperatures, while the methane decomposition reaction dominates above about 650°C. This was supported by their observation that at high temperatures the carbon build up occurred at the front of the bed, where the partial pressure of methane was the greatest.

Lapszewicz *et al* [13] observed that when a mixture of D_2 and CH_4 were passed over Pd on MgO only CH_3D was produced. This suggests that the Pd surface is covered with surface methyl groups not surface carbon species (section 1.4.1). It was also noted that at temperatures above 650°C the formation of coke caused Pd supported on MgO to deactivate. Thus the authors have proposed that amorphous carbon is formed from the products of partial dissociation of methane such as adsorbed methyl groups.

1.4.3 Temperature measurement

Choudhary and co-workers [40] reported that high conversion and selectivity to CO were possible over a variety of catalysts at low temperatures, even as low as 350°C.

In these experiments, the researchers used thermocouples, a conventional method, for temperature measurement.

Heinemann and Chang [36] repeated these results, also using thermocouples, but observed that the catalyst glowed, even at 'low' temperatures. Using an infra-red radiation thermometer Heinemann and Chang measured the catalyst bed temperature to be 1270°C, while the thermocouples at the front and rear of the bed measured 450°C. Even without heating the reaction was sustained, and with additional cooling the reaction was eventually extinguished at 340°C (1150°C using the infrared radiation thermometer).

This discrepancy can be explained by the combustion and reforming mechanism. The initial combustion reactions are highly exothermic (equations 1.8 to 1.10). The energy from these reactions sustain the combustion reactions at low feed-gas temperatures and provide the energy for the endothermic reforming reactions (equations 1.11 to 1.13)[9]. Since energy generated by the combustion stage is utilised in the reforming stage, very little energy is retained by the gas. Thus neither the feed-gas nor the exit-gas temperatures are representative of the temperature on the surface of the catalyst.

Sophisticated temperature measurement is essential for the kinetic studies. Without it measurement of the ignition and autothermal reactor temperatures in the different reaction zones would be impossible. In reaction studies conducted to determine the activity and selectivity of a particular catalyst, conventional techniques are acceptable, bearing in mind their limitations. Most workers have utilised conventional techniques, and thus most of the results reported are with reference to the feed-gas temperature rather than the catalyst temperature. An understanding of the limitations of the method of temperature measurement used by different workers is necessary before comparisons of their work can be made.

[9]The thermodynamic data for these reactions is found in table 1.3.

1.4.4 Catalysts

Since the first work done by Prettre and co-workers [32], supported nickel catalysts have been studied in detail. Based on their observations Prettre *et al* proposed the combustion and reforming mechanism (section 1.4.1), which predicted values in close agreement with their observed exit gas compositions.

Lunsford and his co-workers [33] used XPS and XRD methods to study a 25 wt% Ni/Al_2O_3 catalyst after exposure to the methane partial oxidation reaction. It was found that the composition of the catalyst bed varied with temperature. The workers also found that sufficiently large decreases in contact time caused deviations from equilibrium. At reaction temperatures above 450°C, complete combustion of O_2 takes place in spite of decreased contact times. Thus the deviations from equilibrium were explained as being due to incomplete reaction of CH_4 with CO_2 and H_2O.

They also observed that no carbon formed below 700°C, where only CO_2 and H_2O were produced. Above 750°C a monolayer of carbon was formed. The formation of carbon was related to the methane-to-oxygen ratio. At ratios of $CH_4/O_2 \geq 2$, the reaction produced large amounts of carbon, while for $CH_4/O_2 \geq 1{,}25$ but less than 2, there were no significant deposits of carbon. The products at these low ratios were principally CO_2 and H_2O.

Choudary *et al* have described a series of catalysts of the form NiO/MO_x (M = lanthanides, Al, and Mg, with Ni : M $\geq$ 1 : 1). Carbon deposition was substantial in the presence of the lanthanide catalysts, but had little or no effect on the catalytic activity or selectivity [41]. Using the Ni/MgO catalyst the effect on the reaction of temperature, reduction, Gas Hourly Space Velocity (GHSV) and the ratio of Ni to Mg [42] was studied. With a feed of 67 mol% CH_4 and 33 mol% O_2 and a GHSV of 4.95×10^{-5} h^{-1} at 1 atm, and a 18,7 wt% Ni/Al_2O_3 catalyst, 87,2% conversion and 98,0% selectivity to CO was claimed [43].

Hayakawa *et al* [44] prepared $Ca_{1-x}Sr_xTiO_3$ based mixed oxide catalysts containing chromium, iron, cobalt or nickel. Both the nickel and the cobalt catalysts showed high activity and selectivity to synthesis gas. XRD studies of the nickel and the cobalt catalysts showed that cobalt and nickel metal particles were separated from the perovskite structure, $Ca_{1-x}Sr_xTiO_3$. Prior to pre-treatment the $Ca_{0,8}Sr_{0,2}Ti_{0,8}Co_{0,2}O_{3-\delta}$ catalyst gave 30,6% methane conversion and 16,9% selectivity to coupling products. After treatment in CH_4 at 775°C for an hour, 70,9% conversion of methane and 96,8% selectivity to CO was achieved. The pre-reduction $Ca_{0,8}Sr_{0,2}Ti_{0,8}Co_{0,2}O_{3-\delta}$ yielded a material which had an XRD pattern very similar to that of $CaTiO_3$, while after reduction the pattern showed evidence of metallic Co (JCPDS: 15-806, see section 2.3.4). These metallic sites were thought to be the active catalytic species.

Green *et al* examined transition metal catalysts for the partial oxidation of methane. A series of rare earth pyrochlores, $Ln_2Ru_2O_7$, converted methane to synthesis gas with yields and selectivities closely approaching those expected from thermodynamic calculations. These catalysts showed that reduction had occurred resulting in ruthenium metal particles [45]. They also showed that Ni, Ru, Rh, Pd, Pt and Ir, either supported on Al_2O_3 or present in mixed oxide precursors also catalysed partial oxidation of methane. The Ni and Pd catalysts produced heavy carbon deposits. The Ir and Rh catalysts showed no carbon deposition or deactivation [35].

Schmidt and his co-workers [38, 37, 46, 47] have studied the partial oxidation of methane to synthesis gas over various metal-coated monoliths. The experiments were conducted autothermally with residence times of as low as 10 ms, and gas flow rates of about 4 standard litres per minute at around 1,4 atm. Table 1.4 shows a summary of their results.

They have also shown that CO and H_2 can be produced from methane in a fluidised bed reactor [48]. Conversions of greater than 90% and selectivites of higher than 95% were achieved.

Table 1.4: Comparison of metals for the partial oxidation reaction

Metal and Loading (wt%)	$T_{Reaction}$ (°C)	$\frac{\Delta CH_4}{CH_{4,in}}$	S_{H_2}	S_{CO}	Stability	Changes	Coke Formation
4% Rh	~930	0,80	0,90	0,96	stable		No
3% Ni	~730-830	0,80	0,91	0,93	deactivates slowly	volatilisation, formation of oxide & aluminate	No
2,5% Ir	~920	0,73	0,85	0,94	stable		No
4,7% Pt	~1130	0,87	0,78	0,94	stable		Some
3% Co	~1000	0,20	0,14	0,66	deactivates	formation of aluminate	No
3,5% Pd-La_2O_3	~1200	0,56	0,57	0,63	deactivates	pore blockage	Heavy
0,5/4% Re	deactivates quickly due to volatilisation of the metal						No
5,5% Ru	extinguished in CH_4					phase change	No
6,5% Fe	extinguished in CH_4					phase change	Some

Reproduced in part from [47].

A detailed comparison of supported ruthenium and nickel catalysts was conducted by Poirier and his co-workers [49]. They found that as little as 0,015% Ru on Al_2O_3 gave a higher activity and selectivity than 5% Ni on SiO_2.

Kunimori *et al* [50] found that $RhVO_4/SiO_2$ reached a maximum conversion of 90%, while the unpromoted Rh/SiO_2 reached almost 100% conversion, with very high selectivity to synthesis gas for both catalysts.

Jones and co-workers [51] have shown that the pyrochlore structure of $Eu_2Ir_2O_7$ was destroyed during the initiation of the catalyst, giving an active catalyst that comprised particles of iridium metal of about 30 Å in diameter supported on europium oxide. A sudden increase in synthesis gas production corresponded to the onset of the reduction.

ZSM-5 catalysts containing various metals have also been tested for the oxidation of methane [52]. While methanol was the product of interest, and conversions were low, moderate selectivity to synthesis gas was obtained.

The direct conversion of methane to synthesis gas over cerium oxide was demonstrated by Otsuka and his co-workers [53]. The reaction takes place in the absence of gaseous oxygen. Once the metal has been fully reduced it can be regenerated by converting CO_2 to CO over it.

1.5 Aims of this work

The potential of natural gas as a feedstock for the production of chemicals traditionally produced from petroleum crude, has been highlighted in the previous sections. Most currently available technology uses synthesis gas as an intermediate. The cost of producing synthesis gas is widely recognised as the stumbling block to low investment methane conversion processes. There are two options: either to find processes that can produce synthesis gas cheaply, or to find direct conversion technologies that bypass this intermediate. The technology available for the direct conversion of methane to value-added products such as methanol is still far from viable, but in the medium to long term these processes will mature.

In the short term, processes that could produce synthesis gas at lower capital and operating costs could replace current conversion techniques without affecting downstream processes. Thermodynamically, the partial oxidation of methane to synthesis gas has the potential to be operated autothermally. This has been successfully demonstrated on a laboratory scale by Schmidt and his co-workers [47]. Thus, compared to the endothermic steam-reforming reaction, energy consumption could be dramatically reduced.

Their experiments were conducted at low contact times. The lower the contact time, the smaller the reaction vessel needs to be, and the less the catalyst required. Both result in cost savings.

A fluidised bed reactor has been successfully used for the same reaction [48]. The use of simple reactor technology reduces the capital cost of the process. However, the remaining obstacle to the process is the availability of a suitable catalyst. Most of those catalysts which have shown potential use noble metals. From Schmidt's results (table 1.4) the pick of the noble metals are rhodium and iridium. They are both highly active and selective, and do not deactivate or coke. Not considering the cost of these materials, it is unlikely that there will ever be sufficient production of these

metals for them to be widely implemented. In addition to this, the wide scale use of a metal such as rhodium would cause shortages, resulting in price increases that would negate any benefit derived from other cost savings.

As far as the ferrous metals are concerned, nickel, although active [43, 33], deactivates slowly [47] and is known to result in the formation of coke [33]. Cobalt, is both active [44] and has not been observed to form coke. However, Schmidt and his co-workers [47] reported cobalt deactivation due to phase change and volatilisation.

The aims of this project were twofold: firstly to find a catalyst which could be used to produce synthesis gas actively and selectively. Not only this, but the catalyst should be able to operate at low contact times, and not coke or deactivate. Above all the catalyst must be affordable, robust and easy to produce in bulk.

The second objective was to understand the behaviour of the catalysts to be investigated and relate the behaviour to other published results.

The successful use of cobalt-ruthenium bimetallic catalysts for the Fischer- Tropsch reaction [54] was the first source of inspiration. Although the reaction conditions differ substantially, the F-T reaction is essentially the reverse reaction of the partial oxidation reaction. By adding small amounts of ruthenium to cobalt catalysts, dramatic improvements in catalyst activity and selectivity were achieved for the F-T reaction. It was hoped that the ruthenium and cobalt interaction would result in a stable, active metallic species for the partial oxidation reaction.

Alumina was chosen as the support because of its known use as a support for the activation of methane [55].

Chapter 2

Experimental methods and apparatus

2.1 Reaction studies

To achieve the objectives laid out at the conclusion of the previous chapter, *i.e.* the identification and characterisation of catalysts active and selective in converting natural gas to synthesis gas, required the use of a variety of experimental setups. Most of the equipment needed for the characterisation studies had been constructed by previous researchers in the group. It was however necessary to assemble an installation capable of analysing the product gases of the reaction between methane and oxygen in the presence of a catalyst.

The equipment and techniques used in conducting these studies on the behaviour of various catalysts, are explained in this section.

2.1.1 Installation

A schematic representation of the installation used is shown in figure 2.1.

A mixture of methane and air was fed, via a system of valves housed in the Thermal Conductivity Detector (TCD) oven, A (figure 2.1), to the reactor, R. By switching valve V_R, the reaction mixture could bypass the reactor for analysis. The flow rates of the two gases in the mixture were controlled with mass flow controllers. On/off valves allowed each gas line to be preferentially selected..

The 3-way valve, V_3, on the methane line allowed a third gas to be used, at the same flow rate as the methane. This facility was used for *in situ* reduction of the catalysts in hydrogen.

The product gases after being routed via two pneumatically operated sampling valves, S_1 and S_2, were vented to the atmosphere. The sampling valves were connected to the same actuator to allow simultaneous sampling.

A 30 ml/min stream of hydrogen, controlled with a mass flow controller, was used as the carrier gas for the Flame Ionisation Detector (FID). During sample collection, the product gas stream was routed through the sample loop, and the carrier was bypassed. By switching the valve; the carrier was re-routed through the sample loop, and the product gases in the sample loop at the time of switching were "captured" in the carrier stream. The product gases were then separated in a 3,0 m Porapak QS column at 60°C, B. After this, the products passed through a 0,8 m column packed with a NiO_2/Al_2O_3 catalyst, heated to 350°C, C. The FID, fuelled by the hydrogen carrier, operated at 250°C. An injection port, operated at 150°C, was available for calibration or off-line analysis.

The inert feed was split and both streams were routed via pressure controllers. The reference stream flow rate, 30 ml/min, was controlled with a needle valve. The sample stream passed through the sampling valve and the Carbosieve SII column

prior to detection in the TCD. Both the sampling valves, Carbosieve SII column and the TCD were operated at an oven temperature of 35°C.

The amplified signals from the two detectors were collected and integrated on a Varian 4290 integrator. The integrator also controlled the actuator used to control the sampling valves.

Two variations of this installation configuration were used during the course of this project. The original reactor, figure 2.2, was of a standard design and enabled temperature measurement of the gases above the catalyst bed. This reactor and the corresponding TCD oven temperature (see section 2.1.4) were used during the experiments on the bimetallic catalysts (section 3.1.2), and the screening experiments (section 3.1.3). The large reactor volume of the original reactor was required to accommodate the thermowell, but this resulted in a large residence time of the feed gas and consequently gas-phase reactions (tables 3.1).

The original reactor (figure 2.2) was replaced by one of lower volume (figure 2.3) which reduced the outer diameter from 18 mm to 6 mm. This reduced gas-phase reactions to the extent that they had little influence on the results (table 3.2). The disadvantage of this modification was that accurate measurement of the feed-gas temperature was sacrificed. At the same time as these changes were introduced, modifications in the TCD analysis were also introduced (section 2.1.4). Apart from these adjustments the installation remained unchanged for the duration of the experimental work.

2.1.2 Temperature measurement and control

The reactor jacket and the oven housing the Porapak QS column were controlled with multi-ramping temperature controllers. All the other temperatures were controlled with isothermal controllers.

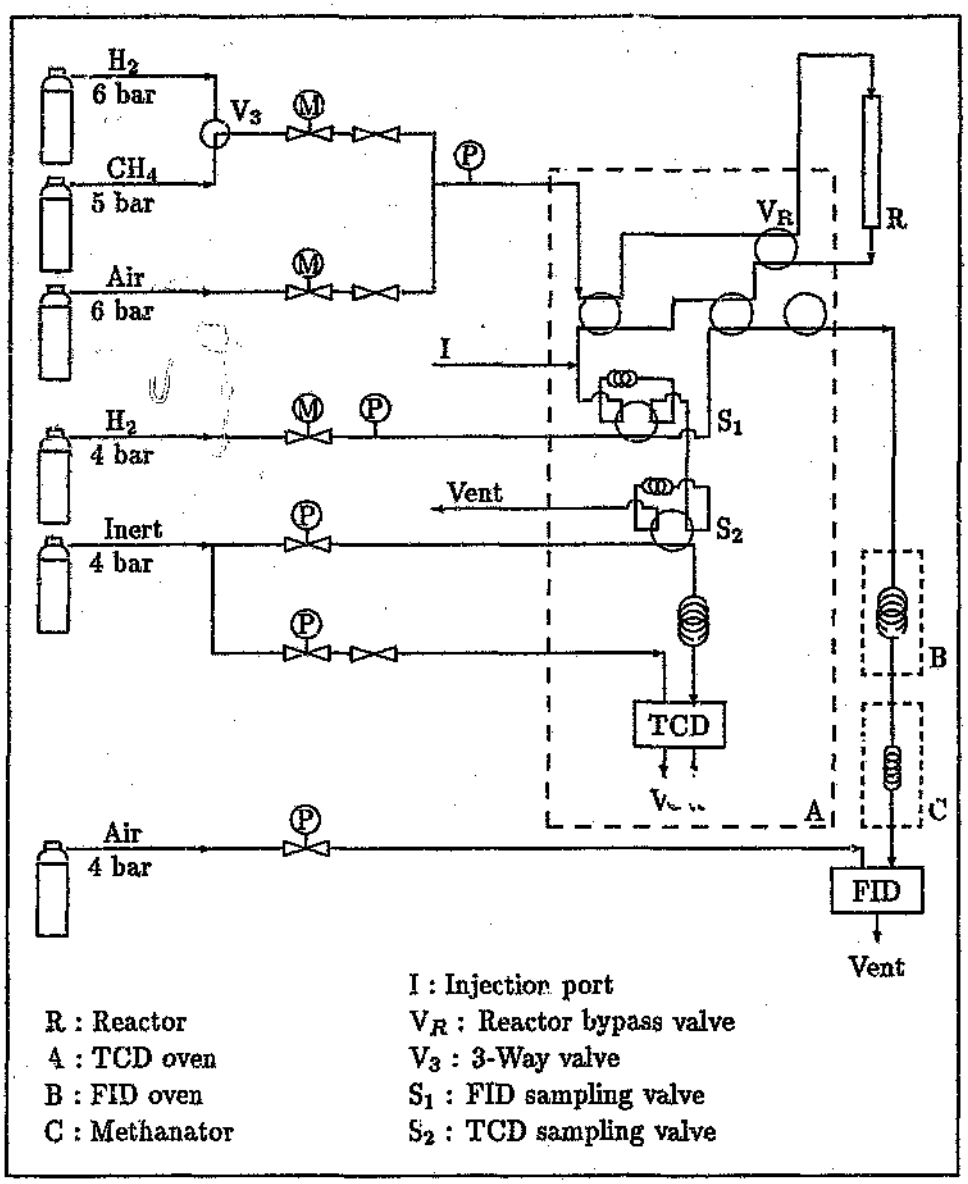

Figure 2.1: The installation used for conducting the reactor studies

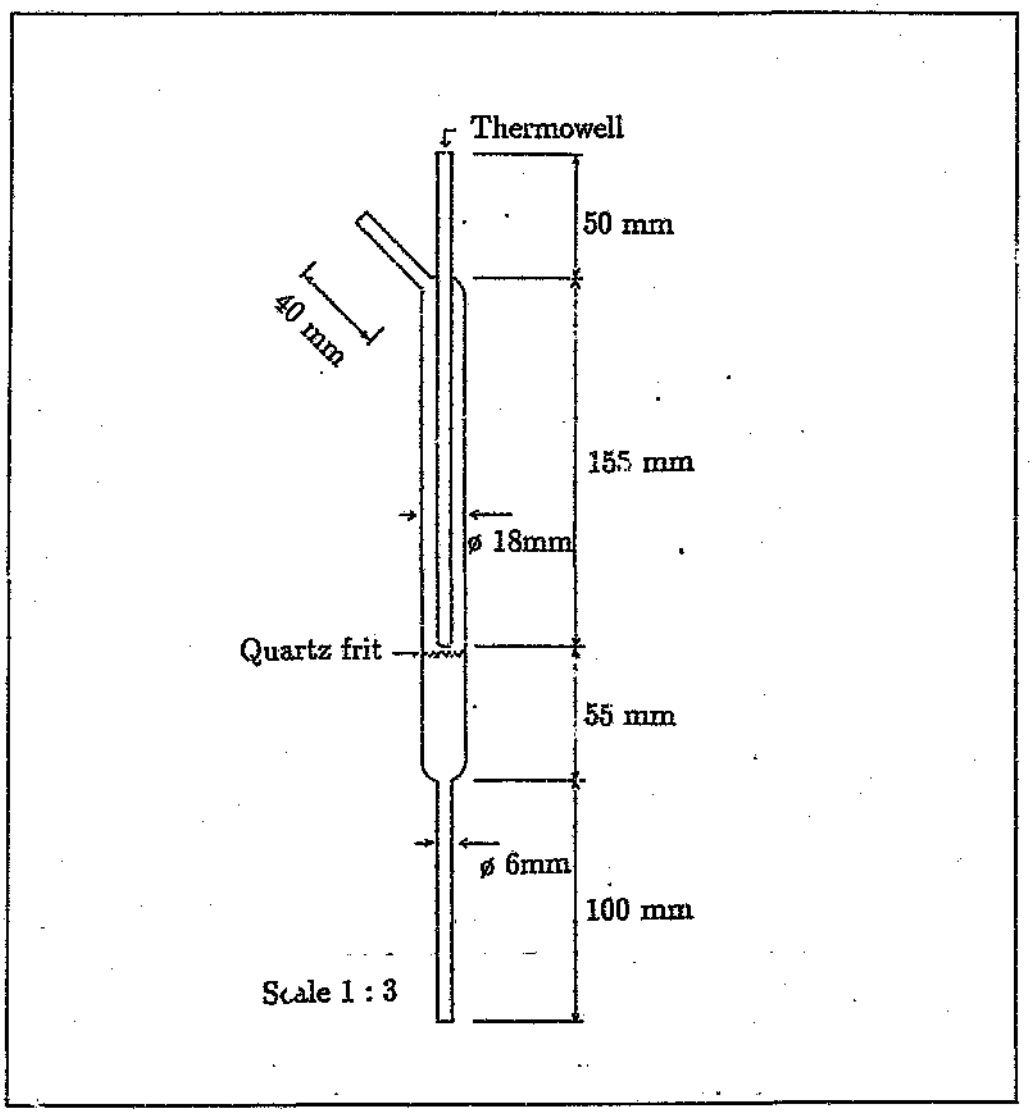

Figure 2.2: The original reactor system

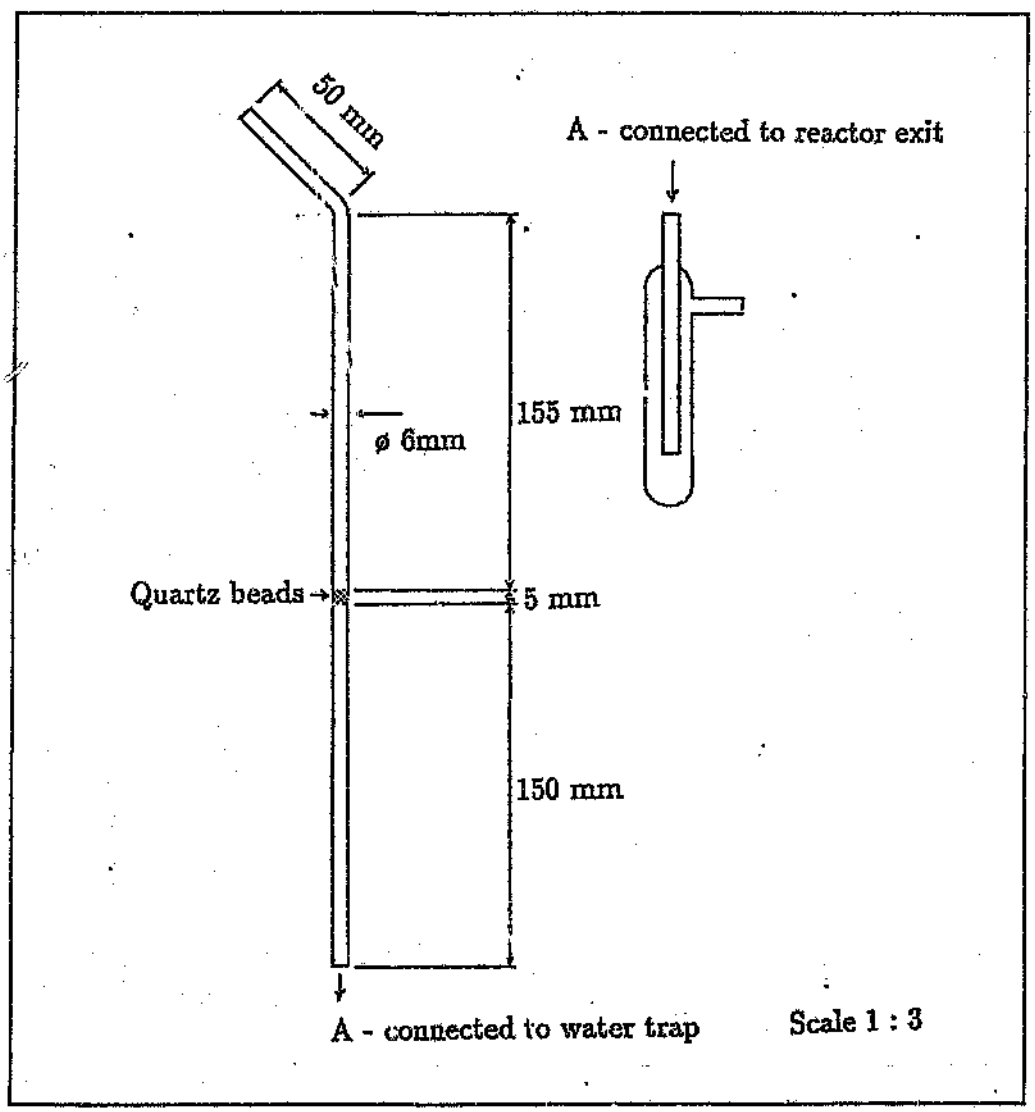

Figure 2.3: The modified reactor system

The reactor jacket temperature was measured by a thermocouple placed inside the jacket, but outside the reactor. This thermocouple was used to control the jacket temperature. A second thermocouple was used to measure the temperatures reported with the results. Using the original reactor (figure 2.2) this thermocouple was positioned inside the thermowell, giving the feed-gas temperature. When the modified reactor was (figure 2.3) installed, this thermocouple was strapped with NiCr wire to the outside of the reactor. This gave the temperature immediately adjacent to the catalyst outside the reactor, as opposed to the temperature adjacent to the heating jacket.

Inside the heating jacket were different temperature zones, the hottest of which was assumed to be at the centre The reactor was positioned such that the catalyst bed coincided with the middle of the heating jacket.

2.1.3 Gas velocities and catalyst mass

The initial criteria for the choice of catalyst mass to be used was governed by the geometry of the original reactor (see figure 2.2). To cover the frit with a layer of catalyst, approximately 100 mg of catalyst was needed.

To minimise gas-phase reactions high gas flow rates are desirable. This meant that the contact time had to be small, and a value of 0.01 s was achieved by setting the mass flow controllers on the air and methane lines to give flow rates (at room temperature and atmospheric pressure) of 428 cm^3/min and 180 cm^3/min respectively. A catalyst density of 1 g/cm^3 was measured for the γ-Al_2O_3 support. The same density was assumed for all the catalysts in order to be able to calculate flow rates from the contact time and catalyst mass.

Assuming that oxygen makes up 21% of air, the ratio of methane/oxygen was two. Over a period of a fortnight a variation of only $\pm 2\%$ in this ratio was observed. This

is well within the accuracy of the measurement technique used to measure the flow rates. The overall flow rate was observed to be marginally lower than the sum of the two individual flows. This may be due to the mixing properties of the gases, or experimental errors.

2.1.4 Analysis

Two different detectors were used for the analysis of the products. Firstly, a Thermal Conductivity Detector (TCD) was used to detect differences in the thermal conductivity between the product gas and a reference stream of the carrier gas. Secondly, a Flame Ionisation Detector (FID), which in essence measures the heat of combustion of the products in air, was used. As the product gas passes through one of the detectors the composition and consequently the chemical properties of the gas change. These changes, due to upstream separation, are translated into electronic signals which are then amplified and recorded by the Varian 4290 integrator.

The shape of the peak recorded indicates a great deal about the product gas. For example, a large sample of a light gas, which easily passes through the gas chromatograph will have low retention time, with a sharp, narrow peak. A sample of a gas of a large or reactive molecule would be retarded by the column packing and thus have a higher retention time and produce a broad, blunt peak. Since each product has different chemical properties, to produce the same area on the integrator requires different amounts of each product. Therefore, in order to compare the amounts of gases produced, it is necessary to find the relative intensity of the signals produced by each product.

One of the features of the installation was the 0,8 m column packed with NiO_2/-Al_2O_3 catalyst. Passage of the product stream over this catalyst with an excess of hydrogen (the carrier gas) resulted in all the carbon containing compounds (*e.g.* CO and CO_2) being converted to methane. Since hydrogen was the carrier and water is

not combustible in air at the detector temperature, the only compound ever detected by the FID was methane. Thus, each carbon compound is detected with the same sensitivity, and the integrated areas reported therefore give a carbon balance.

To test the efficiency of the methanator equal volumes of CO_2 and CH_4 were injected into the FID analysis system. The methanator temperature and the length of the column were adjusted to ensure complete conversion of the CO_2. Since CO_2 is the most stable of the expected products it was assumed that all the other products would be converted to methane.

The only disadvantage of the system is that by using hydrogen as the carrier gas, the hydrogen produced in the reaction is not detected. Hence, in order to determine the hydrogen produced, a TCD was needed.

During the early stages of the project, while the original reactor was being utilised, there appeared to be no need to use the TCD to detect any compounds other than hydrogen. Thus, due to its low cost, nitrogen was used as the inert carrier. Separation of hydrogen from the other components was achievable at 150°C, at which temperature water also remained a gas. However, the advantages of being able to detect the nitrogen content of the air soon became apparent, and the nitrogen carrier was replaced by argon. These changes were introduced at the same time as changes to the reactor system were introduced (section 2.1.1).

The ability to detect nitrogen makes it possible to compensate for the changes in stoicheiometry due to reaction. To illustrate the point: in the feed stream there is a particular amount of CH_4 available for conversion to other carbon containing compounds. The amount of O_2 in the feed is half that of CH_4. The ratio of N_2 to O_2 will thus correspond to the composition of air. Hence the gas ratios are: $\frac{1}{7}$ O_2, $\frac{2}{7}$ CH_4 and $\frac{4}{7}$ N_2.

If all the CH_4 and O_2 were converted to synthesis gas, then the methane and oxygen would form 1 mol CO and 2 mol H_2 for each mol CH_4 and half mol O_2. This means

that, excluding the nitrogen, the product stream would have twice the number of moles found in the feed. If the nitrogen is included the product mixture would contain: $\frac{1}{5}$ CO, $\frac{2}{5}$ H_2 and $\frac{2}{5}$ N_2.

If constant volume samples were taken of the feed and product streams, it would appear that there was less carbon in the product stream than in the feed. This needs to be compensated for, and is easily achieved by using the nitrogen as a measure of the "carbon shrinkage" due to the stoicheiometric expansion.

To achieve the best possible separation of hydrogen and nitrogen, the temperature was reduced to 35°C. Water was condensed out after the reactor, as shown in figure 2.3.

2.1.5 Calibration

In the previous section it was proposed that the FID areas can be used to determine the carbon balance. Since the sample size is arbitrary, and the units of area on the integrator are also arbitrary, one unit area was arbitrarily set to correspond to one mole of CH_4. Since all the carbon-based products are converted to and detected as CH_4, the ratio of areas reported by the integrator is consistent with the ratio of the amounts of each product. Products such as C_2H_4, C_2H_2 and C_3H_6 are considered to be present in appropriate fractions of their areas.

To relate the amount of hydrogen to that of the other products, it is necessary to relate the area of hydrogen on the TCD to the area that the same amount of methane would produce on the FID.

The fraction, x of hydrogen in the TCD sample loop is given by:

$$x = \frac{(\text{area of } H_2 \text{ in a TCD sample})}{(\text{area of pure } H_2 \text{ sample in the TCD})} \tag{2.1}$$

For a sample in the FID containing the same fraction, x of methane:

$$x = \frac{\text{(area of } CH_4 \text{ in a FID sample)}}{\text{(area of pure } CH_4 \text{ sample in the FID)}} \tag{2.2}$$

By equating and rearranging equations 2.1 and 2.2:

$$n_{H_2} = a_{H_2} \frac{\text{(area of pure } CH_4 \text{ in the FID)}}{\text{(area of pure } H_2 \text{ in the TCD)}} \tag{2.3}$$

Where n_{H_2} is the number of moles of hydrogen and a_{H_2} is the area reported by the TCD for a given hydrogen sample.

The area produced by a pure gas sample was obtained by replacing the feed gas with the pure gas, and recording the area of a sample, taken as if it were the product gas.

A problem was encountered during the calibration of methane in the FID. The areas recorded varied by as much as 20%. The experiments were conducted hourly overnight, and the deviations appear to correspond to ambient temperature changes. There is no apparent reason for this behaviour, which is evident in figure 3.1.

To obtain a sensible value for the FID area produced by a pure methane stream a catalyst which appeared to produce no water (10%/C/γ-Al_2O_3) and which was highly selective to CO, was used. Since no condensate was evident, 100% selectivity to hydrogen was assumed. The hydrogen/carbon monoxide ratio was assumed to be two. The area required to give such a result was calculated and used as the calibration value. It needs to be pointed out that the value calculated fell within the measured range of values.

2.1.6 Experimental procedure

Due to the automation possible with the programmable integrator and multi ramping temperature controllers, the experimental procedure was relatively simple and extremely flexible. What is described in this section is a typical series of experiments carried out on a catalyst.

After weighing out 0,1000 g ± 0,0005 g of catalyst, it was poured into the reactor, such that it would either cover the quartz frit (see figure 2.2) or be placed onto the quartz bead support bed (see figure 2.3). The reactor was then secured inside the heating jacket.

Hydrogen gas was directed through the reactor using the three-way valve (V_3, figure 2.1), while the oxygen flow was shut off. The heating jacket temperature controller was programmed to heat and maintain 600°C for 30 minutes, and then decrease the setpoint to 500°C. Once the reactor had reached the setpoint temperature the three-way valve was switched to replace the hydrogen with methane. After a short delay the oxygen was introduced. The time delay depended on the volume of the reactor and consequently on the time taken to flush the hydrogen from the reactor. If the oxygen was introduced too quickly it would ignite the hydrogen, resulting in a sudden increase in temperature, possibly affecting the catalyst.

The reaction system was then allowed to equilibrate at 500°C for about 30 minutes. The sample valves were positioned such that the product stream was routed through the sample loops, *i.e.* "collecting" the sample. Thus, when the sample valves were switched to "sample" the gas in the sample loops represented the steady state product gas of the reactor at 500°C.

During this time the integrator was programmed and the reactor temperature controller reprogrammed. The integrator was programmed to switch the sampling valves from "collecting" to "sampling" at time zero. At the same time the signals from both

the FID and the TCD were recorded. The FID signal was plotted. Negative peak integration and forced tailing were implemented (see section 2.1.7 for an explanation of forced tailing).

Ten minutes after the start of the program, sufficient time to completely flush the sampling valves, the sampling valves were switched back to the "collecting" position. After 28 minutes, sufficient time for all the products to pass through both columns, the integrator stopped collecting data and reported the integrated peak areas and retention times. This sequence of events was programmed to be repeated every 30 minutes.

The reactor temperature controller was reprogrammed so that once reset it would change the setpoint to 800°C for 30 minutes. After 30 minutes the setpoint would again be reset to 1000°C, but for two hours.

After the system had equilibrated at 500°C for half an hour the integrator was activated and the programmed integration sequence repeated itself every 30 minutes. Immediately after the integrator program was implemented the new sequence of reaction temperature setpoints on the temperature controller was started.

The result of these two programs operating in this manner was that while the sample of 500°C product gas was being analysed and its composition recorded, the reactor was heated up to 800°C, and the steady state sample collected. After half an hour at 800°C the products were sampled and analysed while the reactor temperature was increased to 1000°C. The next four samples were all taken at 1000°C. When the last 1000°C sample had been collected and was being analysed, the reactor temperature was reset to zero and the feed gas was manually switched with valve V_R, figure 2.1, to bypass the reactor. Thus after the last 1000°C sample the feed gas was sampled.

The reactor was removed once it had cooled and was cleaned. Deposits were removed either by the glassblowers, or by treatment with strong acids or bases, depending on the nature of the deposit. If there were no deposits the reactor was rinsed with acetone and dried with air.

2.1.7 Data manipulation

Once all the data for a particular set of experiments had been collected, they were translated into usable results. The values reported in the chapters which follow were calculated using the equations listed below, based on the assumptions made in previous discussions.

The factor α: this was used to compensate for the stoicheiometry (section 2.1.4):

$$\alpha = \frac{n^{\circ}_{N_2}}{n_{N_2}} \tag{2.4}$$

where $n^{\circ}_{N_2}$ and n_{N_2} refer to the amount of nitrogen in the feed and product streams respectively.

The conversion of methane, χ, is given by:

$$\chi = \frac{\sum_i n_i}{n_{CH_4} + \sum_i n_i} \tag{2.5}$$

where i = CO, CO_2, C_2H_4, C_2H_2 and C_3H_6.

The selectivities S_i, are expressed as a fraction of the methane converted:

$$S_i = \frac{n_i}{\sum_i n_i} \tag{2.6}$$

The carbon balance, B, is given by:

$$B = \frac{(n_{CH_4} + \sum_i n_i).\alpha}{n^o_{CH_4}} \qquad (2.7)$$

The value of B should be unity if the carbon balance holds. However, these values were consistently greater than one. It appeared that the deviation from unity was related to the amount of hydrogen in the system. Although the hydrogen and nitrogen peaks were separated by over a minute at low concentrations of hydrogen, the size of the hydrogen peak was large enough to overlap the substantially smaller nitrogen peak at high concentrations.

By default, the integrator will integrate two overlapping peaks by dividing the areas perpendicularly at the minimum between the two peaks. Forced tailing requires the integrator to integrate the latter peak as if it were "riding" on the tail of the former. This setting is most applicable if the first peak is larger than the second. Forced tailing was implemented. However, if the tail of the hydrogen peak was poorly integrated the area of the nitrogen peak could be affected. With complete conversion of methane to hydrogen, the nitrogen peak had an area approximately ten times smaller than the hydrogen peak. A small addition to the area of the hydrogen peak would have had a large effect on the size of the nitrogen peak area reported. This would result in an exaggerated value of α (equation 2.4) and consequently of B.

Due to the nature of the FID analysis, the assumption was made that all carbon containing compounds were detected. This assumption was judged to be good since the carbon balance, given by B, indicated that as much as twice the carbon going in was exiting the reactor. Had the reverse been true, heavier products would have condensed in the water trap, clogged up the valves, or been detected by the FID. They would have been noticed.

Dividing the sum of the FID areas, by the average of these values for all the experiments conducted under the same conditions, gave the normalised carbon value, B'. This gave at least some idea of the consistency of the experimental conditions.

The normalised carbon count, B' is given by:

$$B' = \frac{n_{CH_4} + \sum_i n_i}{(n_{CH_4} + \sum_i n_i)_{AVERAGE}} \tag{2.8}$$

2.2 Catalyst preparation

2.2.1 Supports

Alpha alumina (Strem Chemicals) and gamma alumina (Engelhard 4504 T), heavy magnesia (BDM), precipitated silica (Hopkin and Williams), titania (Degussa P25), and a carbon-coated alumina [56] were used. The latter was used as supplied, while the two alumina supports were crushed into particles of mesh size 300-500 μm. The other supports were supplied as powders and needed to be pelletised before being ground into similar-sized particles.

2.2.2 Monometallic catalysts

The incipient wetness technique was used to prepare all the monometallic catalysts used. The solvent and the cobalt salt used varied from support to support.

For the carbon-coated alumina (C/γ-Al_2O_3), cobalt acetate[1] was used. The acetate was dissolved in sufficient nitric acid to prevent saturation. This solution was added to the dry support, which absorbed the solution. Only just enough solution to

[1] $(CH_3COO)_2Co.4H_2O$, Mw = 249,08 g/mol, Merck

completely wet the support was added. It was necessary to make a number of such applications, drying the support at 150°C between each application. After all the solution had been applied, the catalyst was dried overnight.

The 14%Co/C/γ-Al_2O_3 catalyst was prepared in a similar fashion but using cobaltous nitrate[2] in ethanol. Two forms of this catalyst were prepared, one dried at 150°C overnight and the other calcined at 800°C overnight.

The catalysts using MgO, SiO_2 and TiO_2 supports were prepared in a similar way except that water was used as the solvent for the acetate. All these catalysts were calcined overnight at 800°C in an oven with no special atmosphere.

The alumina-supported catalysts were prepared from cobaltous nitrate using water. Due to the porosity of these catalysts and the high solubility of the nitrate in water, even a 10% metal loading could be applied with a single wetting of the solution. The amount of water used was determined by the amount needed to ensure that there was complete soaking but no excess solution, which would result in the metal in the excess solution not being loaded onto the support. These catalysts were calcined overnight at 800°C, with the exception of the catalysts reported in section 3.1.2, which were uncalcined, but dried overnight at 200°C.

The monometallic ruthenium catalyst (section 3.1.2) was prepared in the same way as the uncalcined Co/γ-Al_2O_3. Ruthenium acetate [3] was used as the source of the metal.

---

[2] $Co(NO_3)_2.6H_2O$, Mw = 291,03 g/mol, SAARCHEM

[3] $Ru_3O[OCOCH_3]_6(CH_3OH)_3[OCOCH_3]$, Mw = 828,65 g/mol,prepared according to [57] and [58]

2.2.3 "Aged" catalysts

The "aged" catalysts were calcined at 1125°C for 50 h instead of using the usual drying or calcination stage.

2.2.4 "Diluted" catalysts

Only one catalyst was diluted, 14%Co/C/γ-Al_2O_3. Quartz beads of the same size and with twice the mass of the catalyst were used as a diluent. These were mixed with the catalyst to observe the effect of a heat sink within the catalyst bed.

2.2.5 Bimetallic catalysts

These were prepared in the same way as the monometallic ruthenium catalys (see section 2.2.2), except that the appropriate monometallic catalyst was used. Thus for 0,1% Ru on calcined 1%Co/γ-Al_2O_3, the calcined 1%Co/γ-Al_2O_3 catalyst was used as the "support." The uncalcined version used the uncalcined 1%Co/γ-Al_2O_3 catalyst as the "support."

2.3 Characterisation techniques

2.3.1 Surface area analysis

The method and apparatus [59] used were based on the consecutive adsorption and desorption of nitrogen gas.

A known mass of catalyst was dried *in situ* at 150°C for one hour. Then, with nitrogen flowing over it, the catalyst was cooled to liquid nitrogen temperature to effect the adsorption of the gas onto the catalyst. By rapidly heating the catalyst the nitrogen was desorbed and detected. The surface areas were calculated according to the Brunauer, Emmett, Teller (BET) surface area equation.

2.3.2 Determination of cobalt loading

Atomic absorbtion spectroscopy was conducted, using a Spectravarian 410, to determine the cobalt loading on a number of different catalysts.

The calcined catalysts were found to be insoluble in most strong acids and bases [60]. A method by Barros [61] for the analysis of cobalt containing ores was used to dissolve the $CoAl_2O_4$.

The method involved mixing 0,2 g of the catalyst with 10 ml of boric acid (4 mol %) and 10 ml of concentrated HF. The solution was heated at 60°C for 15 minutes. Then 50 ml of a HNO_3 : 2HCl mixture was added and this solution was heated for a further 30 minutes. After transference to a 100 ml volumetric flask, the solution was made up to the mark to give a 30% by volume HCl solution. The sample solution was then analysed within a day to prevent cobalt adsorption onto the glass flask.

Calcined and uncalcined versions of the same catalyst were compared. The amounts of cobalt detected in both catalysts were almost identical, confirming the applicability of the technique.

2.3.3 Temperature programmed reduction

The equipment used to conduct these experiments was purpose built by a previous researcher [62].

A standard Temperature Programmed Reduction (TPR) consisted of two steps. The first involved drying 100 mg of catalyst at 150°C for one hour under flowing nitrogen. After cooling the catalyst to below 100°C, the second, analysis step was performed. The catalyst was heated to 950°C over a period of 90 minutes, under flowing hydrogen. Changes in the composition or flow rate of the gas flowing over the catalyst would be reflected as changes in intensity by the TCD.

2.3.4 Identification of catalyst structure

Powder X-Ray Diffraction (XRD) techniques were used to identify the dominant chemical species present in a particular catalyst.

Samples were ground into a fine powder (mesh size less than 75 μm). If there was sufficient sample, it was packed into a cell. If not, the sample was coated onto a single SiO_2 crystal using vacuum grease (Dow Corning High Vacuum).

Air-sensitive samples were transported in a sealed reactor, to an air bag, where they were prepared under nitrogen. After preparation they were sealed with a "transparent" coating (Grumbacher Hyplar Gloss Varnish). Blank studies showed that the crystal, grease and varnish have no effect on the diffraction pattern.

The measurements were performed using an X-ray diffractometer (Phillips PW1820) with a graphite monochromator using Cu Kα radiation (40 kV, 20 mA). A gas-phase scintillation detector was used.

Most samples were analysed over four hours between $2\theta = 5°$ to 140°. For samples where the amount of material available was small, the samples were analysed for 16 hours over the same 2θ range.

It needs to be noted that the lower the concentrations of a compound in the sample the less likely it is to be detected by this technique. In other words, these analyses may not detect minor species in the sample.

The observed diffraction patterns were matched, using Phillips PC-APD software, against values in the JCPDS database (table 2.1).

The crystal structures of the unit cells of the 14 Bravais lattices are shown in figure 2.4, which was reproduced from Levine's *Physical Chemistry* [63].

Table 2.1: JCPDS database entries used for XRD pattern matching

Card Number		Compound	Crystal Structure
Set	Pattern		
4	875	Al_2O_3	Not assigned
4	877	Al_2O_3	Not assigned
4	878	Al_2O_3	Not assigned
4	880	Al_2O_3	Cubic
10	173	Al_2O_3	Rhombohedral
10	414	Al_2O_3	Hexagonal
10	425	Al_2O_3	Cubic
11	517	Al_2O_3	Monoclinic
12	539	Al_2O_3	Not assigned
13	373	Al_2O_3	Hexagonal
16	394	Al_2O_3	Tetragonal
21	10	Al_2O_3	Hexagonal
23	1009	Al_2O_3	Monoclinic
26	31	Al_2O_3	Hexagonal
29	63	Al_2O_3	Cubic
35	121	Al_2O_3	Monoclinic
5	727	Co	Hexagonal (close packed)
15	806	Co	Cubic (face centred)
9	402	CoO	Cubic
2	770	Co_2O_3	Hexagonal
9	418	Co_3O_4	Cubic
10	458	$CoAl_2O_4$	Cubic
11	692	$CoCO_3$	Rhombohedral
37	719	CoC_2O_4	Monoclinic
4	829	MgO	Cubic
30	794	MgO	Cubic
19	771	MgO_2	Not assigned

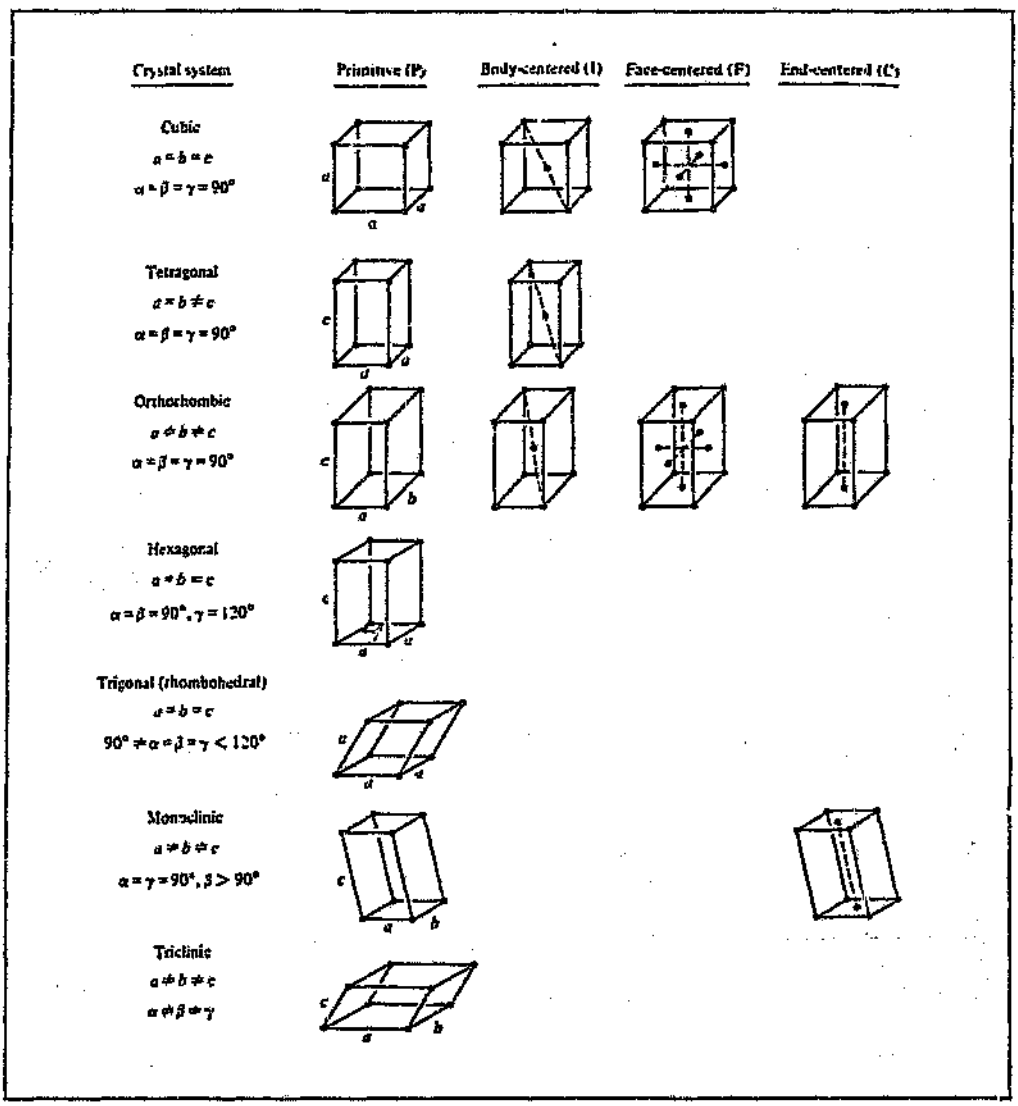

Figure 2.4: Unit cells of the 14 Bravais lattices

Chapter 3

Results

3.1 Reaction studies

In this chapter results[1] from the investigation of the role cobalt-supported catalysts play in the methane partial-oxidation reaction are presented.

3.1.1 Gas-phase reactions

Significant conversions of methane to various carbon-containing products, in the absence of a catalyst, were observed in the original reactor (figure 2.2) at temperatures above 750°C (table 3.1). As the temperature increased, selectivity towards coupled products (produced by reactions *vi* to *viii*, table 1.3) and water decreased, while synthesis gas production increased.

[1]The results in this section have been edited for clarity. All the experimental data collected is presented in Appendix B.

Table 3.1: Gas-phase reactions in the original reactor

Catalyst	Temp (°C)	CH_4 conv. (%)	Selectivity (%) CO	Selectivity (%) CO_2	H_2/CO ratio
Blank Reactor	760	0,8	43,5	13,7	1,88
	860	5,3	54,4	5,5	1,27
	961	14,5	92,3	^,2	1,81

Table 3.2: Gas-phase reactions in the modified reactor

Catalyst	Temp (°C)	CH_4 conv. (%)	Selectivity (%) CO	Selectivity (%) CO_2	H_2/CO ratio
Blank Reactor	435	0,4	0,0	100,0	—
	490	0,0	—	—	—
	545	0,4	0,0	100,0	—
	601	0,0	100,0	0,0	0,62
	657	0,0	—	—	—
	712	0,0	—	—	—
	765	0,0	—	—	—
	874	0,1	0,0	0,0	—
	927	0,3	18,9	0,0	0,77
	980	0,9	24,6	0,0	0,86

The use of a reactor with a lower volume (figure 2.3) had the desired effect of reducing the gas-phase reactions. At about 960°C the gas-phase conversion of methane dropped from 14,5% in the original reactor to just under one percent in the modified reactor, table 3.2. Thus for experiments conducted in the modified reactor, gas-phase reactions could be ignored.

It is important to note that there was no difference in the gas-phase activity on addition of quartz beads to the modified reactor. Nor was there any change in the gas-phase activity, when the modified reactor was retested at the end of the experimental work.

3.1.2 Partial oxidation over Co-Ru bimetallic catalysts

These experiments were conducted in the original reactor. Thus the effect of gas-phase reactions was not negligible at high temperatures (table 3.1).

Although the temperature at which CH_4 reacted to form products in the reactor was lower in the presence of pure γ-Al_2O_3, than in the blank reactor, there was only a marginal improvement in conversion. There was no real improvement in the selectivity to CO and CO_2 with the alumina (compare tables 3.3 and 3.1). The reason alumina showed higher conversions than observed in the gas phase, especially at lower temperatures, is thought to be related to the known activity of the support for C-H bond breaking [55].

Calcined and uncalcined 1%Co/γ-Al_2O_3 catalysts were prepared (section 2.2.2) and tested. The introduction of cobalt generally improved selectivity to the oxide products, particularly in the case of the uncalcined catalyst (table 3.3). Methane conversion was also higher in the presence of the metal, with an increase in activity of ~20% as the feed gas temperature approached 1000°C.

The calcined catalysts had a characteristic blue colour before testing. Interestingly, after reaction, sections of the uncalcined catalysts had begun to change to the same colour. Schmidt and co-workers (section 1.4.4) also observed that areas of the cobalt-coated alumina monolith had changed to a blue colour after reaction. This was attributed to a tetrahedral cobalt complex, probably $CoAl_2O_4$. It was further noted that this region did not appear to be lit, *i.e.* active in the methane conversion reactions.

The reaction of methane with oxygen in the presence of a monometallic 0,1%Ru/γ-Al_2O_3 catalyst was also investigated. This catalyst showed higher activity and selectivity than the 1%Co/γ-Al_2O_3 catalysts (table 3.3). In addition to this the temperature at which products were first observed was significantly lower in the presence of ruthenium, than in the presence of cobalt.

Cobalt-ruthenium bimetallic catalysts were prepared in calcined and uncalcined forms (section 2.2.2), and tested in the same way as the monometallic catalysts. The uncalcined monometallic ruthenium catalyst showed greater activity than the calcined cobalt-ruthenium bimetallic catalyst, which in turn showed greater activity than the uncalcined bimetallic catalyst. Although all three catalysts had similar selectivities at high temperatures, the monometallic ruthenium catalyst showed the greatest selectivity to syngas at temperatures below 700°C. In comparison to their monometallic counterparts, both the calcined and the uncalcined cobalt-ruthenium catalysts had higher conversions of methane and improved selectivity to CO, except when the feed-gas temperature approached 1000°C. Neither of the bimetallic catalysts showed the same dramatic change in activity at ~960°C that had been observed during testing of the two cobalt monometallic catalysts.

Interaction between the ruthenium and cobalt species on the bimetallic catalysts may have resulted in the observed differences in the performance between the monometallic and the bimetallic catalysts. The bimetallic interaction appears to retard the catalytic effect of ruthenium at low temperatures, and that of cobalt at higher temperatures, preventing the increase of activity observed in the monometallic cobalt catalysts near 1000°C.

Reactions were observed in the presence of all three ruthenium-based catalysts at temperatures as low as about 485°C. Poirier and Trudel [49] observed that reactions were initiated at 425°C in the presence of a 0,1%Ru/γ-Al_2O_3 catalyst. They attributed this to the reduction of RuO_2 to Ru metal at this temperature and proposed that the metal is the active catalyst.

Table 3.3: Partial oxidation over Co and Ru mono- and bi-metallic catalysts

Catalyst	Temp (°C)	CH_4 conv. (%)	Selectivity (%) CO	Selectivity (%) CO_2	H_2/CO ratio
γ-Al_2O_3	668	5,2	61,5	9,6	0,9
	767	10,5	54,6	11,2	1,1
	872	18,2	69,8	7,7	1,1
	972	18,7	81,7	1,9	1,8
1%Co/γ-Al_2O_3[a]	664	9,5	59,7	20,5	1,1
	769	19,6	55,5	21,5	0,9
	842	22,8	81,3	7,2	0,9
	972	41,9	99,3	0,2	1,8
1%Co/γ-Al_2O_3[b]	667	8,9	63,0	13,9	1,1
	774	19,5	62,0	19,8	0,8
	870	15,4	70,8	7,6	1,2
	962	35,4	93,6	2,1	1,7
0,1%Ru/γ-Al_2O_3[c]	485	13,9	69,0	31,0	2,4
	572	19,6	88,7	11,3	2,0
	664	23,7	96,5	3,5	1,8
	763	27,6	98,5	0,5	1,8
	862	29,4	98,6	0,1	1,8
	954	30,9	98,7	0,0	1,8
0,1%Ru-1%Co/γ-Al_2O_3[a]	485	6,1	42,6	57,4	2,7
	578	10.8	76,0	24,0	1,8
	670	14,8	88,9	10,7	1,7
	764	22,2	98,4	0,3	1,8
	862	24,3	97,4	0,1	1,8
	957	20,4	97,7	0,0	2,3
0,1%Ru-1%Co/γ-Al_2O_3[b]	484	8,8	53,9	46,1	3,0
	573	19,7	88,1	11,9	1,4
	666	20,1	95,9	3,7	1,7
	761	23,7	97,6	0,6	1,8
	860	24,1	97,3	0,0	1,8
	956	25,9	98,5	0,0	1,8

[a] Uncalcined 1%Co/γ-Al_2O_3 — section 2.2.2.

[b] 1%Co/γ-Al_2O_3 calcined at 800°C — section 2.2.2.

[c] Uncalcined 1%Ru/γ-Al_2O_3 — section 2.2.2.

3.1.3 Partial oxidation over Co on various supports

These experiments were also conducted in the original reactor. Hence the gas-phase reactions reported in table 3.1 need to be considered.

The activity and selectivity of cobalt was tested over five different supports, each with a metal loading of 3±0,2%, table 3.4.

Cobalt supported on MgO proved to be unstable, and metal was observed on cooler downstream sections of the reactor. As a result this catalyst had a lower activity at ~950°C (marginally greater than that of the gas phase) compared to the other catalysts tested.

The cobalt on titania catalyst was exceptional in that it was the only catalyst which showed a gradual improvement in both activity and selectivity with temperature. Nevertheless, it showed the greatest activity and very high selectivity at the maximum temperature. It was however observed that, at the end of the reaction, the catalyst had fused in places, with the quartz frit.

The silica-based catalyst, while not as active as the titania-supported catalyst at lower temperatures, was only slightly less active near 1000°C. Selectivity to synthesis gas was comparable.

The γ-Al_2O_3 and C/γ-Al_2O_3 catalysts both showed moderate conversions at lower temperatures with sudden increases in activity and selectivity at about 950°C. The selectivities achieved were marginally poorer than those of the titania and silica-based catalysts. The C/γ-Al_2O_3-based catalyst appeared black prior to reaction, but after reaction had changed to the same blue colour as the γ-Al_2O_3-based catalyst.

Table 3.4: Partial oxidation of methane over various catalysts

Catalyst	Temp	CH_4	Selectivity (%)		H_2/CO
	(°C)	% conv.	CO	CO_2	ratio
3%Co/γ-Al_2O_3	476	0,00	0,0	0,0	–
	575	0,25	0,0	100,0	–
	670	5,83	56,4	28,3	1,59
	769	8,04	56,0	21,6	0,93
	869	13,53	64,5	9,5	1,05
	959	26,05	98,5	0,1	1,82
3%Co/C/γ-Al_2O_3	473	0,16	0,0	100,0	–
	564	0,27	0,0	100,0	–
	666	2,89	37,9	20,7	1,42
	764	3,97	61,6	20,0	1 01
	863	8,61	62,3	10,9	1,07
	956	26,33	98,2	0,0	1,72
3%Co/MgO	472	0,00	0,0	0,0	–
	566	0,11	0,0	100,0	–
	663	2,02	21,3	48,0	1,44
	760	7,08	17,6	35.7	1,51
	860	6,54	14,4	35,6	3,11
	953	17,78	92,8	0,0	1,85
3%Co/SiO_2	475	0,58	0,0	100,0	–
	569	0,53	0,0	100,0	–
	664	1,87	0,0	85,3	–
	762	7,95	16,4	47,9	1,53
	859	5,36	23,7	25,4	2,04
	949	28,80	99,1	0,0	1,79
3%Co/TiO_2	474	0,06	0,0	100,0	–
	569	0,23	0,0	100,0	–
	664	1,62	29,5	24,7	0,95
	764	11,35	40,5	15,7	0,79
	867	20,00	81,9	4,9	1,48
	955	31,41	99,0	0,2	1,82

3.1.4 Partial oxidation over SiO_2-based catalysts

As a result of the screening tests conducted, MgO and TiO_2 were eliminated as possible supports for further studies. SiO_2 and Al_2O_3 supported catalysts were further investigated in the modified reactor.

The results collected from the original reactor showed that Co on silica was active and selective. However, tests performed in the modified reactor gave results corresponding to half the selectivity and hardly any activity. It is clear from these results (table 3.5) that the gas-phase reactions contributed extensively to methane conversion and CO selectivity.

The results shown in table 3.5 for the tests conducted at ~1000°C in the modified reactor are those collected after two hours. Results were also collected every half an hour prior to this time (see the data collection procedures outlined in section 2.1.6). In the first two hours of reaction, conversions for SiO_2, 3%Co/SiO_2 and 10%Co/SiO_2 dropped from 6,0% to 4,2%, 6,9% to 4,8% and from 5,5% to 3,5% respectively. The selectivity to CO decreased from 53,7% to 49,4%, 49,2% to 45,7% and from 48,4% to 42,2% respectively, over the same period (tables B.9 and B.11).

As a result of the decline in the activity and selectivity of these catalysts, as well as there being little evidence that the cobalt on SiO_2 has any substantial effect on the reaction, no further tests were carried out on silica-based catalysts.

Table 3.5: Comparison of silica-supported catalysts in the original and modified reactors

Catalyst	Temp (°C)	CH_4 conv. (%)	Selectivity (%) CO	Selectivity (%) CO_2	H_2/CO ratio
Original reactor:					
SiO_2	473	0,00	0,0	0,0	–
	566	1,26	76,3	11,6	0,46
	666	15,53	61,7	8,1	0,28
	764	24,77	73,3	4,3	0,35
	856	24,54	73,8	6,6	0,48
	953	46,49	81,8	10,4	0,52
$3\%Co/SiO_2$	475	0,58	0,0	100,0	–
	569	0,53	0,0	100,0	–
	664	1,87	0,0	85,3	–
	762	7,95	16,4	47,9	1,53
	859	5,36	23,7	25,4	2,04
	949	28,80	99,1	0,0	1,79
Modified reactor:					
SiO_2	444	0,1	0,0	100,0	—
	772	0,4	77,6	22,4	0,6
	990	4,2	49,4	4,8	0,7
$3\%Co/SiO_2$	462	0,5	13,0	87,0	0,5
	789	0,7	40,5	59,5	0,4
	1005	4,8	45,7	5,8	0,7
$10\%Co/SiO_2$	468	0,6	3,1	96,9	0,4
	796	2,2	31,5	59,3	0,2
	1006	3,5	42,2	9,4	0,8

3.1.5 Partial oxidation over Al_2O_3-based catalysts

Tests on both α-Al_2O_3 and γ-Al_2O_3 were conducted in the modified reactor.

In the presence of both supports, as temperature increased, so did activity, while selectivity to CO decreased (table 3.6). At the maximum testing temperature activity was low, 23,2% and 20,4% for α-Al_2O_3 and γ-Al_2O_3 respectively, and selectivity to CO poor, 66,6% and 49,0% respectively.

An addition of 3% cobalt to γ-Al_2O_3 reversed the trend, with both activity and selectivity increasing with temperature. Addition of 10% metal to this support resulted in almost complete conversion and close to 100% selectivity at ~1000°C. The 10%Co/α-Al_2O_3 catalyst showed similar activity and selectivity to 10%Co/γ-Al_2O_3 above 1000°C.

The thermal stability of the 10%Co/γ-Al_2O_3 catalyst was tested by calcining it at 1125°C for about 50 hours, in a so called "ageing" process. Only marginal decreases in the activity were observed.

3.1.6 Partial oxidation over C/γ-Al_2O_3-based catalysts

The results from various C/γ-Al_2O_3-based cobalt catalysts are reported in table 3.8.

A comparison of tables 3.6 and 3.8, show that the results obtained from the C/γ-Al_2O_3 support are similar to those of the two pure alumina supports. It was observed that activity increased with increasing temperature, while selectivity decreased. At 1012°C activity was still low (<30%) and selectivity to CO poor (<45%).

The support initially appeared black in colour, due to the carbon coating, but after reaction the colour of the support was white. This implies that the carbon coating was removed at high temperatures. If this is true of the supported catalysts then the

Table 3.6: Partial oxidation over Al_2O_3-based catalysts

Catalyst	Temp (°C)	CH_4 conv. (%)	Selectivity (%) CO	Selectivity (%) CO_2	H_2/CO ratio
α-Al_2O_3	476	0,2	100,0	0,0	9,6
	800	6,5	83,0	17,0	1,6
	1023	23,2	66,6	4,6	0,9
10%Co/α-Al_2O_3	485	0,0	0,0	0,0	—
	831	51,2	89,0	0,0	1,7
	925	89,0	98,2	1,8	1,7
	1024	97,0	99,9	0,1	1,7
γ-Al_2O_3	440	0,1	100,0	0,0	1,0
	772	3,3	77,0	23,0	2,2
	995	20,4	49,0	7,0	1,3
3%Co/γ-Al_2O_3	490	1,0	95,2	4,8	0,0
	807	54,6	87,6	11,5	1,7
	998	77,7	95,6	3,9	1,7
10%Co/γ-Al_2O_3	486	0,1	78,5	21,5	5,8
	845	64,4	94,2	5,8	1,5
	925	81,8	96,0	3,9	1,7
	1042	97,8	100,0	0,0	1,6
10%Co/γ-Al_2O_3[a]	464	0,1	100,0	0,0	7,2
	813	57,1	90,3	8,4	1,7
	1010	96,0	100,0	0,0	1,7

[a] Calcined at 1125°C — section 2.2.2.

results of these studies should resemble those conducted on catalysts using the same Al_2O_3 phase as a support.

Comparison of 10%Co/C/γ-Al_2O_3 at above 1000°C, to those over 10%Co/α-Al_2O_3 and 10%Co/γ-Al_2O_3, showed that the activity of the C/γ-Al_2O_3-based catalyst was slightly lower but the selectivity comparable to the non-carbon-containing catalysts. The variations in the reaction temperature (1010°C, 1023°C and 1042°C for 10%Co/C/γ-Al_2O_3, α-Al_2O_3 and γ-Al_2O_3 respectively) may explain the variations in the conversions.

Comparison of the three alumina-based catalysts at 925°C, table 3.7 shows that the carbon-coated catalyst appears to be more active. This may be due to random experimental error or the presence of the carbon coating.

Calcination at 800°C and 1125°C appear to have little effect on the activity of the 14%Co/C/γ-Al_2O_3 and 10%Co/C/γ-Al_2O_3 catalysts respectively.

The standard 14%Co/C/γ-Al_2O_3 catalyst, and the diluted 14%Co/C/γ-Al_2O_3 catalyst (section 2.2.4) both took an unusually long period to reach steady state; 4 hours and 10 hours respectively. The 14%Co/C/γ-Al_2O_3 catalyst calcined at 800°C, however, reached steady state as rapidly as the 10%Co/C/γ-Al_2O_3 catalyst. The 14%Co catalysts were prepared using cobaltous nitrate in ethanol while the 10%Co catalysts were prepared from cobalt acetate in nitric acid (section 2.2.2). It appears that exposure to high temperatures is needed to activate the catalyst. In the case of the diluted catalyst the heat lost in maintaining the temperature of the quartz beads slows this heat treatment.

3.1.7 Partial oxidation over A_B^R

As a result of the work above and the characterisation studies reported below, a catalyst, labelled A_B^R, was prepared. The results presented in table 3.9 were obtained

Table 3.7: Comparison of Al_2O_3-based catalysts at 925°C

Catalyst	Temp (°C)	CH_4 conv. (%)	Selectivity (%) CO	Selectivity (%) CO_2	H_2/CO ratio
10%Co/α-Al_2O_3	925	89,0	98,2	1,8	1,7
10%Co/γ-Al_2O_3	925	81,8	96,0	3,9	1,7
10%Co/C/γ-Al_2O_3	925	95,9	99,3	0,7	1,2

Table 3.8: Partial oxidation over C/γ-Al_2O_3-based catalysts

Catalyst	Temp (°C)	CH_4 conv. (%)	Selectivity (%) CO	Selectivity (%) CO_2	H_2/CO ratio
C/γ-Al_2O_3	455	0,1	31,8	68,2	0,7
	757	4,6	75,1	24,9	1,8
	1012	28,9	43,5	14,5	1,3
3%Co/C/γ-Al_2O_3	448	0,1	64,1	35,9	0,5
	790	9,9	52,3	44,9	2,4
	1010	83,2	96,7	2,6	1,6
10%Co/C/γ-Al_2O_3	472	1,0	37,5	62,5	0,7
	820	46,0	90,9	9,1	1,9
	925	95,9	99,3	0,7	1,2
	1010	92,0	99,6	0,4	1,8
10%Co/C/γ-Al_2O_3[a]	420	0,1	100,0	0,0	4,1
	763	1,4	55,4	44,6	3,7
	994	94,0	100,0	0,0	1,8
14%Co/C/γ-Al_2O_3	497	0,4	0,0	100,0	—
	833	16,2	46,0	44,7	2,7
	1027	83,4	97,0	2,0	1,7
(after 16 hours)	1027	96,3	98,9	1,1	2,0
14%Co/C/γ-Al_2O_3[b]	507	0,8	0,0	100,0	—
	835	8,6	46,5	53,5	3,4
	1028	39,6	67,4	21,9	2,0
(after 20 hours)	1028	89,7	97,9	2,0	1,5
14%Co/C/γ-Al_2O_3[c]	368	0.4	100,0	0,0	0,3
	730	8.4	54,4	45,6	2,6
	953	87,4	98,5	1,5	1,6

[a] Calcined at 1125°C — section 2.2.2.

[b] Diluted with quartz beads, Quartz : Catalysts = 2 : 1 — section 2.2.4.

[c] Calcined at 800°C — section 2.2.2.

Table 3.9: Partial oxidation over A_B^R

Temp (°C)	CH_4 conv. (%)	Selectivity (%) CO	CO_2	H_2/CO ratio
535	71,3	88,0	12,0	1,9
636	77,4	93,8	6,2	1,8
735	85,6	97,3	2,7	1,9
837	94,0	98,4	1,6	1,8
935	98,4	99,8	0,2	1,8

using this catalyst. It is clear from the table that these results are the best presented in this work for the partial oxidation of methane synthesis gas. The activity and selectivity, at all temperatures, are consistently higher than for any other catalyst tested. The catalyst formulation will be revealed after patents have been taken out on the catalyst.

3.1.8 Stability studies

The stability of 10%Co/C/γ-Al_2O_3 was tested by collecting data at a reaction temperature of 1068°C over a period of 150 hours. This study revealed an almost complete conversion of methane and selectivity to CO over this time period (figure 3.1). The periodic fluctuations in conversion are discussed in section 2.1.5.

The stability of the A_B^R catalyst is demonstrated in figure 3.2. This catalyst was maintained at a reactor setpoint temperature of 900°C for 180 hours. Then the setpoint was decreased to 800°C, and the reaction maintained under these conditions for a further 70 hours. Less extreme conditions were used for this experiment than for the stability test conducted on 10%Co/C/γ-Al_2O_3 (figure 3.1). A lower reaction temperature was introduced since similar results were observed at lower temperatures.

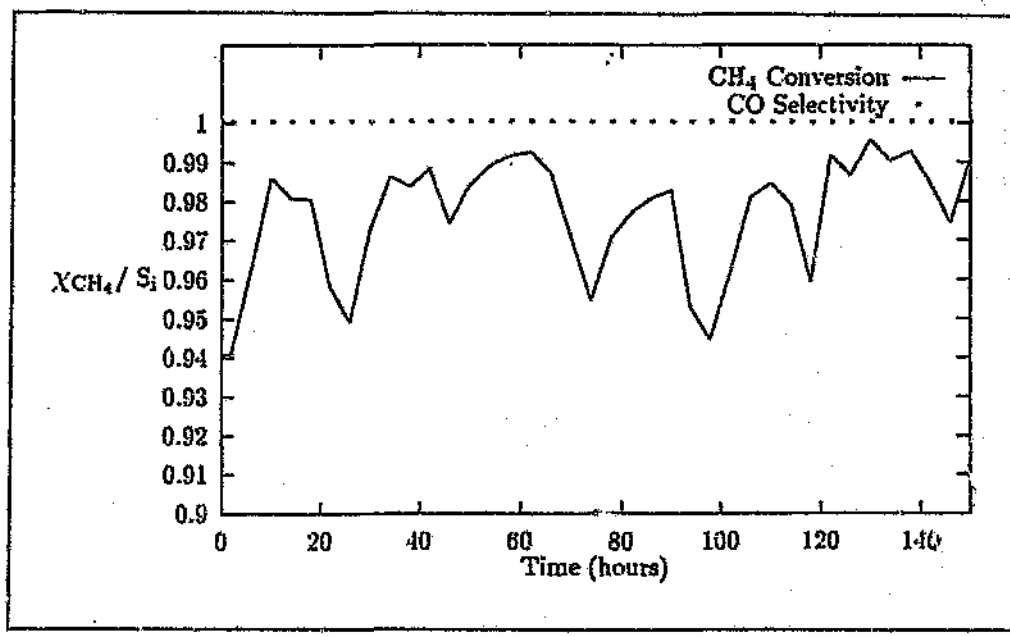

Figure 3.1: 10%/C/γ-Al_2O_3 stability study

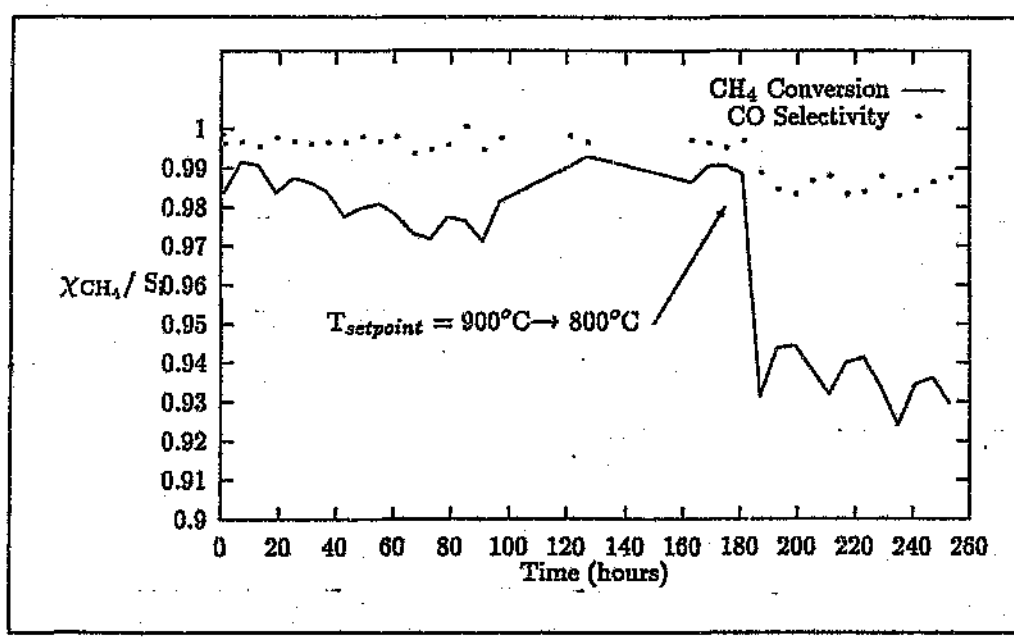

Figure 3.2: A_B^R stability study

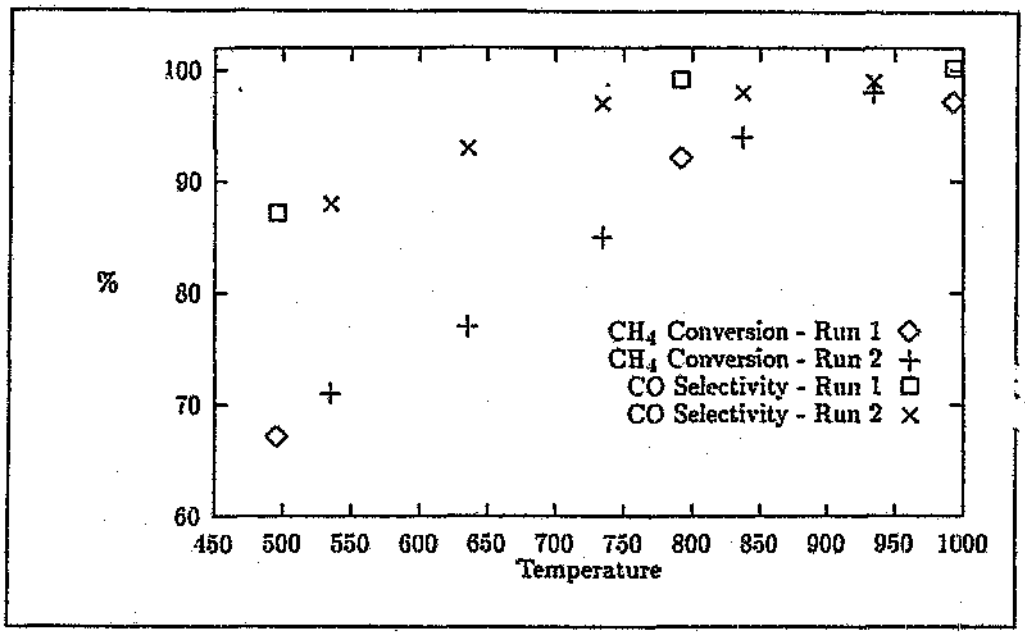

Figure 3.3: Comparison of two different A_B^R experiments

3.2 Reproducibility

It is necessary in any research work to be satisfied that the results reported are accurate, and most importantly reproducible. In order to ascertain the reproducibility of the reactor studies and analysis, two different experiments were conducted on the same catalyst (A_B^R) under the same conditions.

In figure 3.3 the results from the two experiments conducted are plotted. The graph clearly shows that the results from the two experiments show the same trends, and data points at comparable temperatures are within a couple of percent. While it is difficult to perfectly reproduce results, it is clear that a comparison of data from the same catalyst collected at different times is valid.

The reproducibility of the catalyst preparation technique is discussed in sections 4.5.1 and 4.6.1.

Table 3.10: Cobalt loadings of various catalysts.

Catalyst	Calculated [% mass]	Measured [% mass]
α-Al_2O_3 support	0,0	0,0
3%Co/α-Al_2O_3	3,0	2,9
10%Co/α-Al_2O_3	10,0	9,6
γ-Al_2O_3 support	0,0	0,0
3%Co/γ-Al_2O_3	3,0	2,9
10%Co/γ-Al_2O_3[a]	10,0	9,5
10%Co/γ-Al_2O_3[b]	10,0	9,3
C/γ-Al_2O_3 support	0,0	0,0
3%Co/C/γ-Al_2O_3	3,0	2,8
10%Co/C/γ-Al_2O_3[a]	10,0	9,6
10%Co/C/γ-Al_2O_3[b]	10,0	9,5
14%Co/C/γ-Al_2O_3	14,0	13,7

[a] Calcined at 800°C — section 2.3.2

[b] Calcined at 1125°C — section 2.3.2

3.3 Characterisation studies

3.3.1 Determination of cobalt loading

Due to the techniques used in loading metals on support materials and subsequent treatment, it is possible that the actual metal content of a catalyst could be lower than that calculated. For example, in table 3.10, the catalysts calcined at 800°C and 1125°C, although prepared from the same initial material, show small (<0,5%) differences in their metal loadings.

The same preparation techniques and pre-treatment should produce catalysts with similar loadings, for example, all those catalysts calculated to contain 10% cobalt ended up with approximately 9,5% cobalt content. From table 3.10 it would appear that there is consistently 5-10% less cobalt in the catalyst than calculated.

Table 3.11: Surface areas of various catalysts.

Catalyst	Calcination Temperature	Surface Area [m^2/g]
10%Co/α-Al_2O_3	800°C	36,6
10%Co/γ-Al_2O_3	800°C	30,0
10%Co/γ-Al_2O_3	1125°C	4,5
10%Co/C/γ-Al_2O_3	none	96,5
10%Co/C/γ-Al_2O_3	1125°C	6,6

The technique used to obtain these results is described in section 2.3.1

3.3.2 Surface-area analysis

The results of surface-area analyses conducted on various fresh catalysts are reported in table 3.11.

The effect of heat pre-treatment on the catalysts is evident from the results. 10%Co/C/γ-Al_2O_3, that underwent no heat treatment, gave the highest surface area, 96,5 m^2/g. 10%Co supported on γ-Al_2O_3 and α-Al_2O_3, both treated at 800°C, had similar surface areas (30,0 m^2/g and 36,6 m^2/g respectively). The two catalysts calcined at 1125°C also had similar surface areas. The data clearly reflects the loss of surface area expected on heating alumina supports to high temperatures.

3.3.3 Identification of catalyst structure

A summary of the results obtained from the XRD studies conducted are shown in table 3.12.

The structures of α-Al_2O_3 and γ-Al_2O_3 are obviously different (figure 3.4), but it is clear that the structure of C/γ-Al_2O_3 is very similar to that of γ-Al_2O_3. It is worth noting that the α-Al_2O_3 structure observed was not confidently matched with any species in the database. The species found to be most closely related was rhombohe-

Table 3.12: Structures identified using powder diffraction techniques.

Catalyst	Temperature [°C] Calc.	Rxn	Al_2O_3 Rhom.	α	γ	Metallic Co Cubic	Hex.	$CoAl_2O_4$	Co_3O_4
Co/α-Al_2O_3	800	fresh						2	1
Co/α-Al_2O_3	800	1000	1			3		2	
Co/γ-Al_2O_3	800	fresh						1	2
Co/γ-Al_2O_3	800	1000	1			3		2	
Co/γ-Al_2O_3 ("aged")	1125	fresh	1					2	
Co/γ-Al_2O_3 ("aged")	1125	1000	1			2		3	
Co/C/γ-Al_2O_3 (10%)	dried	fresh			1				
Co/C/γ-Al_2O_3 (14%)	dried	fresh			1				
Co/C/γ-Al_2O_3 (in situ)	dried	500	2						1
Co/C/γ-Al_2O_3 (in situ)	dried	1000	1			2			
Co/C/γ-Al_2O_3 (blue)	dried	1000	1			3		2	
Co/C/γ-Al_2O_3 (grey)	dried	1000	1			2			
Co/C/γ-Al_2O_3	800	fresh	3					2	1
Co/C/γ-Al_2O_3	800	1000	1			3		2	
Co/C/γ-Al_2O_3 ("aged")	1125	fresh	1					2	3
Co/C/γ-Al_2O_3 ("aged")	1125	1000	1			3		2	
Co/C/γ-Al_2O_3 (deactivated)	dried	1000	1					2	

The technique used to obtain these results is described in section 2.3.4

A compound marked as being present by a '1' was more confidently matched with a database compound than those with a '2' or '3'.

dral in structure. This was investigated further and it was found that the material supplied by Strem and listed as α-Al_2O_3 was in fact crystalline boehmite.

Crystalline boehmite, after calcination above 1100°C becomes α-Al_2O_3. During calcination, this material transforms to γ-Al_2O_3 at 600°C. Thus the calcined catalysts on this support should be identical to those supported on γ-Al_2O_3 when calcined at 800°C (figure 3.5). The uncalcined Co/C/γ-Al_2O_3 catalyst has a less crystalline structure than the calcined version of the same catalysts. Co/C/γ-Al_2O_3 calcined at 800°C also closely resembles the structure of the other two calcined catalysts at 800°C. However, the confidence with which various compounds were matched varied on the three supports.

The initial calcination appears to cause structural changes to the catalysts. The exact proportions of Co_3O_4 and $CoAl_2O_4$ formed may differ according to the support used, but otherwise the support has little effect on the resulting catalyst structure.

$Co/\gamma\text{-}Al_2O_3$ catalysts calcined at 800°C and 1125°C, both before and after reaction, are shown in figure 3.6. The fresh catalyst calcined at 800°C is the least crystalline and is composed predominantly of $CoAl_2O_4$. After reaction this catalyst is substantially more crystalline and has changed its composition to rhombohedral Al_2O_3, $CoAl_2O_4$ and cobalt metal in a cubic structure.

The $Co/\gamma\text{-}Al_2O_3$ catalyst calcined at 1125°C after reaction is the most crystalline of the catalysts (figure 3.6). Its composition resembles that of the post-reaction $Co/\gamma\text{-}Al_2O_3$ catalyst calcined at 800°C. Both of these catalysts only show evidence of cobalt metal after reaction.

Figure 3.7 shows the progression of $Co/C/\gamma\text{-}Al_2O_3$ through various stages of preparation and reaction. The $C/\gamma\text{-}Al_2O_3$ and fresh $Co/C/\gamma\text{-}Al_2O_3$ show little crystallinity. After reduction at 600°C and exposure to the feed gases at 500°C, the $Co/C/\gamma\text{-}Al_2O_3$ is still poorly crystalline. Under these conditions the $\gamma\text{-}Al_2O_3$ begins to transform into rhombohedral Al_2O_3 and Co_3O_4. After exposure to the feed gases at 1000°C the structure changes to cobalt metal and rhombohedral Al_2O_3.

After the catalysts had been tested in the modified reactor, two distinct zones were observed (the deactivated catalysts (section 4.6.5) did not show this). The zone corresponding to the upper part of the bed, *i.e.* that part exposed to the fresh feed gas, was characteristically blue. This colour was associated with $CoAl_2O_4$ (section 3.1.2). The lower zone had a grey metallic appearance.

After XRD analysis, the composition of the two zones was found to be similar (table 3.12), with both showing cobalt present in the cubic metallic phase. However, while the grey zone showed alumina present in the rhombohedral form, the blue zone exhibited both rhombohedral alumina and $CoAl_2O_4$. The presence of $CoAl_2O_4$ was visually confirmed by the characteristic colour of the zone. After halving a catalyst pellet from the blue zone a white centre and blue concentric "skin" was observed. This suggests that the $CoAl_2O_4$ exists as a surface species.

In contrast to the two catalyst bed zones observed for the active catalysts, the deactivated (labelled $Co/C/\gamma\text{-}Al_2O_3$ deactivated) catalyst showed no evidence of metallic cobalt. The analysis found rhombohedral alumina and $CoAl_2O_4$. This catalyst had the same characteristic blue colouring as the blue zone. A comparison of the two post reaction zones (from $Co/C/\gamma\text{-}Al_2O_3$) and the deactivated catalyst is presented in figure 3.8.

In addition to those species listed in table 2.1, a database search for carbon species was made. Since XRD analyses are sensitive only to crystalline structures in fairly large quantities, amorphous carbon species would not be detected. No amorphous carbon species were ever observed.

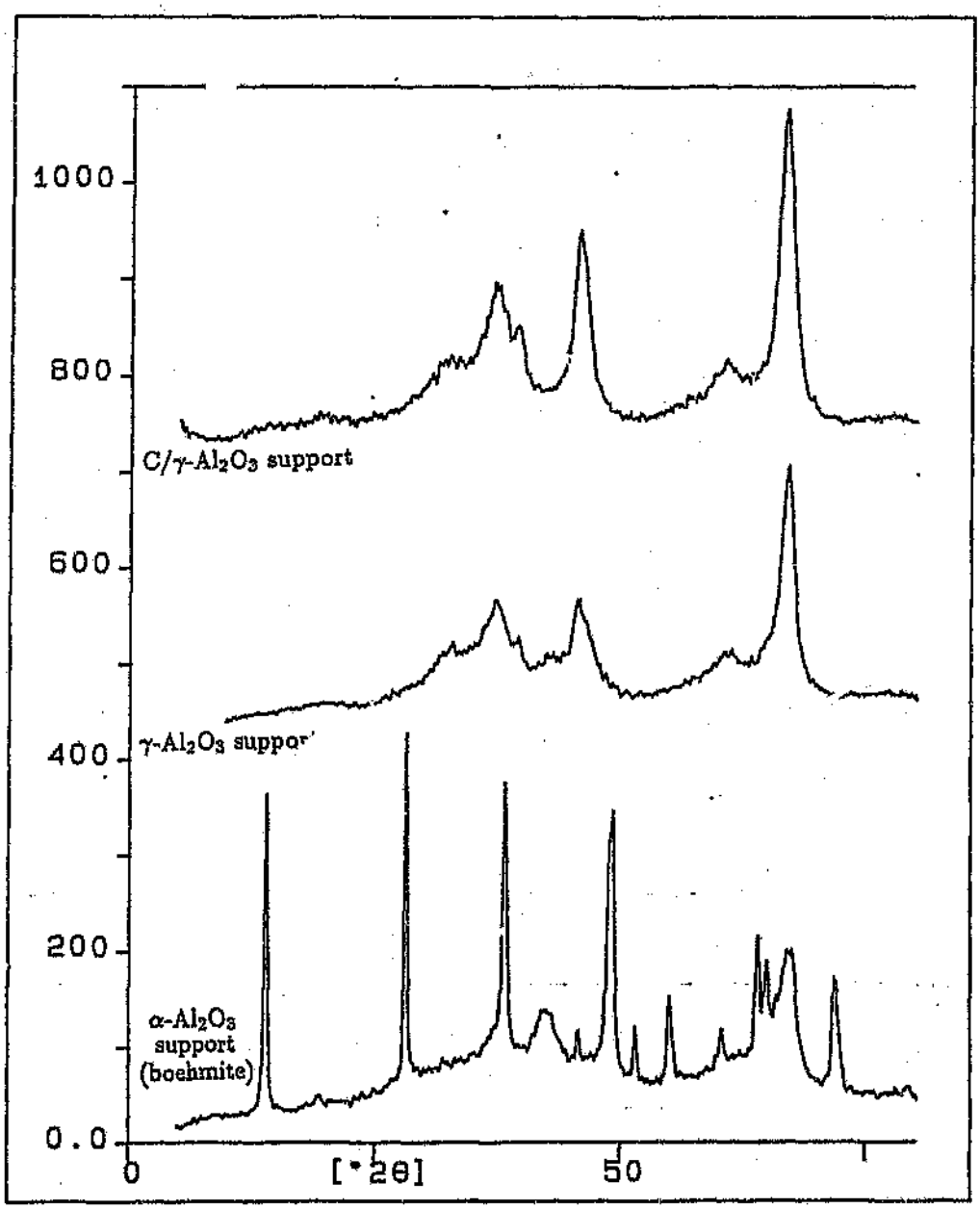

Figure 3.4: XRD of various supports

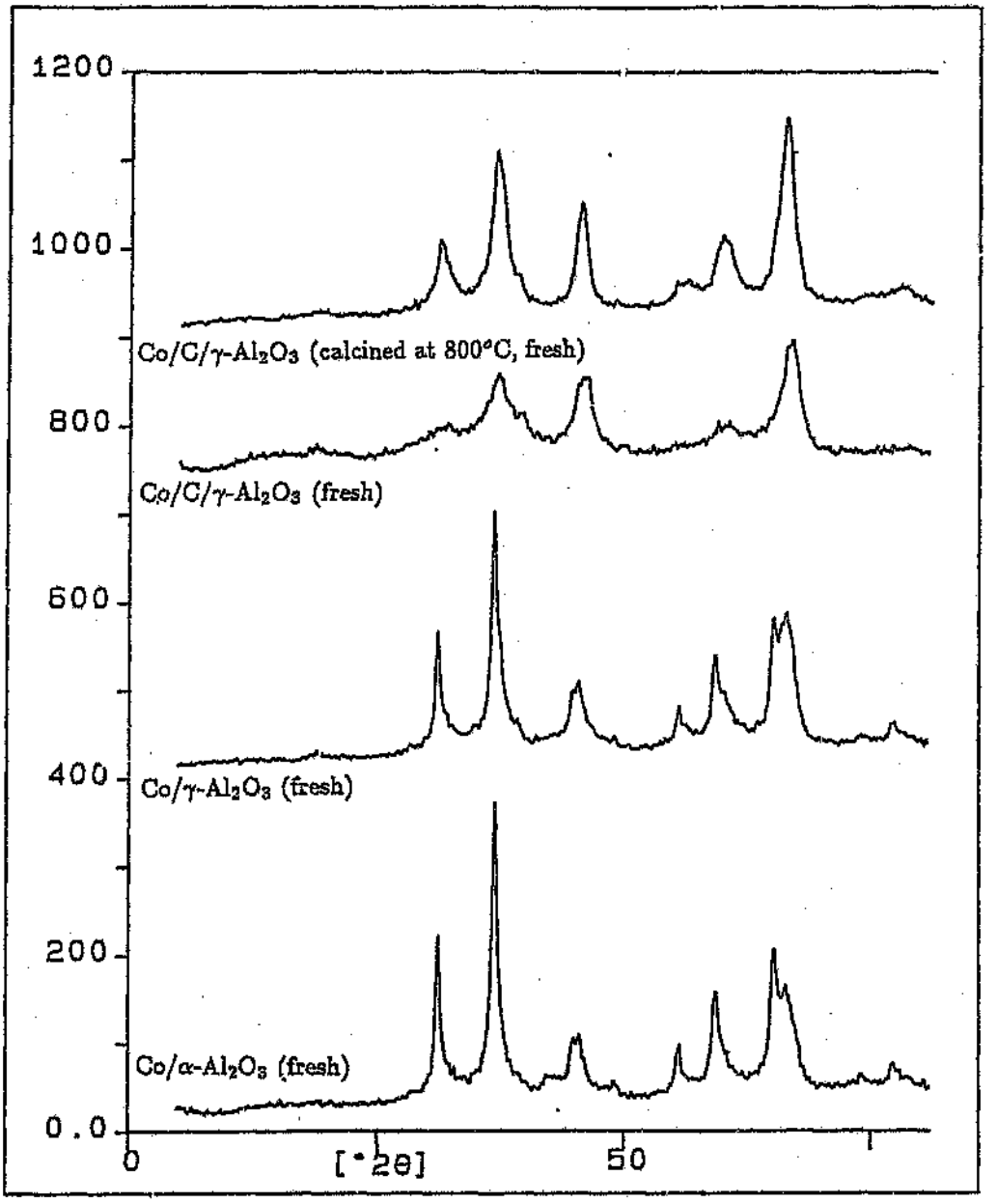

Figure 3.5: XRD of various catalysts prior to reaction

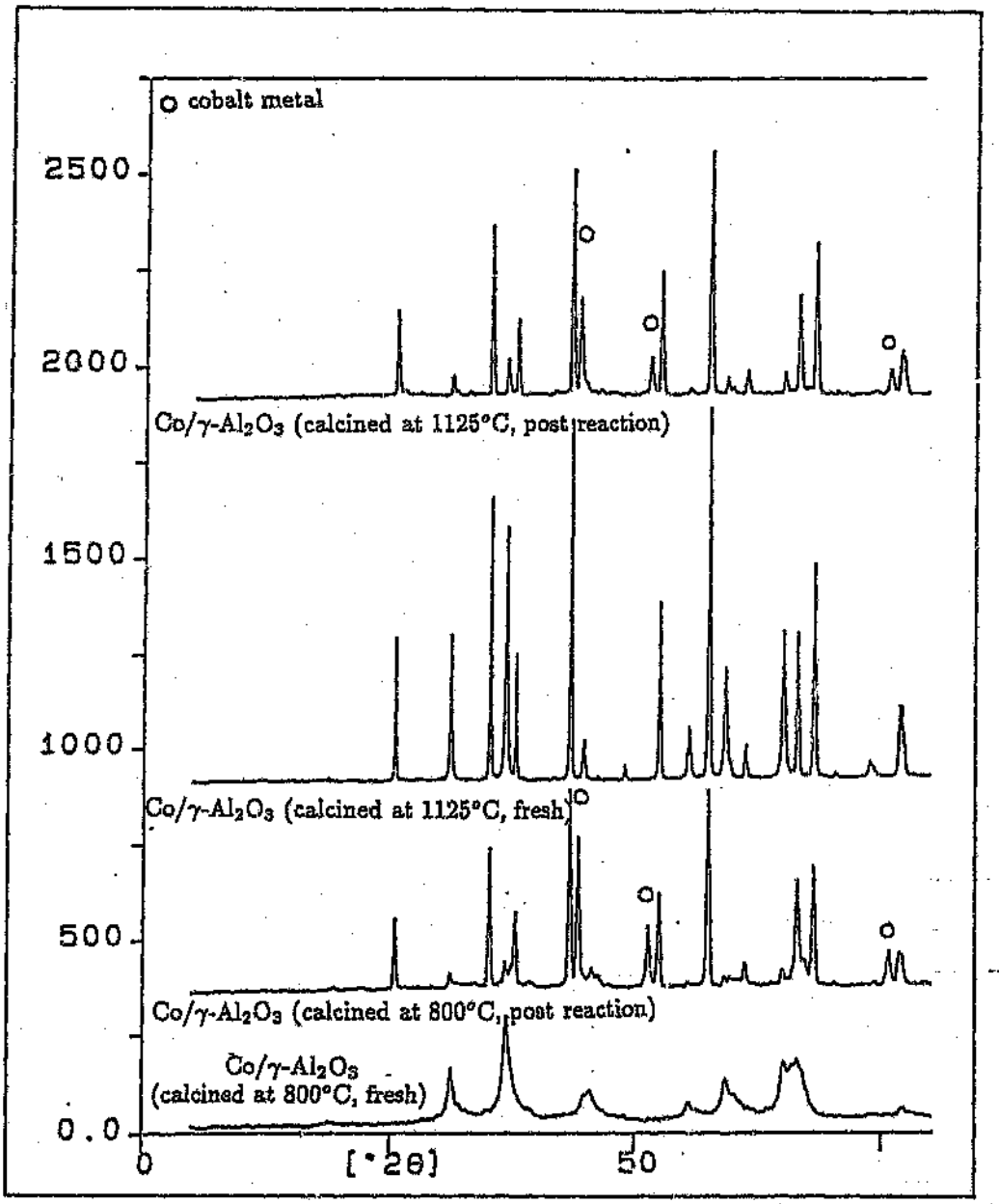

Figure 3.6: XRD of $Co/\gamma\text{-}Al_2O_3$ after various heat treatments

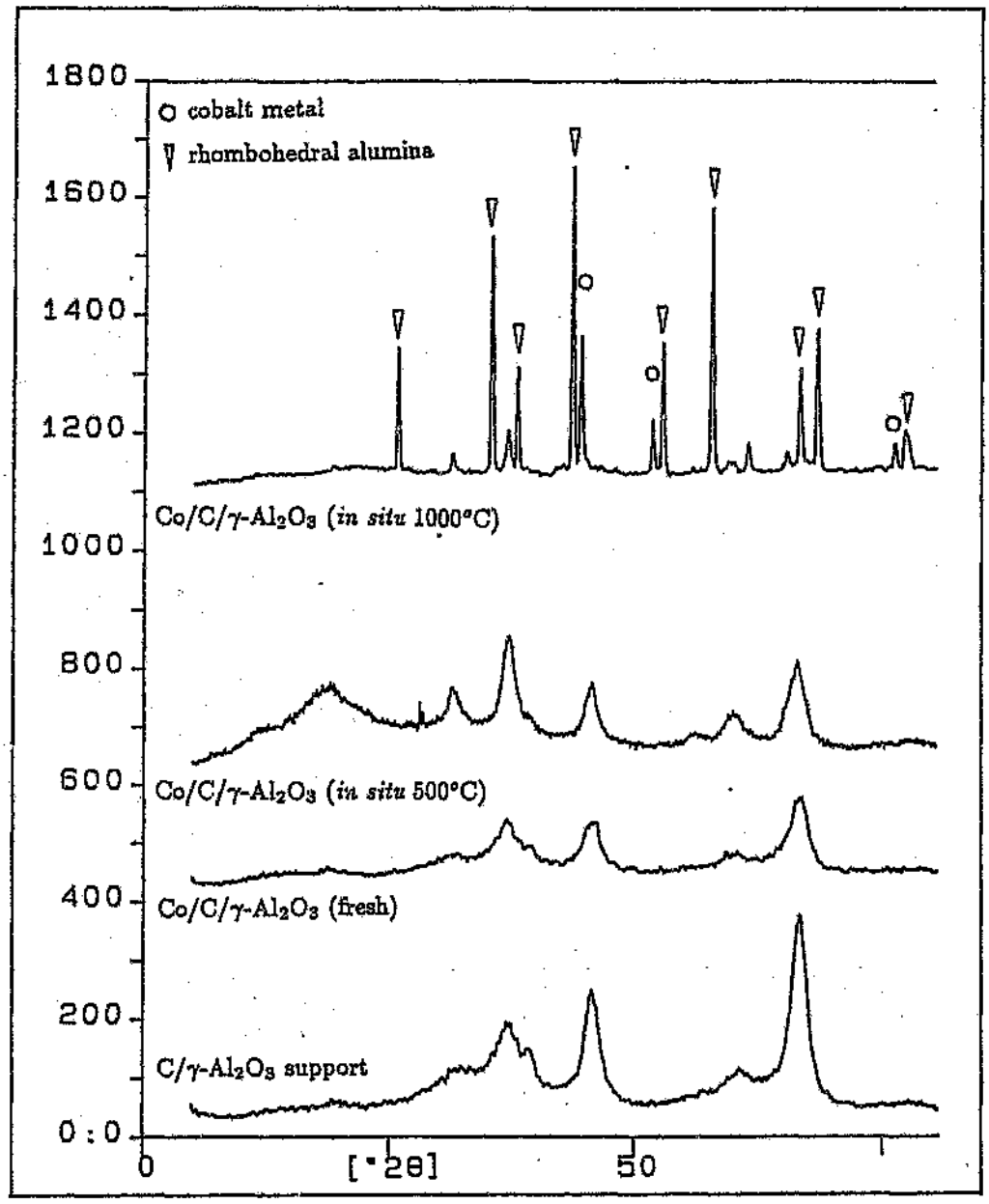

Figure 3.7: XRD of $Co/C/\gamma\text{-}Al_2O_3$ at various temperatures

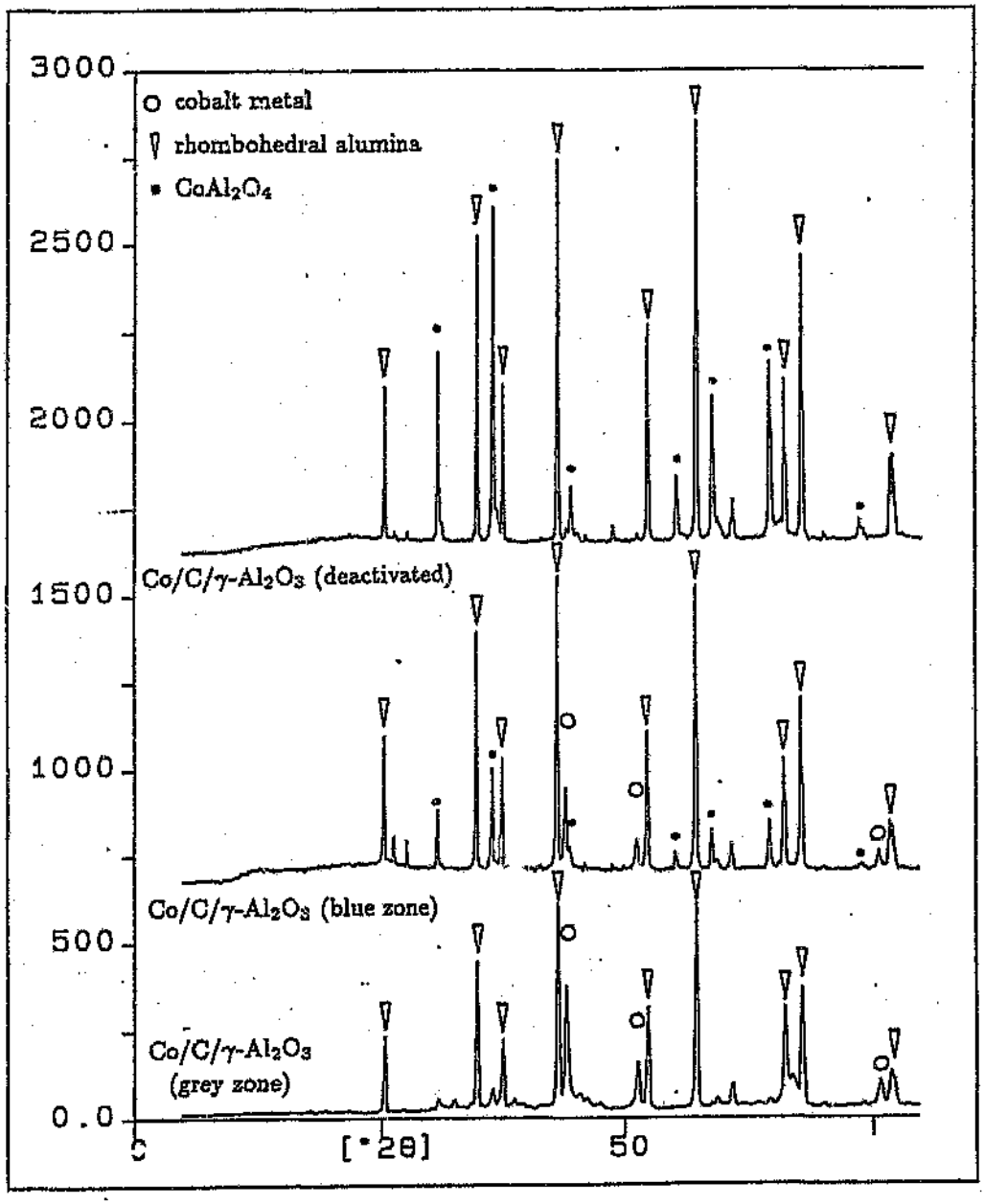

Figure 3.8: Comparison of $Co/C/\gamma\text{-}Al_2O_3$ after reaction and deactivated

Chapter 4

Discussion

4.1 Reactor conditions

4.1.1 Oxygen vs air

Air, rather than oxygen, was used exclusively as the reactant in the experiments conducted in this project. There were two reasons for this, both concerning safety. The first is that without nitrogen as a diluent the methane-oxygen feed gas would very closely approach the explosion limit. Thus a slight fluctuation in the feed composition, resulting in an increase in the oxygen to methane ratio, may have caused explosive combustion. The second is that, since the reaction is exothermic, the nitrogen acts as a heat sink, damping any temperature increases — and consequently preventing any possibility of runaway reactions.

On an industrial scale there are advantages and disadvantages to using air rather than oxygen. In order to achieve the same contact time, the amount of catalyst and consequently the reactor volume needed is greater when using air. In addition to this

it may be advantageous not to have nitrogen present in some downstream processes, and thus using air in the feed would necessitate separation of the nitrogen at some stage of the process. However, these disadvantages of using air need to be considered in the light of the safety and control advantages discussed above.

4.1.2 Reactor design

In the early experiments performed in this project the design of the reactor was found to result in significant gas-phase reactions under the high temperature conditions needed. The objective of modifying the reactor design (section 2.1.1) to minimise gas-phase reactions was successfully achieved (compare tables 3.1 and 3.2). In redesigning the reactor, its diameter decreased and consequently the catalyst bed depth increased from a monolayer of catalyst on the frit to a ~10 mm deep bed. Since both the flow rates through the reactor and the mass of catalyst used remained unchanged, both beds had the same contact time with reactants. However, the change in geometry would favour CO rather than CO_2 as a product (section 4.6.4).

4.1.3 Temperature measurement

The measurement of temperature has been discussed elsewhere (sections 1.4.3 and 2.1.2) and there is very little that needs to be added here. Apart from an internal comparison on the basis of temperature, deductions based on temperature dependent data have been avoided. This has been possible because this research has not involved equilibrium or kinetic studies. To do these, more costly, non-intrusive temperature measurement techniques would be required.

For industrial application, the optimal operating temperature would need to be determined using more sophisticated techniques. However, since the reaction is mildly exothermic overall (table 1.3), energy input would be limited to that lost due to non-adiabatic conditions.

4.2 Contact time experiments with A_B^R

The effect of contact time was investigated using the A_B^R catalyst. Various masses of this catalyst, 10 mg and from 20 mg to 100 mg (in 20 mg increments), were tested at a temperature of 821°C (figure 4.1). Since the feed gas flow rates were held constant, as the catalyst mass was varied so the bed height and contact time varied proportionally.

The conversion and product selection remained constant for catalyst masses above 40 mg. Below this, activity and selection to CO dropped as the catalyst mass decreased. The cause of this change in activity and selectivity is probably due to the corresponding decrease in the contact time. Thus, the amount of catalyst used (100 mg) was more than the mass needed to reach equilibrium[1].

It is also possible that since the depth of the bed decreases with decreasing catalyst mass, there is insufficient catalyst to generate both the combustion and reforming zones. If this is the case, then contact times may be reduced further by decreasing the bed diameter and maintaining the bed height.

[1] Equilibrium values are cited in section 1.4.1, page 23

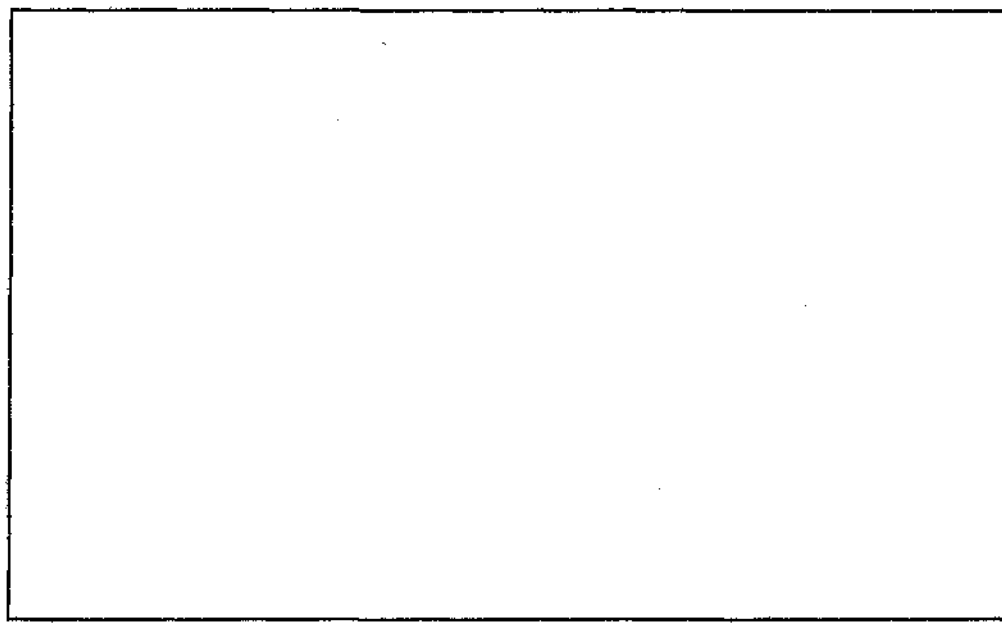

Figure 4.1: Effect of varying A_B^R catalyst mass (821°C)

4.3 Coking

Carbon deposition on a catalyst during the partial oxidation of methane to synthesis gas is undesirable. It is, therefore, one of the important issues to be addressed before this process can be used on an industrial scale. The formation of carbon on metal-supported catalysts for this reaction has been studied in some depth and was discussed briefly in section 1.4.2.

Kinetically, both the Boudouard and methane decomposition reactions, which give undesirable carbon deposition, are known to be exceptionally slow in the absence of a catalyst. However, in the presence of many transition metals both reactions can be readily catalysed. Audier *et al* [64] clearly demonstrated that a significant amount of carbon can be deposited over catalysts containing iron or nickel. In order to avoid carbon deposition on the iron-containing reactor walls, reactions must, therefore, be carried out in a non-ferrous reactor.

Lapszewicz and co-workers [13] observed a relationship between the ability of a catalyst to completely dissociate methane and produce synthesis gas. That is, it appears that there is a relationship between surface carbon and the CO_x products (section 1.4.1). These workers also proposed that amorphous carbon is formed from the products of partial dissociation of methane such as adsorbed methyl groups (section 1.4.2). Thus, there exists a relationship between the coking activity of a catalyst and its inability to cleave C-H bonds.

Lapszewicz *et al* recorded the products of deuterium exchange experiments over various supported transition metal catalysts. Palladium was observed to be most easily deactivated by carbon deposition, and of the less than 2% of the methane feed converted in the deuterium exchange experiments, all was converted to CH_3D. Platinum converted 8,2% of the methane in the feed to 43,9% CH_3D and 56,1% CD_4. Ruthenium was more active, converting 29,3% of the feed; 81,9% to CD_4, 11,9% to CHD_3 and 6,1% to CH_2D_2. Rhodium was the most active of the catalysts tested, showing a 92,3% conversion, but the catalyst exchanged only 71,5% to CD_4. Of the balance 22,1% was changed to CHD_3 and 6,4% to CH_3D.

Claridge *et al* [39] determined the rate of formation of carbon over group VIII B transition metal-supported catalysts. Three different nickel-based preparations all demonstrated greater than 20 mg/h rates of carbon deposition. Rates of 7,48 mg/h, 0,06 mg/h and 0,01 mg/h were recorded for 5% Pd, Rh and Ru supported on Al_2O_3 respectively. No carbon deposition was observed on 1% iridium or platinum supported on Al_2O_3.

Thus within the group VIII B transition elements there appears to be decreasing coking potential from right to left and top to bottom. The difference in characteristics appears to be more marked between groups than between periods.

In the experiments conducted for this research there was never any evidence of coking on the catalysts. Although carbon is amorphous and would not be detected in XRD studies, the catalysts subjected to stability studies showed no evidence of decreasing

activity (section 3.1.8). This does not mean that coking did not occur on these cobalt catalysts, but if it did it showed no ill effects. It is thought that while cobalt is at the top of its group, and thus probably has the greatest coking potential in its group, it ought to show a substantially lower coking ability than nickel. However, if there is a decreasing coking potential trend from right to left, the high coking potential of iron is not explained.

Schmidt and co-workers [47] also reported no evidence of coking on the 3% supported cobalt catalyst that they tested.

4.4 Support materials

The interaction between the metal and the support of a catalyst has great bearing on the activity and stability of the catalyst. Catalysts containing 3% (mass) cobalt were prepared with MgO, TiO_2, SiO_2, γ-Al_2O_3 and C/γ-Al_2O_3, and tested in the original reactor. The results from these experiments are shown in section 3.1.3. All the catalysts screened were prepared in the same fashion, with the exception of the C/γ-Al_2O_3-based catalysts (section 2.2.2).

Metallic deposits were observed on the cooler downstream sections of the reactor while using MgO as the support. In addition to this, the remaining MgO had fused with the quartz frit of the reactor. The 3%Co/TiO_2 catalyst also fused with the quartz frit, although there was no evidence of metal volatility. The other three supports with various metal loadings were tested under the same conditions, but in the modified reactor.

The performance of the silica-based catalysts was significantly poorer in the modified reactor. Table B.11 in appendix B shows the deterioration of the performance of the SiO_2-supported catalysts with time at high temperatures in the modified reactor. α-Al_2O_3 (boehmite), γ-Al_2O_3 and C/γ-Al_2O_3-supported catalysts showed

exceptionally high conversions and selectivity to syngas in the modified reactor (tables B.12, B.13 and B.14 respectively). Thus it appears that for the partial oxidation of methane to synthesis gas alumina supports provide the greatest stability and potential activity.

4.5 Cobalt on γ-Al_2O_3

4.5.1 Preparation

A number of catalysts were prepared using γ-Al_2O_3 as a support. They were prepared with the same starting materials, using the incipient wetness technique (section 2.2.2). One catalyst was prepared with α-Al_2O_3 as the support. Although the XRD patterns of the α-Al_2O_3 and γ-Al_2O_3 supports differed, the pattern of the α-Al_2O_3-supported catalyst was remarkably similar to those of the γ-Al_2O_3-supported catalysts (section 3.3.3). This prompted an investigation into the nature of the α-Al_2O_3 support. It was found that the material supplied by Strem was crystalline boehmite, which after calcination above 1100°C becomes α-Al_2O_3. Calcination above 600°C transforms the boehmite into γ-Al_2O_3. Thus the 10%Co/α-Al_2O_3 catalyst, calcined at 800°C, is more properly described as 10%Co/γ-Al_2O_3.

Two batches of 10%Co/γ-Al_2O_3 were prepared (from γ-Al_2O_3) to test the ability to reproduce results from different batches. Since the same starting materials were used this gives a measure of the reproducibility of the preparation technique. The results are shown in table 4.1.

Although there were differences in the performance of the two catalysts these are well within the reproducibility of the experimental procedures (section 3.2).

Table 4.1: Comparison of different 10%Co/γ-Al_2O_3 batches

Catalyst	Temp	CH_4	Selectivity (%)		H_2/CO
	(°C)	conv. (%)	CO	CO_2	ratio
10%Co/γ-Al_2O_3	486	0,0	0,0	0,0	—
(original batch)	849	48,7	86,6	12,0	1,8
	1041	94,9	98,5	1,5	2,1
10%Co/γ-Al_2O_3	486	0,1	78,5	21,5	5,8
(new batch)	845	64,4	94,2	5,8	1,5
	1042	97,8	100,0	0,0	1,6

4.5.2 Pre-treatment

TPR and XRD techniques were used by Arnoldy and Moulijn [65] to study the properties of a reduced cobalt catalyst which had undergone precalcination at various temperatures. A 9,1%CoO/γ-Al_2O_3 (*i.e.* 7,2% Co metal) material was prepared from cobaltous nitrate and calcined at temperatures from 107°C to 1007°C. The catalyst was heated from room temperature at a rate of 10°C per minute to the desired temperature, and then held at that temperature for a period of 30 minutes.

Catalysts calcined between 100°C and 350°C showed a reduction peak around 225°C, which was attributed to the decomposition of the nitrate. The nitrates were completely removed by calcination above 375°C.

Arnoldy and Moulijn, distinguished from their TPR study, cobalt in four different chemical environments. They observed cobalt as Co_3O_4, a Co^{3+} phase on the surface, a Co^{2+} phase on the surface, and a $CoAl_2O_4$ spinel structure. The relative amounts of these four species depended on the calcination temperature.

Table 4.2: The assignment of TPR reduction temperatures for cobalt species on Co/Al_2O_3 catalysts

Cobalt species	TPR reduction temperature (°C)	
	Arnoldy and Moulijn	Tung, Yeh and Hong
Bulk Co_3O_4	277-357[a]	227
Overlayer Co^{3+}	467	357
Overlayer Co^{2+}	602	597
Spinel	837-957	>577

[a] increased with calcination temperature.
Reproduced from [66].

An investigation into the effect of metal loading on the four cobalt oxide species proposed by Arnoldy and Moulijn was conducted by Tung, Yeh and Hong [66]. In their study the calcination temperature was held constant at 500°C while the cobalt metal loading was varied from 0,1 to 16%. Table 4.2 shows the different TPR reduction temperatures proposed by the two groups.

While the constant loading experiment gave detailed information on the diffusion of cobalt oxides into the support, the variable loading tests gave insight into the layer structures of cobalt oxide deposited on the support. Both groups agreed on the structures formed, but there was a disagreement over the position of the bulk Co_3O_4 peak in the TPR spectra.

The amount of cobalt oxides migrating into the top layers of the alumina to form the spinel depended on the calcination temperature. With higher calcination temperature a larger fraction of cobalt oxides converted into the spinel structure, and a smaller fraction remained on the overlayer to form bulk Co_3O_4 structure.

In this research project the cobalt catalysts supported on γ-Al_2O_3 were calcined at 800°C (section 2.2.2). From the work by Arnoldy and Moulijn [65] these catalysts should consist of diffused Co^{2+} ions in a diluted Co^{2+}-Al^{3+} spinel. As expected, TPR studies of these catalysts calcined at 800°C showed only a single reduction peak above 825°C. This peak was barely distinguishable on an otherwise flat TPR

spectra, indicating that almost all of the cobalt had diffused into the spinel structure. Therefore, during *in situ* reduction at 600°C no changes in the structure of these catalysts would have been anticipated. Any further reduction of Co^{2+} to cobalt metal would take place in the feed gas at temperatures above the calcination temperature of 800°C.

4.6 Cobalt on C/γ-Al_2O_3

4.6.1 Preparation

Cobalt acetate and nitric acid were used to prepare the 3% and 10% cobalt on C/γ-Al_2O_3 catalysts (section 2.2.2). It proved difficult to achieve higher loadings using these starting materials. Thus cobaltous nitrate and ethanol were used to prepare a 14% loading of cobalt on the same support. It appears from the reactor results that the heat pre-treatment of the nitrate-ethanol catalyst was inappropriate. As a result it took much longer to reach steady state than in the presence of the acetate-nitric acid prepared catalysts (table 3.8).

Two batches of 10%Co/C/γ-Al_2O_3 were prepared to test the reproducibility of the preparation technique used for this catalyst. The results are shown in table 4.3. The differences in the performance of the two catalysts tested are well within the reproducibility of the experimental procedures (section 3.2).

Table 4.3: Comparison of different 10%Co/C/γ-Al_2O_3 batches

Catalyst	Temp	CH_4	Selectivity (%)		H_2/CO
	(°C)	conv. (%)	CO	CO_2	ratio
10%Co/C/γ-Al_2O_3	482	0,6	5,6	94,4	9,0
(original batch)	802	32,4	81,0	17,6	1,8
	1001	97,0	99,9	0,1	2,0
10%Co/C/γ-Al_2O_3	472	1,0	37,5	62,5	0,7
(new batch)	820	46,0	90,9	9,1	1,9
	1010	92,0	99,6	0,4	1,8

4.6.2 Loading

The effect of cobalt loading on the activity and selectivity of C/γ-Al_2O_3 based catalysts, at a reaction temperature of ~1000°C, is shown in figure 4.2. The trends established here are also observed over the pure alumina-based supports: at constant temperature, as the cobalt loading increases, so the activity increases. Selectivity also improves dramatically with the introduction of the metal, but shows little improvement as the metal content is increased above 3%. Thus there seems to be little advantage in cobalt metal loadings in excess of 10%.

4.6.3 Pre-treatment

The cobalt supported on carbon-coated alumina catalysts were only calcined at 200°C (section 2.2.2). Since there are no published studies of the temperature programmed reduction of these catalysts, a study was conducted to assess the effect that a carbon coating would have on the cobalt TPR spectra. Figure 4.3 shows the TPR spectra obtained from the C/γ-Al_2O_3 support and the 10%Co/C/γ-Al_2O_3 material.

In spite of the carbon coating on the alumina the TPR obtained for 10%Co/C/γ-Al_2O_3 was similar to that found for Co/γ-Al_2O_3 (section 4.5.2). The peaks observed around 250°C, 450°C and 600°C are attributable to the decomposition of the nitrate,

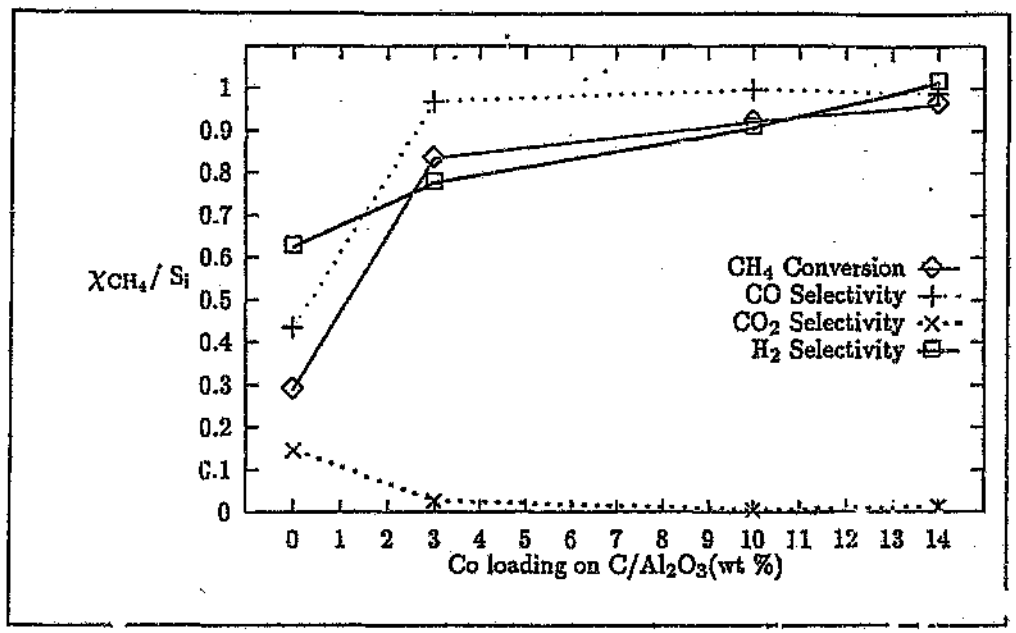

Figure 4.2: Effect of varying cobalt loading on $Co/C/Al_2O_3$ catalysts (1000°C)

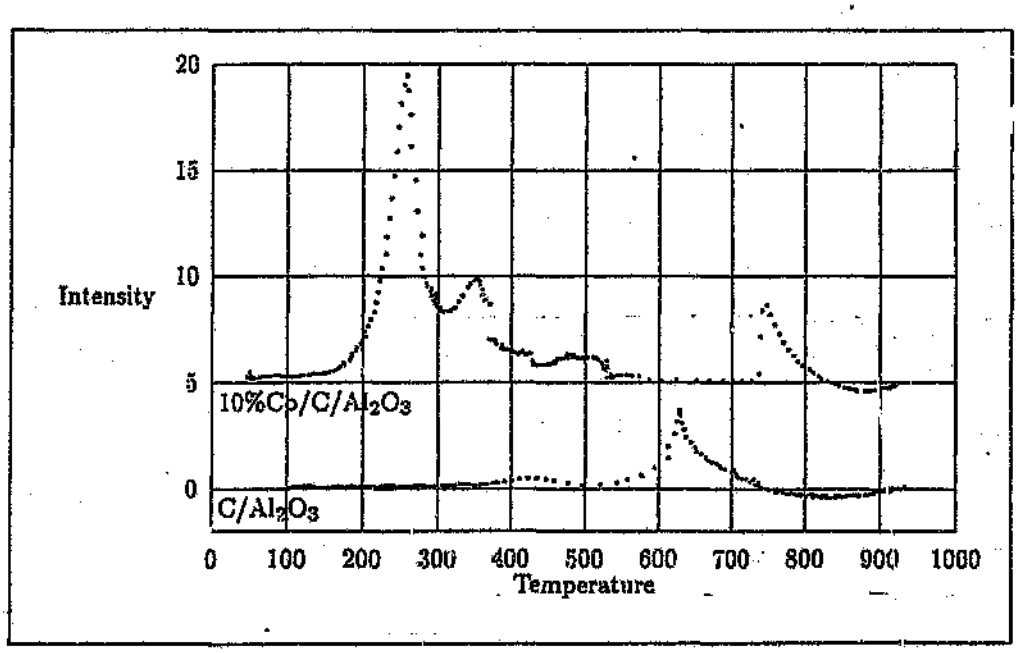

Figure 4.3: TPR of $C/\gamma\text{-}Al_2O_3$ and $10\%Co/C/\gamma\text{-}Al_2O_3$

reduction to Co_3O_4 and a surface Co^{3+} species, respectively [65]. These are all reported to be surface species. The last peak observed, around 750°C, falls between the regions which Arnoldy and Moulijn described as corresponding to reduction to the surface Co^{2+} species and the spinel structure respectively (section 4.5.2). It is likely, due to the carbon layer, that this corresponds to reduction to the Co^{2+} surface species, rather than diffusion into the alumina and reduction to the spinel.

Under reaction conditions the carbon layer burned off the pure C/γ-Al_2O_3 support material (section 3.1.6). From the XRD study conducted and the presence of the blue zone in the post reaction catalyst $CoAl_2O_4$ must be present. This implies that the carbon layer is not necessarily stable under the reaction conditions. It is likely that the carbon layer burns off in the reactor, resulting in a pure gamma alumina support. This would explain the similarity between the XRD patterns found for the C/γ-Al_2O_3 and pure alumina-supported catalysts (figure 3.5).

Thus, during the *in situ* reduction of $10\%Co/C/\gamma$-Al_2O_3 (calcined at 200°C) at 600°C, it would be expected that the nitrate would decompose, and that Co_3O_4 would reduce to surface Co^{3+} and perhaps even surface Co^{2+}. At high temperatures in the reaction mixture, after the combustion of the carbon layer, further reduction to cobalt metal supported on a spinel layer takes place.

4.6.4 The blue zone

Lunsford *et al* [33] found that the composition of their Ni/Al_2O_3 catalyst bed varied with reaction temperature. After precalcination at 600°C, the nickel in the near surface region was predominantly $NiAl_2O_4$. This material exhibited a moderate 6% conversion of methane to CO_2 and H_2O at 550°C. This increased to 16% at 700°C. With further increases in temperature and consequently oxygen consumption in the methane oxidation reaction, the oxygen concentration decreased. Eventually, at 750°C, the layer of $NiAl_2O_4$ near the inlet had decomposed thermally, regenerating

α-Al_2O_3 and a surface NiO phase. Since the NiO phase is a better catalyst for the reaction than $NiAl_2O_4$, complete consumption of the feed oxygen occurred over the NiO phase, resulting in higher methane conversion to CO_2 and H_2O. The highly exothermic complete combustion of methane resulted in a 50°C rise in temperature over the narrow NiO zone.

The resulting $CH_4/CO_2/H_2O$ mixture quickly reduced the remainder of the bed to metallic Ni supported on α-Al_2O_3. The metal then catalysed the reforming of the remaining methane. This sequence of reactions is the same as that proposed by Prettre [32] and his co-workers (see section 1.4.1).

After the initial formation of metallic nickel at 750°C, the composition of the reaction mixture was found to conform to that expected at thermodynamic equilibrium corresponding to the catalyst bed temperature. This occurred throughout the range 450 - 900°C. Within this temperature range, as the temperature decreased from 900°C to 450°C, the NiO zone broadened and moved downward. This effect was found to be completely reversible, within this temperature range. However, at reaction temperatures below 450°C, or at exceptionally low contact times, unreacted O_2 breaks through the NiO zone causing the reoxidation of Ni to $NiAl_2O_4$. After this all reaction ceased.

Two distinct zones in the catalyst bed were observed after reaction for all the alumina-based catalysts tested in this work, in the modified reactor (section 3.3.3). The upper zone had a characteristic blue colour, which was attributed to the presence of $CoAl_2O_4$ [47] and confirmed by XRD analysis (figure 3.8). Rhombohedral alumina and cobalt metal in a cubic structure (table 3.12) were also found in the blue zone. The second zone was grey in appearance and was found to consist of cubic metallic cobalt and rhombohedral alumina.

Bai and co-workers [67] found no appreciable reduction of bulk $CoAl_2O_4$ in an Ar/H_2 (85/15) atmosphere at 320°C. Increasing the temperature to 950°C for 4 hours resulted in an 8,37% weight loss, which corresponded to a reduction of 92,5% of the

Table 4.4: Partial oxidation over the blue zone

Temp (°C)	CH_4 conv. (%)	Selectivity (%) CO	CO_2	H_2/CO ratio
479	0,3	100,0	0,0	0,2
818	20,2	81,8	16,3	2,5
1016	47,5	78,8	5,6	1,6

reducible cobalt present. In a pure hydrogen atmosphere at the same temperature, a reduction of 98,7% of the reducible cobalt was achieved. X-ray analysis showed this existed as cubic cobalt. In other words, the authors reported a reduction of Co_3O_4 to surface cubic cobalt. Hence it is entirely possible that the diffusion of cobalt metal into alumina (section 4.5.2) is reversible, especially at higher loadings. The catalysts tested by Bai and co-workers contained 11,29% cobalt on γ-Al_2O_3.

Approximately 20 mg of the blue zone of a catalyst was separated from the grey zone after reaction and tested in the same manner as a regular catalyst. The results are shown in table 4.4. Considering the effect of the increased contact time (section 4.2) and comparing the results to those of the deactivated catalyst (table 4.5) it is clear that this zone was active. Further, after this catalyst was removed from the reactor it too exhibited the characteristic blue and grey zones.

Schmidt and his co-workers also described the formation of two zones on a 3% cobalt supported on an alumina monolith catalyst that they studied [47]. The formation of $CoAl_2O_4$ was noted and it was assumed that this zone was inactive for the partial oxidation of methane to synthesis gas. The reaction mechanism proposed by these workers (section 1.4.1) would have led them to believe that this zone played no part in the catalytic reaction, and that the spinel would grow from the leading edge of the monolith ultimately deactivating the entire catalyst. Since the loading used by Schmidt *et al* was only 3% it is possible that all the metal diffused into the alumina, and was in too low a concentration to be reduced back to surface metal. Further studies by Schmidt, either confirming the growth of the "deactivated" zone or the absence of cobalt metal, would have confirmed or denied this hypothesis.

Table 4.5: Partial oxidation over the deactivated 10%Co/C/γ-Al_2O_3 at 938°C

Time	CH_4	Selectivity (%)		H_2/CO
(hours)	conv. (%)	CO	CO_2	ratio
1	8,2	67,1	21,4	0,8
4	6,0	54,5	37,2	1,3
10	9,7	63,0	26,5	0,7
15	6,0	62,8	29,3	1,0

It is therefore proposed that the cobalt supported on alumina catalysts tested in this research behaved in a similar fashion to the nickel on alumina catalysts studied by Lunsford and his co-workers. The formation of the zones observed are consistent with the sequential combustion and reforming mechanism proposed by Prettre [32] and his co-workers.

4.6.5 Deactivation

In this work, during one of the reactions, a regulator controlling the methane flow malfunctioned (table B.21). This resulted in a dramatic decrease in the flow of methane, and a corresponding increase in oxygen to the reactor in the presence of a 10%Co/γ-Al_2O_3 catalyst (labelled 10%Co/C/γ-Al_2O_3 deactivated, table 3.12). It was noted that after this reaction that the catalyst consisted of a single blue zone, rather than the blue and grey zones usually observed.

Unlike the typical blue zone formed in other reactions (section 4.6.4) this catalyst showed no restoration of activity or selectivity upon retesting, even after 15 hours on line (table 4.5).

Under normal conditions CH_4 in the feed reacts with all the O_2 to form CO_2. The remaining CH_4 is then reformed to CO and H_2. During the combustion stage large amounts of energy are evolved, but these are consumed by the subsequent endothermic reforming reactions (section 1.4.1).

In the presence of excess O_2, as was the case during the regulator malfunction, methane is completely converted to CO_2, but since there was no methane it could not be reformed. In addition, the energy generated by the reaction is not consumed by subsequent reactions, resulting in high catalyst-surface temperatures. The result is a high-temp oxidising environment.

XRD studies (section 3.3.3, table 3.12 and figure 3.8) of the deactivated catalyst showed that it differed from the active catalysts in one respect: there was no evidence of cobalt as metal in the catalyst. Thus, the active phase must be the cubic metallic cobalt. Hirakawa *et al* [44] reached the same conclusion for reduced $Ca_{0,8}Sr_{0,2}Ti_{0,8}Co_{0,2}O_{3-\delta}$ (section 1.4.4).

Since no metal was observed on the cooler downstream regions of the reactor after retesting of the deactivated catalyst, it is unlikely that metallic cobalt or a cobalt oxide volatilised. Under the oxidising conditions caused by the regulator malfunction, it is likely that most of the metal diffused into the support, forming $CoAl_2O_4$. This is the same process that occurs during calcination (section 4.5.2). Under the extreme conditions in the reactor at that time, the metal may have diffused into the core of the catalyst, leaving a thin surface layer of alumina surrounding the $CoAl_2O_4$ core. This outer layer, exposed to heat and oxidising conditions, might then have been transformed into low surface area α-Al_2O_3, thus trapping the metal in the core, not allowing re-reduction to the active metal phase. This would explain why no metal was observed downstream, the blue colour of the catalyst and the loss of activity.

Chapter 5

Conclusions

10%Co/γ-Al_2O_3 and 10%Co/C/γ-Al_2O_3 were found to convert a 2:1, methane : oxygen feed, with a contact time of 0,01 s, to greater than 90% synthesis gas at ~1000°C.

Based on the study of the above catalysts it was proposed that the reaction of partial oxidation to synthesis gas takes place via a two-stage reaction in the presence of cobalt metal. The first step involves combustion of CH_4 to CO_2, which consumes all the feed O_2, while the second involves reforming of the excess CH_4 and CO_2. The overall reaction is the partial oxidation of methane to syngas, a mildly exothermic reaction.

The catalyst thus performs two distinct roles in two distinct zones of the catalyst bed. The blue zone, which first comes into contact with the feed and involves the highly-exothermic combustion reactions, is subject to high temperatures and oxygen concentrations. This zone is blue in appearance and contains cobalt as $CoAl_2O_4$ and cubic metal. The $CoAl_2O_4$ arises from the diffusion of the metal into the support under the reaction conditions. Thus this zone consists of an alumina core with a layer of $CoAl_2O_4$ and surface metallic cobalt.

The second zone forms at that point where there is no longer any oxygen in the gas phase and therefore is associated with the reforming reactions. These reactions utilise the energy from the combustion reactions to drive the endothermic reforming reactions. In this region cobalt predominantly exists as metallic cobalt, while the alumina exists in the rhombohedral phase. The structure of the catalyst pellets in this zone is the same as for those in the blue zone, except that the concentration of metallic cobalt on the surface is higher giving this zone its grey metallic colour.

It is thus proposed that the active phase for both reactions is metallic cobalt. Volatilisation of the metal is prevented by the ability of the metal to diffuse into the alumina support under combustion conditions. Activity for reduction of CO_2 is regained in the second zone by the re-reduction of the $CoAl_2O_4$ back to metallic cobalt. However, when exposed to extreme temperatures and high oxygen concentrations, the catalyst's structure collapses, and this no longer allows the diffusion of cobalt, and hence results in catalyst deactivation.

Not only are these catalysts easily prepared by the incipient wetness technique, from a relatively inexpensive metal and widely available support materials, but the catalyst shows no evidence of coking.

In order to validate this understanding of the catalyst's behaviour, a catalyst was designed to embody the characteristics outlined above as being necessary for stable, active and selective conversion of methane to synthesis gas. A catalyst, called A_B^R was synthesised, which proved to be more active, selective and stable than the catalysts mentioned above. The materials required for this catalyst are as inexpensive and as readily available as those required for the cobalt catalysts discussed in this work, prepared by the incipient wetness technique. However, the preparation procedures for the A_B^R catalyst are more complex.

In section 1.5 the aims of this project were presented in two parts. These aims were firstly to find a cheap, robust and easily manufactured catalyst capable of active and selective syngas production. The catalyst was to operate at low contact times,

and not coke or deactivate. The second aim was to gain an understanding of the behaviour of this catalyst using the available literature and the studies conducted in the project. The investigation of the cobalt on γ-Al_2O_3 catalysts met the stated aims and provided the background knowledge to be able to design a catalyst capable of improved performance, the A^B_B catalyst.

Appendix A

The crystal structure of alumina

Many oxides, including Al_2O_3 show close packing of their oxygen atoms. There are two types, hexagonal and cubic. Consider a single layer of oxygen anions, considered to behave as hard spheres, as shown in figure A.1. The layer has a trigonal symmetry, with each oxygen "touching" 6 other anions in the layer. A second layer, similar to the first, is positioned such that each anion is positioned above a hole in the first.

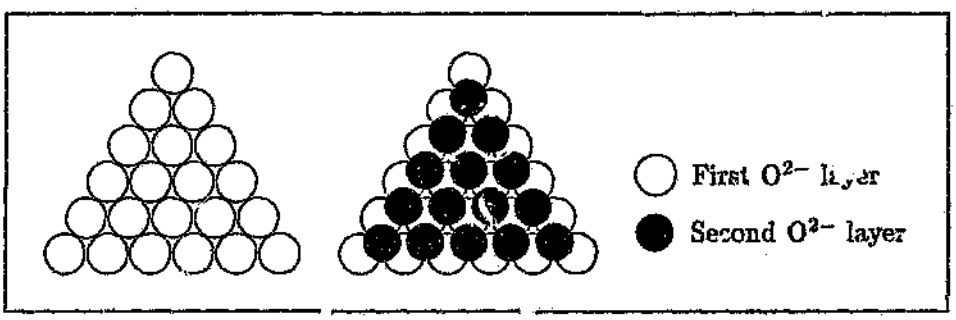

Figure A.1: Single and double layers of close packed spheres

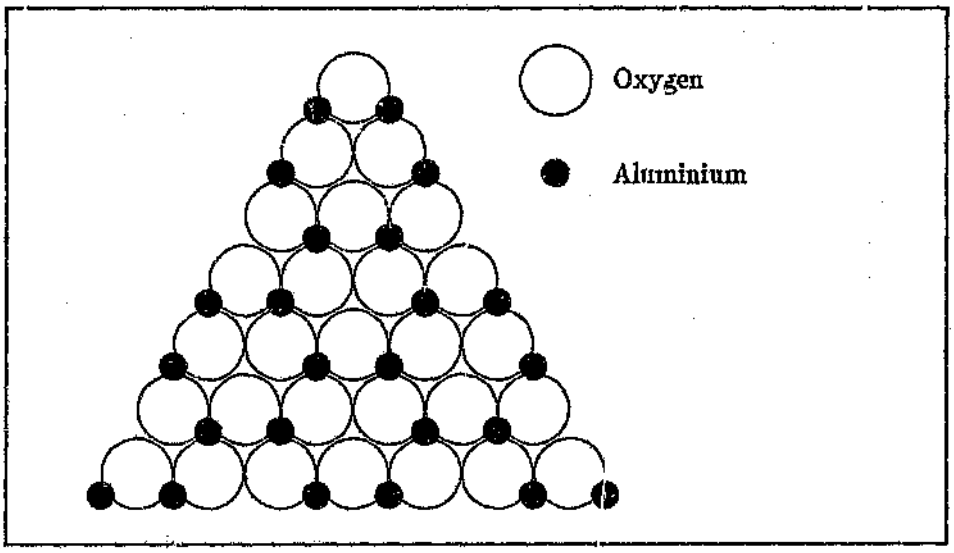

Figure A.2: Structure of α-Al_2O_3 showing Al^{3+} positions

In **hexagonal close-packed** the third layer is placed in the same position as the first. α-Al_2O_3 has this type of packing, where in place of the second oxygen anion layer, there is a layer of Al^{3+}. Since there are equal numbers of sites in both layers, to maintain electrical neutrality one of every three sites must remain vacant in the metal oxide, figure A.2.

In **cubic close-packed** or face-centred cubic the third layer is placed above another set of holes. The fourth layer follows the trend, which is the same position as the first layer. This type of packing applies to γ-Al_2O_3. There are two types of holes in this type of packing, octahedral and tetrahedral[1]. Figure A.3 shows a model of γ-Al_2O_3 with both sites. The two layers are packed ABABABAB...[69].

[1] A good explanation of the differences between the two can be found in *Inorganic Chemistry* [68].

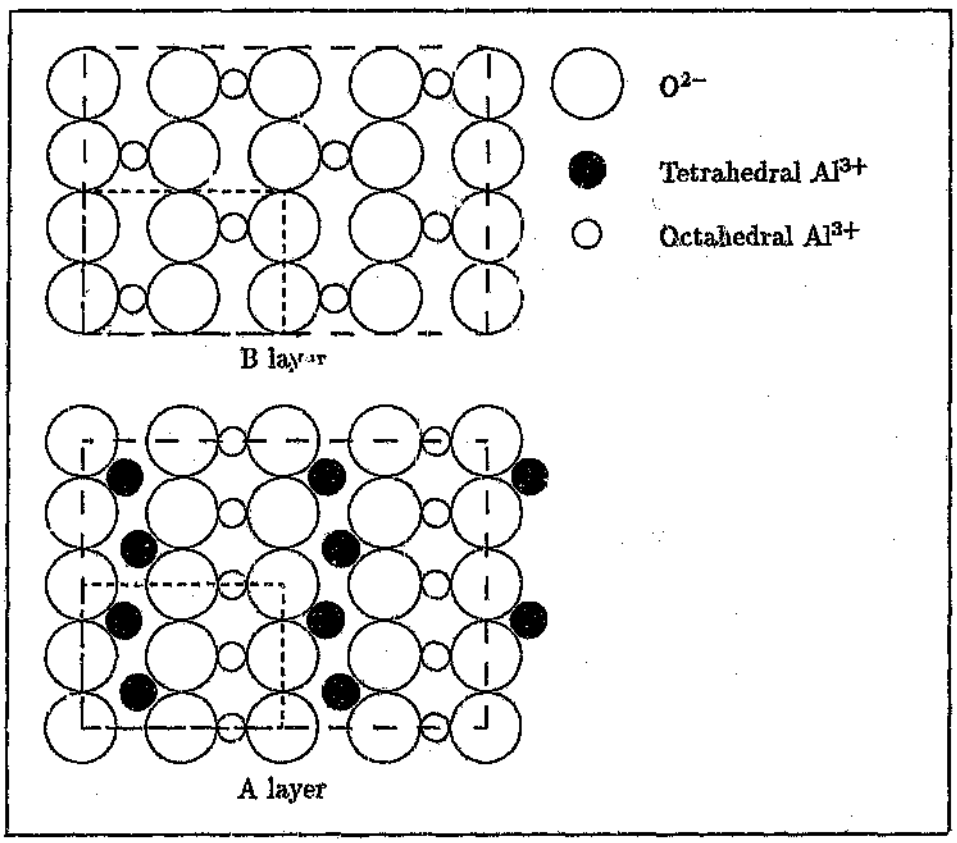

Figure A.3: Structure of γ-Al_2O_3 showing tetrahedral and octahedral Al^{3+}

Appendix B

Reactor studies — all data

In this appendix all the results obtained from the reactor studies are presented in their entirety. All catalysts or supports were reduced *in situ*, for 30 minutes, at 600°C, in ~180 ml/min of H_2. In a feed mixture of 180 ml/min CH_4 and 426 ml/min air, the experimental procedures detailed in section 2.1.6 were carried out. Explanations of the calculations performed to obtain the results reported are given in section 2.1.7.

After the title of each table in this appendix, the number of the dependant main-body table is given in parenthesis.

Original reactor

These experiments were conducted in the original reactor (section 2.1.1) and used nitrogen as the carrier gas in the TCD (section 2.1.4).

Table B.1: Partial oxidation in the gas-phase — original reactor (Table 3.1)

Temp	Time	CH_4	Selectivity (%)					
(°C)	(h)	conv. (%)	CO	CO_2	C_2H_4	C_2H_2	C_3H_6	H_2/CO
756	0,5	0,5	50,0	19,5	0,0	0,0	30,5	2,1
760	1,0	0,8	43,5	13,7	7,0	0,0	35,7	1,9
859	1,5	3,5	58,3	6,7	23,5	0,0	11,5	1,3
860	2,0	5,3	54,4	5,5	27,4	0,0	12,8	1,3
959	2,5	8,1	73,9	1,1	21,4	0,0	3,5	—
959	3,0	10,2	86,0	0,8	11,5	0,0	1,7	2,0
959	3,5	3,2	72,1	0,0	24,4	0,0	3,7	2,7
959	4,0	11,6	89,1	0,4	9,6	0,0	0,9	1,9
960	4,5	13,1	87,8	0,6	8,3	0,0	3,4	1,9
961	5,0	14,5	92,3	0,2	7,5	0,0	0,0	1,8

Table B.2: Partial oxidation over monometallic Co on γ-Al_2O_3 (Table 3.3)

Metal	Temp	CH_4	Selectivity (%)		
Loading	(°C)	conv. (%)	CO	CO_2	H_2/CO
none	668	5,2	61,5	9,6	0,9
	767	10,5	54,6	11,2	1,1
	872	18,2	69,8	7,7	1,1
	972	18,7	81,7	1,9	1,8
1%Co[a]	664	9,5	59,7	20,5	1,1
	769	19,6	55,5	21,5	0,9
	842	22,8	81,3	7,2	0,9
	972	41,9	99,3	0,2	1,8
1%Co[b]	667	8,9	63,0	13,9	1,1
	774	19,5	62,0	19,8	0,8
	870	15,4	70,8	7,6	1,2
	962	35,4	93,6	2,1	1,7

[a] Uncalcined 1%Co/γ-Al_2O_3 — section 2.2.2.

[b] 1%Co/γ-Al_2O_3 calcined at 800°C — section 2.2.2,

Table B.3: Partial oxidation over monometallic Ru on γ-Al_2O_3 (Table 3.3)

Metal Loading	Temp (°C)	CH_4 conv. (%)	Selectivity (%) CO	CO_2	H_2/CO
0,1%Ru[a]	485	13,9	69,0	31,0	2,4
	572	19,6	88,7	11,3	2,0
	664	23,7	96,5	3,5	1,8
	763	27,6	98,5	0,5	1,8
	862	29,4	98,6	0,1	1,8
	954	30,9	98,7	0,0	1,8

[a] Uncalcined 1%Ru/γ-Al_2O_3 — section 2.2.2.

Table B.4: Partial oxidation over bimetallic Co-Ru on γ-Al_2O_3 (Table 3.3)

Metal Loading	Temp (°C)	CH_4 conv. (%)	Selectivity (%) CO	CO_2	H_2/CO
0,1%Ru-1%Co[a]	485	6,1	42,6	57,4	2,7
	578	10,8	76,0	24,0	1,8
	670	14,8	88,9	10,7	1,7
	764	22,2	98,4	0,3	1,8
	862	24,3	97,4	0,1	1,8
	957	20,4	97,7	0,0	2,3
0,1%Ru-1%Co[b]	484	8,8	53,9	46,1	3,0
	573	19,7	88,1	11,9	1,4
	666	20,1	95,9	3,7	1,7
	761	23,7	97,6	0,6	1,8
	860	24,1	97,3	0,0	1,8
	956	25,9	98,5	0,0	1,8

[a] Uncalcined 1%Co/γ-Al_2O_3 — section 2.2.2.

[b] 1%Co/γ-Al_2O_3 calcined at 800°C — section 2.2.2.

Table B.5: Screening — partial oxidation over 3%Co/γ-Al_2O_3 (Table 3.4)

Metal	Temp	Time	CH_4	Selectivity (%)					
Loading	(°C)	(h)	conv. (%)	CO	CO_2	C_2H_4	C_2H_2	C_3H_6	H_2/CO
3%Co	476	0,5	0,0	0,0	0,0	0,0	0,0	0,0	—
	476	1,0	0,0	0,0	0,0	0,0	0,0	0,0	—
	575	1,5	0,4	0,0	100,0	0,0	0,0	0,0	—
	575	2,0	0,3	0,0	100,0	0,0	0,0	0,0	—
	669	2,5	5,5	56,0	29,4	3,4	0,0	11,2	—
	670	3,0	5,8	56,4	28,3	1,7	0,0	10,6	1,6
	768	3,5	8,3	54,6	23,9	12,5	0,0	9,0	—
	769	4,0	8,0	56,0	21,6	12,9	0,0	9,6	0,9
	868	4,5	11,9	61,6	11,7	24,4	0,0	2,4	—
	869	5,0	13,5	64,5	9,5	24,6	0,0	1,3	1,0
	958	5,5	24,3	98,5	0,0	1,5	0,0	0,0	—
	959	6,0	25,0	98,9	0,1	1,0	0,0	0,0	—
	959	6,5	25,4	98,9	0,0	1,1	0,0	0,0	—
	959	7,0	26,1	98,5	0,1	1,4	0,0	0,0	1,3

Table B.6: Screening — partial oxidation over 3%Co/C/γ-Al_2O_3 (Table 3.4)

Metal	Temp	Time	CH_4	Selectivity (%)					
Loading	(°C)	(h)	conv. (%)	CO	CO_2	C_2H_4	C_2H_2	C_3H_6	H_2/CO
3%Co	473	0,5	0,35	0,0	100,0	0,0	0,0	0,0	—
	473	1,0	0,18	0,0	100,0	0,0	0,0	0,0	—
	568	1,5	0,13	0,0	100,0	0,0	0,0	0,0	—
	564	2,0	0,13	0,0	100,0	0,0	0,0	0,0	—
	665	2,5	2,79	64,3	26,7	0,7	0,0	8,2	—
	666	3,0	2,89	67,9	20,7	1,9	0,0	9,4	1,4
	761	3,5	4,96	60,4	22,8	6,9	0,0	9,9	—
	764	4,0	3,97	61,6	20,0	10,6	0,0	8,8	1,0
	862	4,5	7,48	63,8	10,9	21,2	0,0	4,1	—
	863	5,0	8,61	62,3	10,9	22,5	0,0	4,3	1,1
	955	5,5	15,58	96,6	0,0	2,8	0,0	0,6	—
	955	6,0	20,30	97,8	0,0	2,2	0,0	0,0	—
	955	6,5	24,31	98,2	0,0	1,6	0,0	0,2	—
	956	7,0	26,33	98,2	0,0	1,7	0,0	0,2	1,7

Table B.7: Screening — partial oxidation over 3%Co/MgO (Table 3.4)

Metal Loading	Temp (°C)	Time (h)	CH_4 conv. (%)	Selectivity (%)					H_2/CO
				CO	CO_2	C_2H_4	C_2H_2	C_3H_6	
3%Co	473	0,5	0,1	0,0	100,0	0,0	0,0	0,0	—
	472	1,0	0,0	0,0	0,0	0,0	0,0	0,0	—
	565	1,5	0,2	0,0	84,6	0,0	0,0	15,4	—
	566	2,0	0,1	0,0	100,0	0,0	0,0	0,0	—
	662	2,5	2,5	29,9	43,9	0,0	0,0	26,2	—
	663	3,0	2,0	21,3	48,0	6,1	0,0	24,6	1,4
	760	3,5	7,1	14,6	38,[illegible]	[illegible]7,3	0,0	20,7	—
	760	4,0	7,1	17,6	35,7	25,1	0,0	21,6	1,5
	859	4,5	6,5	12,0	39,1	41,9	0,0	7,0	—
	860	5,0	6,5	14,4	35,6	42,5	0,0	7,5	3,1
	951	5,5	16,2	95,5	0,0	4,2	0,0	0,3	—
	952	6,0	16,8	97,2	0,0	2,2	0,0	0,7	—
	952	6,5	16,7	93,1	0,0	2,6	0,0	4,4	—
	953	7,0	17,8	92,8	0,0	5,2	0,0	2,0	1,9

Table B.8: Screening — partial oxidation over 3%Co/TiO_2 (Table 3.4)

Metal Loading	Temp (°C)	Time (h)	CH_4 conv. (%)	Selectivity (%)					H_2/CO
				CO	CO_2	C_2H_4	C_2H_2	C_3H_6	
3%Co	475	0,5	0,1	0,0	100,0	0,0	0,0	0,0	—
	474	1,0	0,1	0,0	100,0	0,0	0,0	0,0	—
	568	1,5	0,2	0,0	100,0	0,0	0,0	0,0	—
	569	2,0	0,2	0,0	100,0	0,0	0,0	0,0	—
	663	2,5	1,4	33,3	27,9	8,3	0,0	30,5	—
	664	3,0	1,6	29,5	24,7	12,4	0,0	33,4	1,0
	763	3,5	10,7	38,2	18,0	26,8	0,0	17,1	—
	764	4,0	11,4	40,5	15,7	28,4	0,0	15,5	0,8
	867	4,5	18,0	77,4	13,9	7,9	0,0	1,1	—
	867	5,0	20,0	81,9	12,1	4,9	0,0	1,1	1,5
	954	5,5	32,1	98,9	0,5	0,7	0,0	0,0	—
	955	6,0	32,8	98,[illegible]	0,4	0,8	0,0	0,0	—
	955	6,5	33,4	99,1	0,2	0,7	0,0	0,0	—
	955	7,0	31,4	99,0	0,2	0,8	0,0	0,0	1,8

Table B.9: Screening — partial oxidation over 3%Co/SiO_2 (Tables 3.4 and 3.5)

Metal Loading	Temp (°C)	Time (h)	CH_4 conv. (%)	Selectivity (%)					H_2/CO
				CO	CO_2	C_2H_4	C_2H_2	C_3H_6	
none	474	0,5	0,0	0,0	0,0	0,0	0,0	0,0	—
	473	1,0	0,0	0,0	0,0	0,0	0,0	0,0	—
	565	1,5	1,4	77,8	10,8	0,0	0,0	11,4	—
	566	2,0	1,3	76,3	11.6	0,0	0,0	12,2	0,5
	664	2,5	16,1	61,2	8,1	19,0	0,0	11,7	—
	666	3,0	15,5	61,7	8,1	18,4	0,0	11,8	0,3
	762	3,5	15,7	66,0	5,0	22,4	0,0	6,6	—
	764	4,0	24,8	73,3	4,3	17,8	0,0	4,7	0,4
	856	4,5	22,9	72,5	6,3	20,1	0,0	1,1	—
	856	5,0	24,5	73,8	6,6	18,5	0,0	1,1	0,5
	953	5,5	54,2	79,5	13,3	7,1	0,0	0,1	—
	953	6,0	41,8	79,6	12,0	8,4	0,0	0,0	—
	952	6,5	27,8	79,2	7,4	13,4	0,0	0,0	—
	95?	7,0	46,5	81,8	10,4	8,0	0,0	0,0	0,5
3%Co	477	0,5	0,5	0,0	100,0	0,0	0,0	0,0	—
	475	1,0	0,6	0,0	100,0	0,0	0,0	0,0	—
	568	1,5	1,0	0,0	100,0	0,0	0,0	0,0	—
	569	2,0	0,5	0,0	100,0	0,0	0,0	0,0	—
	663	2,5	2,1	0,0	84,9	0,0	0,0	15,1	—
	664	3,0	1,9	0,0	85,3	0,0	0,0	14,7	—
	762	3,5	7,9	16,5	50,5	18,3	0,0	14,7	—
	762	4,0	8,0	16,4	47,9	20,7	0,0	15,0	1,5
	864	4,5	14,5	42,1	23,9	30,2	0,0	3,8	—
	859	5,0	5,4	23,7	25,4	41,6	0,0	9,3	2,0
	948	5,5	26,6	98,9	0,0	1,1	0,0	0,0	—
	949	6,0	26,9	98,9	0,0	1,1	0,0	0,0	—
	949	6,5	27,5	99,0	0,0	1,0	0,0	0,0	—
	949	7,0	28,8	99,1	0,0	0,9	0,0	0,0	1,8

Modified reactor

These experiments were conducted in the modified reactor (section 2.1.1). At the same time argon was introduced as the carrier gas for the TCD (section 2.1.4), which allowed an independent method of evaluating the carbon balance (sections 2.1.4, 2.1.5 and 2.1.7).

Table B.10: Partial oxidation in the gas-phase — modified reactor (Table 3.2)

Temp	Time	CH_4		Selectivity (%)					
(°C)	(h)	conv. (%)	CO	CO_2	C_2H_4	C_2H_2	C_3H_6	H_2/CO	B'
435	0,5	1,36	0,0	100,0	0,0	0,0	0,0	—	1,03
490	1,0	0,00	0,0	0,0	0,0	0,0	0,0	—	0,98
545	1,5	0,35	0,0	100,0	0,0	0,0	0,0	—	0,93
601	2,0	0,02	100,0	0,0	0,0	0,0	0,0	0,62	0,93
657	2,5	0,05	0,0	0,0	0,0	0,0	100,0	—	0,99
712	3,0	0,00	0,0	0,0	0,0	0,0	0,0	—	0,99
765	3,5	0,00	0,0	0,0	0,0	0,0	0,0	—	0,98
874	4,0	0,06	0,0	0,0	0,0	0,0	100,0	—	1,01
927	4,5	0,28	18,9	0,0	0,0	0,0	81,1	0,77	1,07
980	5,0	0,88	4,6	0,0	4,2	0,0	71,2	0,86	1,08

Table B.11: Partial oxidation over cobalt on SiO_2 (Table 3.5)

Metal Loading	Temp (°C)	Time (h)	CH_4 conv. (%)	Selectivity (%)					H_2/CO	B'
				CO	CO_2	C_2H_4	C_2H_2	C_3H_6		
none	444	0,5	0,1	0,0	100,0	0,0	0,0	0,0	—	1,01
	772	1,0	0,4	77,6	22,4	0,0	0,0	0,0	0,6	1,04
	990	1,5	6,0	53,7	3,5	13,4	0,0	29,4	0,6	1,02
	990	2,0	5,0	51,2	3,5	13,2	0,0	32,1	0,7	0,99
	990	2,5	3,8	54,1	2,6	11,0	0,0	32,3	0,8	0,97
	990	3,0	4,2	49,4	4,8	11,6	0,0	34,2	0,7	0,97
3%Co	462	0,5	0,5	13,0	87,0	0,0	0,0	0,0	0,5	1,01
	789	1,0	0,7	40,5	59,5	0,0	0,0	0,0	0,4	1,01
	1005	1,5	6,9	49,2	5,4	16,2	0,0	29,2	0,7	0,94
	1005	2,0	6,5	51,9	6,2	13,5	0,0	28,4	0,6	1,01
	1005	2,5	5,3	49,3	4,4	13,9	0,0	32,4	0,7	1,00
	1005	3,0	4,8	45,7	5,8	13,9	0,0	34,7	0,7	1,03
10%Co	468	0,5	0,6	3,1	96,9	0,0	0,0	0,0	0,4	0,99
	796	1,0	2,2	31,5	59,3	0,0	0,0	9,2	0,2	1,01
	1006	1,5	5,5	48,4	8,9	12,9	0,0	29,8	0,7	0,99
	1006	2,0	4,4	48,0	7,6	12,7	0,0	31,7	0,7	1,00
	1006	2,5	3,8	45,8	8,2	12,0	0,0	34,0	0,8	0,96
	1006	3,0	3,5	42,2	9,4	13,7	0,0	34,7	0,8	1,05

Table B.12: Partial oxidation over cobalt on α-Al_2O_3 (Table 3.6)

Metal Loading	Temp (°C)	Time (h)	CH_4 conv. (%)	Selectivity (%)					H_2/CO	B'
				CO	CO_2	C_2H_4	C_2H_2	C_3H_6		
none	476	0,5	0,2	100,0	0,0	0,0	0,0	0,0	9,6	1,03
	800	1,0	6,5	83,0	17,0	0,0	0,0	0,0	1,6	0,95
	1023	1,5	21,5	64,5	6,0	28,4	0,0	1,2	1,1	1,02
	1023	2,0	22,9	64,8	5,7	26,9	0,0	2,6	1,0	1,06
	1023	2,5	27,1	66,1	5,3	25,5	0,0	3,1	1,0	0,93
	1023	3,0	23,2	66,6	4,6	26,8	0,0	2,1	0,9	1,02
10%Co	485	0,5	0,0	0,0	0,0	0,0	0,0	0,0	—	1,28
	831	1,0	51,2	89,0	0,0	10,2	0,0	0,8	1,7	1,04
	925	1,5	89,0	98,2	1,8	0,0	0,0	0,0	1,7	0,93
	1023	2,0	81,3	99,6	0,0	0,4	0,0	0,0	1,8	0,99
	1023	2,5	96,7	100,0	0,0	0,0	0,0	0,0	1,7	0,93
	1023	3,0	96,8	100,0	0,0	0,0	0,0	0,0	1,7	0,93
	1024	3,5	97,0	100,0	0,0	0,0	0,0	0,0	1,7	0,90

Table B.13: Partial oxidation over cobalt on γ-Al_2O_3 (Table 3.6)

Metal Loading	Temp. (°C)	Time (h)	CH_4 conv. (%)	Selectivity (%)					H_2/CO	B'
				CO	CO_2	C_2H_4	C_2H_2	C_3H_6		
none	440	0,5	0,1	100,0	0,0	0,0	0,0	0,0	1,0	0,93
	772	1,0	3,3	77,0	23,0	0,0	0,0	0,0	2,2	0,98
	995	1,5	20,0	40,4	6,9	26,4	0,3	17,0	1,2	1,03
	995	2,0	20,1	49,5	6,5	26,0	0,0	13,1	1,1	1,00
	995	2,5	21,9	51,3	8,5	24,0	0,0	16,2	1,3	1,03
	995	3,0	20,6	49,4	6,4	27,7	0,0	16,5	1,3	1,00
	995	3,5	20,4	49,0	[illegible]	27,3	0,0	16,7	1,3	0,99
3%Co	490	0,5	1,0	95,2	4,8	0,0	0,0	0,0	0,0	1.06
	807	1,0	54,6	87,6	11,5	0,1	0,0	0,7	1,7	0,99
	998	1,5	78,6	95,0	4,4	0,5	0,0	0,2	1,5	1,04
	998	2,0	77,0	[illegible] 8	3,6	0,3	0,0	0,3	1,7	0,95
	998	2,5	78,0	95,3	4,4	0,3	0,0	0,2	1,6	0,99
	998	3,0	77,7	95,[illegible]	3,9	0,3	0,0	0,2	1,7	0,96
10%Co	486	0,5	0,0	0,0	0,0	0,0	0,0	0,0	—	1,24
	849	1,0	48,7	86,6	12,0	0,8	0,0	0,6	1,8	1,13
	1041	1,5	88,5	98,8	1,1	0,2	0,0	0,0	2,1	0,91
	1041	2,0	93,0	98,8	1,2	0,0	0,0	0,0	2,3	0,83
	1041	2,5	94,3	99,0	1,0	0,0	0,0	0,0	2,1	0,93
	1041	3,0	95,0	98,5	1,5	0,0	0,0	0,0	2,1	0,96
10%Co[a]	486	0,5	0,1	78,5	21,5	0,0	0,0	0,0	5,8	1,33
	845	1,0	64,4	94,2	5,8	0,0	0,0	0,0	1,5	1,07
	925	—	81,8	96,0	3,9	0,0	0,0	0,0	1,7	0,91
	1042	1,5	97,2	99,9	0,1	0,0	0,0	0,0	1,7	0,88
	1042	2,0	98,3	100,0	0,0	0,0	0,0	0,0	1,6	0,92
	1042	2,5	98,0	100,0	0,0	0,0	0,0	0,0	1,6	0,96
	1042	3,0	97,8	100,0	0,0	0,0	0,0	0,0	1,6	0,93
10%Co[b]	464	0,5	0,1	100,0	0,0	0,0	0,0	0,0	7,2	1,32
	813	1,0	57,1	90,3	8,4	0,4	0,0	0,0	1,7	1,03
	1010	1,5	82,6	99,8	0,2	0,0	0,0	0,0	1,8	0,95
	1010	2,0	97,2	100,0	0,0	0,0	0,0	0,0	1,6	0,93
	1010	2,5	96,5	100,0	0,0	0,0	0,0	0,0	1,8	0,95
	1010	3,0	96,0	100,0	0,0	0,0	0,0	0,0	1,7	0,93

[a] A second batch prepared in the same way.

[b] From the second batch, calcined at 1125°C— section 2.2.2.

Table B.14: Partial oxidation over cobalt on C/γ-Al_2O_3 (Table 3.8)

Metal Loading	Temp (°C)	Time (h)	CH_4 conv. (%)	Selectivity (%)					H_2/CO	B'
				CO	CO_2	C_2H_4	C_2H_2	C_3H_8		
none	455	0,5	0,1	31,8	68,3	0,0	0,0	0,0	0,7	0,99
	757	1,0	4,6	75,1	24,9	0,0	0,0	0,0	1,8	0,96
	1012	1,5	29,4	47,6	20,8	23,1	3,5	4,9	1,3	0,99
	1012	2,0	32,9	50,6	17,5	20,4	5,0	6,3	1,2	1,03
	1012	2,5	33,3	47,3	16,3	27,2	2,3	7,0	1,2	1,01
	1012	3,0	28,2	43,5	14,5	30,8	1,2	10,1	1,3	1,02
3%Co	448	0,5	0,1	64,1	35,9	0,0	0,0	0,0	0,5	1,09
	790	1,0	9,9	52,8	41,9	2,1	0,0	3,8	2,4	1,12
	1010	1,5	76,2	94,4	3,9	1,5	0,0	0,3	1,6	0,97
	1010	2,0	80,0	97,0	1,6	5,1	0,0	0,3	1,6	0,95
	1010	2,5	81,5	95,8	2,3	1,6	0,0	0,2	1,6	0,93
	1010	3,0	83,2	96,7	2,6	0,5	0,0	0,2	1,6	0,94
10%Co	482	0,5	0,6	5,6	94,4	0,0	0,0	0,0	0,0	1,18
	802	1,0	32,4	81,1	17,6	0,3	0,0	1,1	1,8	1,13
	1001	1,5	93,0	99,8	0,2	0,0	0,0	0,0	2,0	0,91
	1001	2,0	96,1	99,8	0,2	0,0	0,0	0,0	2,0	0,93
	1001	2,5	96,7	99,9	0,1	0,0	0,0	0,0	2,0	0,91
	1001	3,0	97,0	99,9	0,1	0,0	0,0	0,0	2,0	0,93
10%Co[a]	472	0,5	1,0	37,5	62,5	0,0	0,0	0,0	0,7	1,27
	820	1,0	46,1	90,9	9,1	0,0	0,0	0,0	1,9	0,97
	925	—	95,6	99,3	0,2	0,0	0,0	0,0	1,2	1,19
	1010	1,5	89,3	99,6	0,4	0,0	0,0	0,0	1,7	0,91
	1010	2,0	91,6	99,8	0,2	0,0	0,0	0,0	1,7	0,91
	1010	2,5	92,2	99,8	0,2	0,0	0,0	0,0	1,7	0,90
	1010	3,0	92,0	99,6	0,4	0,0	0,0	0,0	1,8	0,85
10%Co[b]	420	0,5	0,1	100,0	0,0	0,0	0,0	0,0	4,1	1,26
	763	1,0	1,4	55,4	44,6	0,0	0,0	0,0	3,7	1,23
	994	1,5	80,4	99,8	0,2	0,0	0,0	0,0	1,9	0,95
	994	2,0	93,9	100,0	0,0	0,0	0,0	0,0	2,0	0,78
	994	2,5	93,9	99,9	0,1	0,0	0,0	0,0	1,9	0,90
	994	3,0	94,0	100,0	0,0	0,0	0,0	0,0	1,8	0,89

[a] A second batch prepared in the same way.

[b] From the second batch, calcined at 1125°C— section 2.2.2.

Table B.15: Partial oxidation over cobalt on C/γ-Al_2O_3 — alternative preparation (Table 3.8)

Metal Loading	Temp (°C)	Time (h)	CH_4 conv. (%)	Selectivity (%)					H_2/CO	B'
				CO	CO_2	C_2H_4	C_2H_2	C_3H_6		
14%Co	497	0,5	0,4	0,0	100,0	0,0	0,0	0,0	—	1,16
	833	1,0	16,2	46,0	44,7	3,3	0,0	6,0	2,7	1,14
	1027	1,5	83,4	97,0	2,0	0,9	0,0	0,1	1,7	1,09
	1027	2,0	62,8	95,3	4,5	0,2	0,0	0,0	2,8	0,95
	1027	3,0	90,3	99,2	0,8	0,0	0,0	0,0	2,2	0,85
	1027	4,0	92,6	99,7	0,3	0,0	0,0	0,0	2,1	0,91
	1027	5,0	94,1	99,8	0,2	0,0	0,0	0,0	2,1	0,91
	1027	6,0	95,[illegible]	99,3	0,7	0,0	0,0	0,0	2,2	0,86
	1027	7,0	95,5	99,3	0,7	0,0	0,0	0,0	1,9	1,00
	1027	8,0	95,8	99,7	0,3	0,0	0,0	0,0	1,8	1,02
	1027	9,0	95,9	99,3	0,7	0,0	0,0	0,0	1,8	1,06
	1027	10,0	96,0	99,2	0,8	0,0	0,0	0,0	1,7	1,11
	1027	11,0	96,3	98,9	1,1	0,0	0,0	0,0	2,0	0,94
14%Co[a]	368	0,5	0,4	100,0	0,0	0,0	0,0	0,0	0,3	1,21
	730	1,0	8,5	54,4	45,6	0,0	0,0	0,0	2,6	1,11
	953	1,5	76,7	96,2	3,0	0,8	0,0	0,0	1,5	0,97
	953	2,0	82,2	97,4	2,[illegible]	0,4	0,0	0,0	1,7	0,86
	953	2,5	85,1	97,8	1,9	0,2	0,0	0,0	1,6	0,93
	953	3,0	87,4	98,5	1,5	0,0	0,0	0,0	1,6	0,93
14%Co[b]	507	0,5	0,8	0,0	100,0	0,0	0,0	0,0	—	1,24
	835	1,0	8,6	46,5	53,5	0,0	0,0	0,0	3,4	1,10
	1028	1,5	39,6	67,4	21,9	7,9	0,0	2,8	2,0	0,99
	1028	2,0	57,8	83,[illegible]	9,6	4,4	0,0	2,8	1,9	1,02
	1028	2,5	61,3	87,9	7,1	4,2	0,0	0,3	1,9	0,99
	1028	3,0	65,3	89,7	3,8	4,2	0,0	0,3	1,9	0,9[illegible]
	1028	3,5	67,9	93,2	5,0	1,9	0,0	0,0	1,8	0,97
	1028	4,0	72,6	93,6	5,7	0,7	0,0	0,0	1,7	1,01
	1028	8,0	84,8	97,2	2,4	0,4	0,0	0,0	1,7	1,03
	1028	12,0	88,5	98,0	1,[illegible]	0,1	0,0	0,0	1,6	1,04
	1028	16,0	89,9	98,3	1,7	0,0	0,0	0,0	1,7	1,00
	1028	20,0	89,7	97,9	2,0	0,2	0,0	0,0	1,5	1,10
	1028	24,0	90,1	98,2	1,9	0,0	0,0	0,0	1,6	1,03
	1028	28,0	90,2	98,4	1,5	0,1	0,0	0,0	2,0	0,87
	1028	32,0	90,4	98,4	1,4	0,1	0,0	0,0	2,0	0,84
	1028	36,0	89,6	98,3	1,[illegible]	0,1	0,0	0,0	1,8	0,95
	1028	40,0	89,3	98,1	1,8	0,2	0,0	0,0	1,7	1,03
	1028	44,0	88,7	97,9	1,9	0,2	0,0	0,0	1,6	1,06
	1028	48,0	88,8	97,8	2,1	0,1	0,0	0,0	1,7	1,02
	1028	52,0	88,6	98,1	1,7	0,2	0,0	0,0	1,7	0,9[illegible]
	1028	56,0	88,5	98,6	1,3	0,1	0,0	0,0	2,0	0,85
	1028	60,0	87,7	98,2	1,6	0,2	0,0	[illegible],0	1,7	0,98
	1028	64,0	87,1	98,0	1,8	0,1	0,0	0,0	1,6	1,04
	1028	68,0	87,0	98,1	1,6	0,3	0,0	0,0	1,7	1,04
	1028	72,0	87,9	98,1	1,6	0,3	0,0	0,0	2,0	0,84

[a] Calcined at 800°C— section 2.2.2,

[b] Diluted with 200 mg of quartz beads,

Table B.16: Partial oxidation over the "blue" zone (Table 4.4)

Temp	Time	CH_4	Selectivity (%)						
(°C)	(h)	conv. (%)	CO	CO_2	C_2H_4	C_2H_2	C_3H_6	H_2/CO	B'
479	0,5	0,3	100,0	0,0	0,0	0,0	0,0	0,2	1,07
818	1,0	20,2	81,8	16,3	0,0	0,0	1,9	2,5	0,97
1016	1,5	40,8	82,7	4,6	8,9	0,0	3,9	2,0	0,93
1016	2,0	43,3	78,7	3,8	13,8	0,0	3,8	2,0	1,00
1016	2,5	43,9	78,4	4,3	13,9	0,0	3,5	2,1	0,92
1016	3,0	47,5	78,8	5,6	12,5	0,0	3,2	1,6	1,11

Table B.17: Partial oxidation over deactivated 10%Co/C/γ-Al_2O_3 (Table 4.5)

Temp	Time	CH_4	Selectivity (%)						
(°C)	(h)	conv. (%)	CO	CO_2	C_2H_4	C_2H_2	C_3H_6	H_2/CO	B'
958	0,5	5,2	50,4	30,5	19,1	0,0	0,0	1,7	0,94
958	1,0	8,2	67,1	21,4	11,4	0,0	0,0	0,8	0,98
958	1,5	5,7	46,5	34,8	18,7	0,0	0,0	1,7	0,97
958	4,5	6,0	54,5	37,2	8,4	0,0	0,0	1,3	0,96
958	7,5	8,7	61,1	25,9	13,0	0,0	0,0	0,7	1,09
958	10,5	9,7	63,0	26,5	10,5	0,0	0,0	0,7	0,99
958	13,5	8,2	62,9	27,8	10,3	0,0	0,0	0,8	1,05
958	16,5	6,0	62,8	29,3	7,9	0,0	0,0	1,0	1,01

Table B.18: Partial oxidation studies over A_B^R (Figure 3.3)

Temp	Time	CH_4	Selectivity (%)						
(°C)	(h)	conv. (%)	CO	CO_2	C_2H_4	C_2H_2	C_3H_6	H_2/CO	B'
496	0,5	67,3	87,7	12,3	0,0	0,0	0,0	1,9	1,10
792	1,0	92,3	99,1	0,9	0,0	0,0	0,0	1,7	1,00
993	1,5	97,2	100,0	0,0	0,0	0,0	0,0	1,7	1,01
993	2,0	96,0	100,0	0,0	0,0	0,0	0,0	1,7	1,02
993	2,5	95,5	100,0	0,0	0,0	0,0	0,0	1,7	1,00
993	3,0	95,2	100,0	0,0	0,0	0,0	0,0	1,7	1,00
993	6,0	97,6	100,0	0,0	0,0	0,0	0,0	1,9	0,87
993	9,0	98,8	100,0	0,0	0,0	0,0	0,0	1,6	1,03
993	12,0	99,0	99,8	0,2	0,0	0,0	0,0	1,6	1,06
993	15,0	98,9	99,8	0,2	0,0	0,0	0,0	1,3	0,96
993	18,0	99,5	100,0	0,0	0,0	0,0	0,0	1,8	0,95

Table B.19: GHSV tests using A_B^R (Figure 4.1)

Temp	Mass	CH_4	Selectivity (%)						
(°C)	(mg)	conv. (%)	CO	CO_2	C_2H_4	C_2H_2	C_3H_6	H_2/CO	B'
821	80,0	98,5	97,7	2,3	0,0	0,0	0,0	1,7	1,00
821	60,0	97,5	98,6	1,4	0,0	0,0	0,0	1,5	1,00
821	40,0	96,0	97,8	2,2	0,0	0,0	0,0	1,5	1,00
825	20,0	87,8	98,6	1,4	0,0	0,0	0,0	1,1	1,00
825	10,0	42,5	95,4	4,6	0,0	0,0	0,0	2,0	1,00

Table B.20: 10%Co/C/γ-Al_2O_3 stability — 0 to 150 hours (Figure 3.1)

Temp	Time	CH_4	Selectivity (%)						
(°C)	(h)	conv. (%)	CO	CO_2	C_2H_4	C_2H_2	C_3H_6	H_2/CO	B'
563	0,5	0,6	83,3	16,7	0,0	0,0	0,0	1,6	1,32
889	1,0	48,1	90,2	8,0	0,6	0,0	1,2	1,9	1,18
1068	1,5	94,1	100,0	0,0	0,0	0,0	0,0	2,2	0,93
1068	2,0	93,7	100,0	0,0	0,0	0,0	0,0	1,9	1,05
1068	2,5	93,8	100,0	0,0	0,0	0,0	0,0	2,2	0,93
1068	3,0	93,8	100,0	0,0	0,0	0,0	0,0	2,1	0,97
1068	3,5	94,1	100,0	0,0	0,0	0,0	0,0	1,9	1,07
1068	7,5	96,3	100,0	0,0	0,0	0,0	0,0	2,1	0,95
1068	11,5	98,6	100,0	0,0	0,0	0,0	0,0	1,8	1,08
1068	15,5	98,1	100,0	0,0	0,0	0,0	0,0	1,7	1,17
1068	19,5	98,0	100,0	0,0	0,0	0,0	0,0	1,9	1,06
1068	23,5	95,8	100,0	0,0	0,0	0,0	0,0	1,9	1,09
1068	,5	94,9	100,0	0,0	0,0	0,0	0,0	1,8	1,09
1068	1,5	97,3	100,0	0,0	0,0	0,0	0,0	1,9	1,07
1068	35,5	98,6	100,0	0,0	0,0	0,0	0,0	1,9	1,07
1068	39,5	98,4	100,0	0,0	0,0	0,0	0,0	1.5	1,33
1068	43,5	98,8	100,0	0,0	0,0	0,0	0,0	1,7	1,23
1068	47,5	97,4	100,0	0,0	0,0	0,0	0,0	1,8	1,14
1068	51,5	98,4	100,0	0,0	0,0	0,0	0,0	1,7	1,16
1068	55,5	98,9	100,0	0,0	0,0	0,0	0,0	1,7	1,21
1068	59,5	99,2	100,0	0,0	0,0	0,0	0,0	1,8	1,12
1068	63,5	99,3	100,0	0,0	0,0	0,0	0,0	1,7	1,17
1068	67,5	98,7	100,0	0,0	0,0	0,0	0,0	1,7	1,21
1068	71,5	97,1	100,0	0,0	0,0	0,0	0,0	1,8	1,12
1068	75,5	95,5	100,0	0,0	0,0	0,0	0,0	1,8	1,14
1068	79,5	97,1	100,0	0,0	0,0	0,0	0,0	1,8	1,10
1068	83,5	97,7	100,0	0,0	0,0	0,0	0,0	1,8	1,11
1068	87,5	98,1	100,0	0,0	0,0	0,0	0,0	1,7	1,14
1068	91,5	98,3	100,0	0,0	0,0	0,0	0,0	1,8	1,10
1068	95,5	95,3	100,0	0,0	0,0	0,0	0,0	1,8	1,11
1068	99,5	94,5	100,0	0,0	0,0	0,0	0,0	1,9	1,07
1068	103,5	96,2	100,0	0,0	0,0	0,0	0,0	2,1	0,92
1068	107,5	98,1	100,0	0,0	0,0	0,0	0,0	1,9	1,06
1068	111,5	96,5	100,0	0,0	0,0	0,0	0,0	1,8	1,09
1068	115,5	98,0	100,0	0,0	0,0	0,0	0,0	1,7	1,14
1182	119,5	96,0	100,0	0,0	0,0	0,0	0,0	1,9	1,07
1064	123,5	99,2	100,0	0,0	0,0	0,0	0,0	1,8	1,05
1064	127,5	98,7	100,0	0,0	0,0	0,0	0,0	1,9	1,01
1064	131,5	99,6	100,0	0,0	0,0	0,0	0,0	1,7	1,10
1064	135,5	99,0	100,0	0,0	0,0	0,0	0,0	1,7	1,11
1064	139,5	99,3	100,0	0,0	0,0	0,0	0,0	1,7	1,10
1064	143,5	98,5	100,0	0,0	0,0	0,0	0,0	2,1	0,91
1064	147,5	97,5	100,0	0,0	0,0	0,0	0,0	1,9	1,00
1064	151,5	99,1	100,0	0,0	0,0	0,0	0,0	2,1	0,90

Table B.21: 10%Co/C/γ-Al_2O_3 stability — deactivation

Temp (°C)	Time (h)	CH_4 conv. (%)	Selectivity (%)					H_2/CO	B'
			CO	CO_2	C_2H_4	C_2H_2	C_3H_6		
1064	151,5	99,1	100,0	0,0	0,0	0,0	0,0	2,1	0,90
1064	155,6	99,1	100,0	0,0	0,0	0,0	0,0	2,1	0,95
1064	159,5	99,1	99,8	0,2	0,0	0,0	0,0	1,8	1,06
1064	163,5	99,2	99,9	0,1	0,0	0,0	0,0	1,2	1,66
1064	167,5	98,3	100,0	0,0	0,0	0,0	0,0	2,0	0,97
1064	171,5	98,8	100,0	0,0	0,0	0,0	0,0	1,8	1,07
1064	175,5	97,7	100,0	0,0	0,0	0,0	0,0	1,7	1,16
1064	179,5	98,0	99,1	0,9	0,0	0,0	0,0	1,5	1,31
1064	183,5	97,8	96,1	3,9	0,0	0,0	0,0	1,5	1,08
1064	187,5	97,0	95,1	4,9	0,0	0,0	0,0	1,4	1,07
1064	191,5	94,7	93,0	7,0	0,0	0,0	0,0	1,5	0,90
1064	195,5	89,9	68,0	18,8	3,2	0,0	10,1	0,9	0,62
1064	199,5	99,8	33,6	66,4	0,0	0,0	0,0	0,5	0,48
1064	203,5	100,0	4,8	95,2	0,0	0,0	0,0	12,4	0,07
1064	207,5	98,8	5,2	94,8	0,0	0,0	0,0	1,0	0,05
1064	211,5	100,0	11,0	89,0	0,0	0,0	0,0	0,7	0,03
1064	215,5	100,0	1,4	98,6	0,0	0,0	0,0	1,2	0,13
1064	219,5	15,1	51,0	14,8	33,2	0,0	1,1	1,5	1,34
1064	223,5	14,6	51,2	18,2	29,4	0,0	1,1	1,4	1,42
1064	227,5	22,1	53,6	17,9	27,9	0,0	0,7	1,0	1,02
1064	231,5	100,0	17,8	82,2	0,0	0,0	0,0	0,7	0,41
1064	235,5	100,0	0,8	99,2	0,0	0,0	0,0	0,8	0,23

Table B.22: A_B^R stability (Table 3.9, figures 3.2 and 3.3)

Temp	Time	CH_4	Selectivity (%)						
(°C)	(h)	conv. (%)	CO	CO_2	C_2H_4	C_2H_2	C_3H_6	H_2/CO	B'
535	0,5	71,3	88,1	11,9	0,0	0,0	0,0	1,9	1,08
636	1,0	77,4	93,8	6,2	0,0	0,0	0,0	1,8	1,03
735	1,5	85,6	97,3	2,7	0,0	0,0	0,0	1,9	0,95
837	2,0	94,1	98,4	1,6	0,0	0,0	0,0	1,8	0,98
935	2,5	98,4	99,8	0,2	0,0	0,0	0,0	1,8	0,97
935	3,0	98,4	99,6	0,4	0,0	0,0	0,0	1,8	0,96
935	9,0	99,1	99,6	0,4	0,0	0,0	0,0	1,7	1,01
935	15,0	99,0	99,5	0,5	0,0	0,0	0,0	1,6	1,06
935	21,0	98,4	99,7	0,3	0,0	0,0	0,0	1,7	1,01
935	27,0	98,7	99,6	0,4	0,0	0,0	0,0	1,8	0,93
935	33,0	98,6	99,6	0,4	0,0	0,0	0,0	1,5	1,09
935	39,0	98,4	99,6	0,4	0,0	0,0	0,0	1,6	1,05
935	45,0	97,7	99,6	0,4	0,0	0,0	0,0	1,9	0,88
935	51,0	98,0	99,7	0,3	0,0	0,0	0,0	1,8	0,94
935	57,0	98,1	99,6	0,4	0,0	0,0	0,0	1,7	0,97
935	63,0	97,8	99,8	0,2	0,0	0,0	0,0	1,7	0,99
935	69,0	97,3	99,3	0,7	0,0	0,0	0,0	1,7	1,00
935	75,0	97,2	99,4	0,6	0,0	0,0	0,0	1,8	0,94
935	81,0	97,7	99,5	0,5	0,0	0,0	0,0	1,8	0,92
935	87,0	97,6	100,0	0,0	0,0	0,0	0,0	1,8	0,93
935	93,0	97,1	99,4	0,6	0,0	0,0	0,0	1,7	1,00
935	99,0	98,1	99,7	0,3	0,0	0,0	0,0	1,8	0,94
935	123,0	99,0	99,8	0,2	0,0	0,0	0,0	1,9	0,88
935	129,0	99,3	99,6	0,4	0,0	0,0	0,0	1,7	1,00
935	165,0	98,6	99,7	0,3	0,0	0,0	0,0	1,9	0,87
935	171,0	99,1	99,6	0,4	0,0	0,0	0,0	1,5	1,13
935	177,0	99,1	99,5	0,5	0,0	0,0	0,0	1,6	1,04
935	183,0	98,8	99,7	0,3	0,0	0,0	0,0	1,6	1,06
837	189,0	93,4	98,8	1,2	0,0	0,0	0,0	1,9	0,89
837	195,0	94,4	98,4	1,6	0,0	0,0	0,0	1,7	0,98
837	201,0	94,4	98,3	1,7	0,0	0,0	0,0	1,6	1,06
837	207,0	93,8	98,6	1,4	0,0	0,0	0,0	1,7	0,99
837	213,0	93,2	98,8	1,2	0,0	0,0	0,0	1,8	0,97
837	219,0	94,0	98,3	1,7	0,0	0,0	0,0	1,7	0,99
837	225,0	94,1	98,4	1,6	0,0	0,0	0,0	1,6	1,03
837	231,0	93,4	98,8	1,2	0,0	0,0	0,0	1,8	0,93
837	237,0	92,4	98,2	1,8	0,0	0,0	0,0	2,0	0,88
837	243,0	93,4	98,4	1,6	0,0	0,0	0,0	1,8	0,95
837	249,0	93,6	98,6	1,4	0,0	0,0	0,0	1,7	1,01
837	255,0	93,0	98,7	1,3	0,0	0,0	0,0	1,7	0,98

References

[1] G. C. Bond. *Heterogeneous Catalysis: Principles and Applications.* Clarendon Press, Oxford, second edition, 1987.

[2] R. E. Kirk, D. F. Othmer, M. Grayson, and D. Eckroth. *Kirk-Othmer Encyclopedia of Chemical Technology*, volume 11. John Wiley & Sons, Inc, New York, third edition, 1980.

[3] M. D. Lemonick. *TIME*, page 51, December 1993.

[4] M. G. Poirier, A. R. Sanger, and K. J. Smith. *The Canadian Journal of Chemical Engineering*, 69:1027, 1991.

[5] J. Haggin. *C&EN*, page 33, April 1992.

[6] J. Haggin. *C&EN*, page 6, January 1993.

[7] J. R. Anderson. *Applied Catalysis*, 47:177, 1989.

[8] J. Haggin. *C&EN*, page 45, May 1988.

[9] D. L. Trimm. In *Methane Conversion*, volume 36 of *Studies in Surface Science and Catalysis*, page 39, Amsterdam, 1988. Elsevier.

[10] S. Strelzoff. *Technology and Manufacture of Ammonia.* John Wiley & Sons, Inc, New York, 1981.

[11] J. Rostrup-Nielsen. In *Methane Conversion*, volume 36 of *Studies in Surface Science and Catalysis*, page 73, Amsterdam, 1988. Elsevier.

[12] M. E. Dry. In *Preprints - Catalysis & Catalytic Processing*, page 57, Cape Town, October 1993. Catalysis Society of South Africa.

[13] J. A. Lapszewicz, A. Ekstrom, Q. Daiyi, and X.-Z. Jiang. In *Preprints - Catalysis & Catalytic Processing*, page 273, Cape Town, October 1993. Catalysis Society of South Africa.

[14] H. Pines. *The Chemistry of Catalytic Hydrocarbon Conversions.* Academic Press, New york, 1981.

[15] W. Keim. *Catalysis in C_1 Chemistry.* D. Reidel Publishing Company, Dortrecht, 1983.

[16] M. S. Wainwright. In *Methane Conversion*, volume 36 of *Studies in Surface Science and Catalysis*, page 95, Amsterdam, 1988. Elsevier.

[17] C. J. Maiden. In *Methane Conversion*, volume 36 of *Studies in Surface Science and Catalysis*, page 1, Amsterdam, 1988. Elsevier.

[18] A. A. Avidan. In *Methane Conversion*, volume 36 of *Studies in Surface Science and Catalysis*, page 307, Amsterdam, 1988. Elsevier.

[19] J. Topp-Jørgensen. In *Methane Conversion*, volume 36 of *Studies in Surface Science and Catalysis*, page 293, Amsterdam, 1988. Elsevier.

[20] S. I. Sandler. *Chemical and Engineering Thermodynamics.* John Wiley and Sons, Singapore, second edition, 1989.

[21] R. J. Gillespie, D. A. Humphreys, N. C. Baird, and E. A. Robinson. *Chemistry.* Allyn and Bacon, Inc., Boston, 1986.

[22] M. M. Bhasin and K. D. Campbell. In *Preprints - Catalysis & Catalytic Processing*, page 25, Cape Town, October 1993. Catalysis Society of South Africa.

[23] J. C. Q. Fletcher. *S. A. Journal of Chemical Engineering*, 6:26, 1994.

[24] J. F. Walker. *Formaldehyde.* Reinhold Publishing Corporation, New York, 1986.

[25] R. E. Kirk, D. F. Othmer, M. G., and D. Eckroth. *Kirk-Othmer Concise Encyclopedia of Chemical Technology.* John Wiley & Sons, Inc, New York, third edition, 1985.

[26] G. Weiss. *Hazardous Chemicals Data Book.* Noyes Data Corporation, New York, second edition, 1986.

[27] J. N. Theron, J. C. Q. Fletcher, and M. S. Scurrell. In *Preprints - Catalysis & Catalytic Processing*, page 291, Cape Town, October 1993. Catalysis Society of South Africa.

[28] G. A. Foulds and ... S. Walker. In *Preprints - Catalysis & Catalytic Processing*, page 213, Cape Town, October 1993. Catalysis Society of South Africa.

[29] R. Pitchai and K. Klier. *Catal. Rev.-Sci. Eng.*, 28:13, 1986.

[30] A. Coghlan. *New Scientist*, page 17, January 1993.

[31] R. P. Noceti and C. E. Taylor. *U.S. Patent No. 4769504*, 1988.

[32] M. Prettre, CH. Eichner, and M. Perrin. *Transactions of the Faraday Society*, 43:335, 1946.

[33] D. Dissanayake, M. P. Rosynek, K. C. C. Kharas, and J. H. Lunsford. *Journal of Catalysis*, 132:117. 1991.

[34] W. J. M. Vermeiren, E. Blomsa, and P. A. Jacobs. *Catalysis Today*, 13:L1, 1992.

[35] P. D. F. Vernon, M. L. H. Green, A. K. Cheetham, and A. T. Ashcroft. *Catalysis Letters*, 6:181, 1990.

[36] Y.-F. Chang and H. Heinemann. *Catalysis Letters*, 21:215, 1993.

[37] D. A. Hickmann and L. D. Schmidt. *Science*, 259:343, 1993.

[38] D. A. Hickmann and L. D. Schmidt. *AIChE Journal*, 39:1164, 1993.

[39] J. B. Claridge, M. L. H. Green, S. C. Tsang, A. P. E. York, A. T. Ashcroft, and P. D. Battle. *Catalysis Letters*, 22:299, 1993.

[40] V. R. Choudhary, A. S. Mamman, and S. D. Sansare. *Applied Catalysis*, 90:L1, 1992.

[41] V. R. Choudhary, V. H. Rane, and A. M. Rajput. *Catalysis Letters*, 22:289, 1993.

[42] V. R. Choudhary, A. S. Mamman, and S. D. Sansare. *Ange. Chem. Int. Ed. Engl.*, 31:1189, 1992.

[43] V. R. Choudhary, A. M. Rajput, and B. Prabhakar. *Journal of Catalysis*, 139:326, 1993.

[44] T. Hayakawa, A. G. Andersen, M. Shimizu, K. Suzuki, and K. Takehira. *Catalysis Letters*, 22:307, 1993.

[45] A. T. Ashcroft, A. K. Cheetham, J. S. Foord, M. L. H. Green, C. P. Grey, A. J. Murrell, and P. D. F. Vernon. *Nature*, 344:319, March 1990.

[46] D. A. Hickman, E. A. Haupfear, and L. D. Schmidt. *Catalysis Letters*, 17:223, 1993.

[47] P. M. Torniainen, X. Chu, and L.D. Schmidt. *Journal of Catalysis*, 146:1, 1994.

[48] S. S. Bharadwaj and L.D. Schmidt. *Journal of Catalysis*, 146:11, 1994.

[49] M. G. Poirier and J. Trudel. *Catalysis Letters*, 21:99, 1993.

[50] K. Kunimori, S. Umeda, J. Nakamura, and T. Ushijima. *Bulletin of the Chemical Society of Japan*, 65:2563, 1992.

[51] R. H. Jones, A. T. Ashcroft, D. Waller, A. K. Cheetham, and J. M. Thomas. *Catalysis Letters*, 8:169, 1991.

[52] S. Han, D. J. Martenal , R. E. Palermo, J. A. Pearson, and D. E. Walsh. *Journal of Catalysis*, 148:134, 1994.

[53] K. Otsuka, T. Ushiyama, and I. Yamanaka. *Chemistry Letters*, page 1517, 1993.

[54] J. G. Price, N. J. Coville, D. Glasser, and D. Hildebrandt. In *Preprints - Catalysis & Catalytic Processing*, page 137, Cape Town, October 1993. Catalysis Society of South Africa.

[55] Li Quanzhi and Y. Amenomiya. *Applied Catalysis*, 23:173, 1986.

[56] *Soviet Union Patent No. 1330783*, 1987.

[57] M. Priet, P. Pichat, and M. V. Mathieu. *Journal of Physical Chemistry*, 75:1216, 1971.

[58] M. Priet, P. Pichat, and M. V. Mathieu. *Journal of Physical Chemistry*, 75:1221, 1971.

[59] J. R. Mellor. PhD thesis, University of the Witwatersrand, 1993.

[60] R. C. Weast ed. *CRC Handbook of Chemistry and Physics*. CRC Press, Inc., Boca Raton, Florida, 63rd edition, 1982.

[61] J. S. Barros. *Analyst*, 114:369, 1989.

[62] D. J. Duvenhage. PhD thesis, University of the Witwatersrand, 1993.

[63] I. N. Levine. *Physical Chemistry*. McGraw-Hill Book Company, Singapore, third edition, 1988.

[64] M. Audier, A. Oberlin, M. Oberlin, M. Coulon, and L. Bonnetain. *Carbon*, 19:217, 1981.

[65] P. Arnoldy and J. A. Moulijn. *Journal of Catalysis*, 93:38, 1985.

[66] H.-C. Tung, C.-T. Yeh, and C.-T. Hong. *Journal of Catalysis*, 122:211, 1990.

[67] C-S. Bai, S. Soled, K. Dwight, and A. Wold. *Journal of Solid State Chemistry*, 91:148, 1991.

[68] D. F. Shriver, P. W. Atkins, and C. H. Langford. *Inorganic Chemistry*. Oxford University Press, Oxford, second edition, 1994.

[69] B. C. Gates, J. R. Katzer, and G. C. A. Schuit. *Chemistry of Catalytic Processes.* McGraw-Hill Book Company, New York, second edition, 1979.